PREDICTION OF AN AXIAL
COMPRESSOR STAGE CHARACTERISTIC
FROM A ONE-POINT MEASUREMENT

THESIS

Shahnaz M. Punjani

AFIT/GAE/ENY/95D-21

DTIC QUALITY INSPECTED 3

DEPARTMENT OF THE AIR FORCE

AIR UNIVERSITY

AIR FORCE INSTITUTE OF TECHNOLOGY

Wright-Patterson Air Force Base, Ohio

PREDICTION OF AN AXIAL
COMPRESSOR STAGE CHARACTERISTIC
FROM A ONE-POINT MEASUREMENT

THESIS

Shahnaz M. Punjani

AFIT/GAE/ENY/95D-21

DTIC QUALITY INSPECTED 3

PREDICTION OF AN AXIAL

COMPRESSOR STAGE CHARACTERISTIC

FROM A ONE-POINT MEASUREMENT

THESIS

Presented to the Faculty of the School of Engineering

of the Air Force Institute of Technology

Air University

In Partial Fulfillment of the

Requirements for the Degree of

Master of Science in Aeronautical Engineering

Shahnaz M. Punjani

November 1995

ACKNOWLEDGEMENTS

TABLE OF CONTENTS

LIST OF FIGURES

LIST OF TABLES

LIST OF SYMBOLS

A	area (ft^2)
C	absolute velocity (ft/s)
A, B, C	constant coefficients for parabolic functions, i.e. $Ax^2 + Bx + C$
C_p	specific heat (ft-lbf/lbm-°R)
DF	diffusion factor
e	true error
E	linearized error
G	observation relation
H	$\dfrac{\partial G}{\partial \Delta\alpha_1}$
m	mass flow (lbm/s)
m	slope of a line
M_{rel}	relative Mach number
MSE	mean sum squared error
N	rotational velocity (rotations per second)
N	total number of data points
NR_{cor}	corrected speed
P	pressure (psi)
P	gaussian probability function
r	radius (ft)

r	residual
R	gas constant (ft^2/s^2-°R)
Q	instrumental covariance
S	scalar quantity used in non-linear estimation: $E^T Q^{-1} E$
T	temperature (°R)
U	blade speed (ft/s)
V	relative velocity (ft/s)
W	work (ft-lbf)
$\dot{W}$	power input (ft-lbf/s)

Greek

α	absolute flow angle (degrees)
β	relative flow angle (degrees)
$\delta\Delta\alpha_1$	incremental change in $\Delta\alpha_1$
δC	incremental change in the parabolic coefficient, C
$\delta\epsilon'$	incremental change in the deflection curve slope
$\Delta\alpha_1$	change in stator outlet angle (degrees)
Δh	change in static enthalpy per unit mass (ft-lbf/lbm)
ΔT	change in temperature (°R)
ΔP	change in pressure (psi)
ϵ	deflection angle (degrees)
ϵ'	slope of ϵ versus β_1 curve

Φ	flow coefficient
Φ_A	flow coefficient used to calculate the parabolic coefficient, A
Φ_o	flow coefficient which gives maximum value of efficiency
γ	ratio of specific heats
η	efficiency
η_{max}	maximum efficiency
κ	incremental change in $\Delta\alpha_1$ used to estimate H
Λ	degree of reaction
μ	test tolerance for non-linear least squares algorithm to check C
ρ	density (lbm/ft^3)
σ	solidity
σ^P	square root of mean sum squared error for pressure (psi)
σ^T	square root of mean sum squared error for temperature (°R)
τ	test tolerance for non-linear least squares algorithm to check ε'
υ	test tolerance for one-point algorithm
ς	test tolerance for non-linear least squares algorithm to check $\Delta\alpha_1$
ξ	incremental change in the parabolic coefficienct, C, used to estimate H
Ψ^T	work coefficient
Ψ^P	pressure coefficient

Subscripts

1	inlet to stage

2	outlet to stage
a	axial
calc	calculated
D	DYNTECC data
G	generated
i	data point designator
m	mean
max	maximum
o	stagnation
o	true value in non-linear least squares
P	predicted
R	reference
REF	calculated reference value
t	value at the tip
T	test
w	tangential

ABSTRACT

This study focuses on predicting axial compressor stage characteristics using a single performance point comprised of mass flow, temperature rise and pressure rise coefficients (Φ, Ψ^T, and Ψ^P) obtained in experimental testing and a generic stage temperature characteristic. A new temperature characteristic is generated using a mapping technique where changes in stage blade angles are iterated from assumptions of free vortex flow and constant increment of flow turning angle with increased flow incidence. If additional data corresponding to the new curve are available, the characteristic is adjusted using non-linear least squares estimation. Essentially, the modified mapped curve results from a re-estimated change in the stator outlet angle which is iterated to minimize the total error between the new curve and the new aggregate of the given data.

A pressure characteristic for the single data point may be predicted from the new temperature characteristic and an assumption of constant efficiency. Upon collection of additional data points, three being sufficient, an improved pressure characteristic is obtained using an improved model for efficiency.

The predicted characteristics agreed well with calibration data in pre-stall regions. For those data near stall, the assumed linear relationship between incidence and flow turning is invalid, and a new model for flow turning is required.

I. __INTRODUCTION__

1.1 Background

A plot of temperature and pressure changes versus mass flow, compressor stage characteristics display the entire operating range for a stage. The mass flow, temperature and pressure rise are often non-dimensionalized and typically redesignated as flow (Φ), temperature (Ψ^T), and pressure (Ψ^P) coefficients. The superscripts "T" and "P" denote temperature and pressure, respectively. Figure 1.1 is an example of a compressor characteristic. This figure also shows the efficiency characteristic which can be calculated from the pressure and temperature characteristics.

Characteristic curves are developed during the design process and verified by testing. In the first case, they are developed from first principles (and computer codes) using blade and machine geometry and the semi-empirical methods of cascade theory to adjust for losses due to separation and boundary layer effects. Off-design performance, i.e., the characteristic, due to profile loss on the surfaces of the blades, annulus skin friction and secondary losses due to three-dimensional flow effects, may be estimated using empirical data and relationships as described in Ref. 7. Figure 1.2 shows a comparison of a characteristic calculated using first principles augmented with cascade theory and the actual characteristic determined by testing the compressor.

In the testing phase, mass flow, temperature and pressure data are non-dimensionalized to account for different environmental operating conditions (such as

inlet temperature and pressure), rotor speeds and the size of the compressor. Ideally (barring Reynolds number effects and excessive losses), the data acquired in this manner should collapse to a single curve independent of rotor speed and environment. For fixed relative blade geometry, the temperature and pressure rise for a given stage could be determined by geometrically scaling up or scaling down from a characteristic curve representative of a family of compressor stages. Figure 1.3 illustrates the correlation of head coefficient versus flow coefficient along a single curve for a centrifugal pump. The head coefficient (a measure of the energy transfer) is a scaled form of the temperature coefficient used in axial compressors.

It is useful at this point to review possible methods of developing characteristics for variable geometry. For stages of a given rotor geometry, a change in inlet gas angles due to variable inlet geometry will create a family of characteristics with inlet gas angles as the parameter. A change in blade angles, such as occurs with variable inlet guide vanes (IGV) or stator vanes, will cause the stage characteristics to be shifted up or down relative to the original curve. Figure 1.4 shows an example of how the pressure characteristic (Ψ^P vs. Φ) may be changed due to a change in the stator outlet angle. This figure was developed using a computer code, STGSTK (described in Ref. 12), capable of predicting the overall performance of an axial compressor. Ref. 12 describes the method by which STGSTK changes individual stage characteristics due to blade angle resets. The program user must input the design pressure rise and efficiency characteristics. (If the characteristics are unavailable, they are estimated by parabolas through the design pressure rise and

efficiency for the design flow coefficient.) The design pressure characteristic is adjusted for changes in speed and blade angles through changes in flow angles, mass flow rate, and pressure and temperature rise. A change in the stator outlet angle is precluded from causing a change in any of the other angles (relative flow angles inlet and outlet to the rotor) through an adjustment of the flow coefficient. The algorithm also assumes that the efficiency for the new pressure characteristic remains unaltered. STGSTK, however, requires design-level knowledge of the compressor. For example, all of the blade angles as well as the resets or changes in those angles must be known. The design pressure and efficiency stage characteristics for each stage are also essential inputs to the model and must be fully developed before the model may be used.

With individual stage characteristics known or estimated, the stage stacking analysis determines the overall compressor performance. The meanline velocity diagram inlet to the first stage along with the pressure ratio and efficiency for the given flow coefficient determines the outlet meanline velocity and this gives the inlet conditions of the second stage. The second stage outlet conditions are the inlet of the third stage and so on to the final stage until, finally, the overall temperature and pressure rise of the compressor are determined.

In an indirect procedure, individual stage characteristics can be developed from the generalized compressor stage characteristic typical of that shown in Figure 1.5. Ref. 10 describes the procedure which involves a stage-stacking approach and iteration of the design point values, Ψ_{REF}^{P}, Φ_{REF}, at the maximum efficiency point.

The general pressure characteristic shown in Figure 1.5 was developed using pressure rise data for a number of different compressor stages as referenced in the figure. Since the stage-stacking method requires knowledge of the blade angles, the initial absolute flow angle inlet to the first stage is assumed to be 15 degrees if the compressor has inlet guide vanes. Without IGV's, the initial angle is zero degrees. A variable angle geometry schedule is estimated based on field measurements of the compressor in question. A stage-stacking analysis given a mass flow, inlet temperature and pressure, and estimated inlet flow angle, yields the general stage characteristics. The characteristics are updated for new reference design points (Φ_{REF}, Ψ_{REF}^{P}) for each stage until agreement occurs between the calculated overall temperature and pressure rise and those of the given compressor.

So far, a direct and indirect way have been described to develop stage characteristics. The degree to which characteristics are straight rather than parabolic can allow for simpler analysis. For example, one may account for variable geometry as given in Ref. 2 which describes a model for off-design performance using ideal, straight-line-design stage characteristics. The model is accurate only for small deviations from the stage design point (within 4 percent of the design flow coefficient), since for large deviations the characteristic is curved due to losses and separation of the flow. A benefit of the straight-line-characteristic assumption is its use in studying perturbation effects and possible design changes.

1-4

1.2 The DYNTECC Analysis Program

The analysis and resulting code formulated during this research will become an integral part of the DYNamic Turbine Engine Compressor Code developed at Arnold Engineering Development Center at Arnold Air Station. DYNTECC [Ref. 6] is a one-dimensional, stage-by-stage axial compression system mathematical model designed to analyze dynamic instabilities of any compression system. DYNTECC numerically solves the mass, momentum, and energy equations with turbomachinery source terms (mass bleed, blade forces, and shaft work). Stage characteristics are an essential part of the compressor model and are required as inputs to DYNTECC.

Generally, stage characteristics required for DYNTECC are acquired from tests on the actual compressor being modeled. The test data is curvefit using an external program, PACFIT, which separates the test data into subsets, fits a parabolic curve through each subset and records a series of constant coefficients for each segment accounting for temperature and pressure coefficients as a parabolic function of flow coefficient. PACFIT coefficients along with the appropriate flow coefficient ranges are inputs to the DYNTECC model and used subsequently within the model to determine the pressure and temperature rise over each stage for any given mass flow.

Other required inputs to DYNTECC include hub and tip radii, rotor blade speed, the axial location of the entrance and exit to each stage, and a number of parameters defining the operating environment of the compressor, such as inlet temperature and pressure. These inputs are outlined in Ref. 13. DYNTECC does not require and cannot accept any specific blade geometry.

Currently, AEDC is modifying DYNTECC so that it can be applied as an on-line test data validation software package to allow for rapid on-site determination of data outliers or inconsistencies. Essentially, it will run while a compressor is being tested and before fully-developed stage characteristics are defined. Requisite to that modification is an ability to develop the stage characteristics during the test itself using an initial data point (temperature and pressure rise for a given mass flow rate) acquired for each stage characteristic.

1.3 Problem Statement

In an effort to stay within the limits of the current DYNTECC inputs, the use of first principles which requires blade angles, thickness, spacing, height, and chord length of the actual blades, information which is usually proprietary to the compressor designer, and thus unavailable, was eliminated. The problem finally reduced to: Given only a single performance point, comprised of temperature and pressure rise versus mass flow rate, overall stage geometry, and operating environment data, determine the pressure and temperature characteristics for the stage over the entire range of flow coefficient.

1.4 Approach

The solution method involved relating a performance point acquired real-time, stage-specific parameters and a general reference curve, to obtain a new characteristic through the performance point. The reference curve could be that of the stage being tested, perhaps one that was acquired during scale model tests, or a general curve

representing the performance of a number of other compressor stages. An essential requirement was that the reference curve be non-dimensionalized with respect to radius, operating environment and blade speed in a way consistent with the governing equations for mass flow, momentum and energy.

The performance point for a stage must also be similarly non-dimensionalized and compared to the reference curve. The algorithm assumes that the performance point is not on the reference curve and has possibly experienced a blade angle reset. Based on the references cited earlier (Ref. , 10 and 12), the curve generation methodology presented in this thesis assumes that because stage characteristics of fixed geometry should collapse any differences between the reference curve and the given performance point are due solely to a change in the absolute gas flow inlet angle, α_1.

Figure 1.6 is a graphical depiction of the problem statement and its solution. Since the pressure curve is related to temperature curve through the efficiency, a new temperature curve is generated first. The test values, Φ_T and Ψ_T^T, are used to determine both the change in α_1 from the reference curve and the point on the reference temperature curve (Φ_R, Ψ_R^T) that transforms to the test point. This is accomplished by determining the vector sum of the change in Ψ_R^T due to $\Delta\alpha_1$ along a line of constant flow coefficient and the change in Φ_R due to $\Delta\alpha_1$ along a line of constant temperature coefficient. With a new α_1 computed, the temperature curve through the test point, Φ_T, Ψ_T^T, is generated using the flow and temperature coefficients of the reference curve. From Ψ_T^T and Ψ_T^P, the efficiency at the test point

is calculated and initially assumed constant for the whole range of flow coefficient. Finally, a new pressure curve is generated using the constant efficiency and the new temperature curve.

Once the new temperature and pressure characteristics are generated, another portion of the algorithm uses additional data points acquired real-time to improve the estimated curves. For the temperature curve, this is accomplished using a non-linear least square algorithm to adjust the calculated $\Delta\alpha_1$ such that it minimizes the sum-squared error between the test data and calculated temperature coefficients. Additional data points can also be used to improve the efficiency model which up to this point had been assumed constant. The additional test data are used to develop a parabolic function for the efficiency, and the pressure curve is recalculated using the new efficiency and temperature curves.

The following items were accomplished during the validation of the methods presented in this thesis:

1. A curve generation algorithm was developed to generate new stage characteristics from a reference curve for the same stage and one test data point comprised of Φ, Ψ^T, Ψ^P.

2. The algorithm was also used to predict the characteristics for other stages using a reference curve from one stage and one test data point from a different stage.

3. The effect of changing the input data point, Φ, Ψ^T, on the accuracy of the curve generation was studied.

4. Finally, an improvement scheme for the generated curves due to additional test data points was examined.

The remaining chapters in this thesis are devoted to: Chapter II, a development of the governing equations and algorithms used to predict a new characteristic from a single data point and to update the prediction as new data is accumulated; Chapter III, the selection and development of reference curves to be used in the prediction algorithms; Chapter IV, application of the prediction algorithms to stage performance data for a three-stage axial compressor and a summary of the results; and Chapter V, conclusions and recommendations for the project.

II. DEVELOPMENT OF GOVERNING EQUATIONS AND CURVEFIT ALGORITHMS

2.1 Introduction

There are four steps in determining the temperature and pressure stage characteristics from a test performance point comprised of Φ, Ψ^T, Ψ^P. First, a reference temperature curve is compared to the test data flow and temperature coefficient. Second, if they do not lie along the same line, parameters for a new temperature characteristic are computed based on a change in stator outlet angle. Third, a new temperature curve is developed and the efficiency at the given point calculated using the test data temperature and pressure coefficients. Fourth, with the efficiency initially assumed constant over the entire range of flow coefficient, a new pressure curve is generated using the new temperature curve and the constant efficiency.

The theory and necessary equations used to solve this problem as described above are presented in this chapter. First, non-dimensionalized stage characteristic parameters for the performance point and reference curve are defined. Second, theoretical relationships between the flow, temperature and pressure coefficients are derived. Third, the equations employed in adjusting the curve assuming a change in the stator outlet angle are derived. Fourth, the development of the reference curve angles is described. Finally, the solution algorithms are presented.

The derivations presented below are based on the following assumptions:

1. Compressibility effects over the stage may be ignored. This is common in many derivations as seen in Ref. 3. For example, the density change for first stage of the test compressor used to verify this approach is only seven percent of the initial value. The density is treated as a step change between stages.

2. The flow is in radial equilibrium (i.e., the radial component of the flow velocity is negligible) and follows free-vortex flow theory such that the product of the tangential flow velocity and the radius is constant. With these assumptions and assuming incompressibility, the work done by the compressor is equal at all radii. Thus, the total stage performance may be determined from mean radius calculations.

3. The increment in deflection angle for an increment in incidence for a stage is constant. This limits the analysis to pre-stall effects. At stall and post-stall, the slope of the deflection versus incidence curve can vary considerably with changes in flow coefficient.

4. For a given rotor speed, the stator outlet angle, α_1, remains constant for the entire flow coefficient range although the stator blades may be reset for a change in rotor speed.

2.2 Non-Dimensionalization of the Stage Characteristic

There are many ways to define the flow, temperature and pressure coefficients in order to non-dimensionalize the stage characteristics. For example, using the definitions from Ref. 4, the flow, temperature and pressure coefficients are given by:

$$\Phi = \frac{m}{2\rho_m \pi N r_m A_m} \qquad (2.1)$$

$$\Psi^T = \frac{Cp\Delta T_{os}}{\left(2\pi\ N\ r_m\ \right)^2} \qquad (2.2)$$

$$\Psi^P = \frac{\Delta P_{os}}{\rho_{o1}\left(2\pi\ N\ r_m\ \right)^2} \qquad (2.3)$$

where m = the mass flow rate, N = the rotor speed in rotations per second, r_m = the mean radius of the stage, A_m = the mean area of the stage, ΔT_{os} = temperature change over the stage, ΔP_{os} = pressure rise over the stage, ρ_m = the mean density of the stage, and ρ_{o1} = the inlet stagnation density of the stage. Equations (2.1-3) are also the characteristic coefficients used in this analysis.

Since variations due to speed, operating temperature and geometry are accounted for by nondimensionalization of the performance parameters, all performance data for a stage should collapse into one curve. When this does not occur, the deviation of the data from a single curve is generally attributed to Reynolds number, stall and secondary loss effects. The deviation can also be due to changes in the blade geometry such as variable vanes. As this analysis is limited to pre-stall performance by assumption 3, stall and loss effects on the performance data are minimal when compared to the effect of changing blade geometry. Thus, deviations of the data from a single curve are assumed primarily due to changes in the blade angles, particularly changes in the upstream stator outlet angle (α_1).

2.3 Adjusting the Characteristic for Changes in IGV or Stator Angles

2.3.1 Basic Compressor Equations

Shown in Figure 2.1 are the various angles of the compressor stage that will be referenced in this derivation. The subscripts "1" and "2" denote the inlet and exit to the rotor, respectively; thus, absolute air angles inlet and outlet to the rotor are designated α_1 and α_2, respectively. The direction of the flow with respect to the rotor blade is given by β_1 and β_2. The deflection angle, ε, is equal to $\beta_1 - \beta_2$. This is the overall angle through which the rotor turns the flow. The outlet angles of the stage are the inlet angles to the next stage. Hence, α_3 for the first stage in a compressor is α_1 for the second stage.

The absolute inlet flow angle, α_1, is zero for the first stage unless an inlet guide vane (IGV) is present. The IGV turns the flow from a purely axial direction before it enters the compressor. C denotes the absolute velocity while V is the flow velocity relative to the rotor.

As seen by the velocity triangles, the inlet and outlet blade speeds, U_1 and U_2, and the flow's absolute axial velocities, C_{a1} and C_{a2}, are related to the flow angles by:

$$\frac{U_1}{C_{a1}} = \tan\alpha_1 + \tan\beta_1 \qquad (2.4)$$

$$\frac{U_2}{C_{a2}} = \tan\alpha_2 + \tan\beta_2 \qquad (2.5)$$

Using conservation of mass principles and assuming no bleed flow from the stage, the mass flow rates entering and exiting the rotor are equal and given by:

2-4

$$m_1 = m_2 \tag{2.6}$$

$$m_1 = \rho_1 C_{a1} A_1 \tag{2.7}$$

$$m_2 = \rho_2 C_{a2} A_2 \tag{2.8}$$

The power input to the stage due to a change in angular momentum is given by:

$$\dot{W} = m(U_2 C_{w2} - U_1 C_{w1}) \tag{2.9}$$

where C_{w1} and C_{w2} denote the inlet and outlet tangential velocities. The power input can also be determined by the difference in the stagnation temperature between the stage's inlet and outlet:

$$\dot{W} = m C_p \Delta T_{os} \tag{2.10}$$

where C_p is the specific heat of the gas taken as constant across the rotor.

Setting (2.9) and (2.10) equal and simplifying:

$$C_p \Delta T_{os} = (U_2 C_{w2} - U_1 C_{w1}) \tag{2.11}$$

Using (2.6-2.8) and the velocity triangles, the right hand side of (2.11) can be determined in terms of the mass flow. Starting with the velocity triangles:

$$C_{w1} = C_{a1} \tan \alpha_1 \tag{2.12}$$

$$C_{w2} = U_2 - C_{a2} \tan \beta_2 \tag{2.13}$$

Using (2.7-2.8):

$$C_{a1} = m_1 / \rho_1 A_1 \tag{2.14}$$

$$C_{a2} = m_2 / \rho_2 A_2 \tag{2.15}$$

Substituting the above into (2.12-2.13):

$$C_{w1} = m_1 \tan \alpha_1 / \rho_1 A_1 \qquad (2.16)$$

$$C_{w2} = U_2 - m_2 \tan \beta_2 / \rho_2 A_2 \qquad (2.17)$$

Substituting (2.16) and (2.17) into the right hand side of (2.11) and using conservation of mass:

$$C_p \Delta T_{os} = \left[U_2^2 - \frac{U_2 m \tan \beta_2}{\rho_2 A_2} - \frac{U_1 m \tan \alpha_1}{\rho_1 A_1} \right] \qquad (2.18)$$

Replacing the mass flow and the temperature change by Φ (2.1) and Ψ^T(2.2) we have an equation solely in terms of the flow and temperature coefficients:

$$\Psi^T = \left[\frac{U_2^2}{\left(2\pi \, Nr_m \right)^2} - \frac{U_2 \, A_m \Phi \tan \beta_2}{A_2 2\pi \, Nr_m} - \frac{U_1 A_m \Phi \tan \alpha_1}{A_1 2\pi \, Nr_m} \right] \qquad (2.19)$$

The above equation also assumes that the flow is essentially incompressible over the stage, i.e. $\rho_1 = \rho_2 = \rho_m$.

The temperature coefficient can be recast in terms of the flow angles using velocity triangles, conservation of mass, and the definition of the flow coefficient. Substituting (2.14) into (2.4) and solving for the mass flow:

$$m = \frac{\rho_1 A_1 U_1}{\tan \alpha_1 + \tan \beta_1} \qquad (2.20)$$

Dividing through by the mean radius and area and substituting $U_1 = 2\pi Nr_1$:

$$\frac{m}{A_m r_m} = \left(\frac{\rho_1 A_1 2\pi \, Nr_1}{\tan \alpha_1 + \tan \beta_1} \right) \frac{1}{A_m r_m} \qquad (2.21)$$

Dividing both sides by $2\pi N \rho_1$:

2-6

$$\frac{m}{\rho_1 A_m 2\pi \ N r_m} = \left(\frac{A_1 r_1}{\tan\alpha_1 + \tan\beta_1}\right)\frac{1}{A_m r_m} \qquad (2.22)$$

Substituting (2.22) into (2.1) and again assuming the flow across the stage is incompressible:

$$\Phi = \left(\frac{1}{\tan\alpha_1 + \tan\beta_1}\right)\frac{A_1 r_1}{A_m \ r_m} \qquad (2.23)$$

Substituting (2.23) into the right hand side of (2.19) results in:

$$\Psi^T = \left[\frac{U_2^2}{(2\pi \ Nr_m)^2} - \frac{U_2 A_1 r_1 \tan\beta_2}{A_2 2\pi \ N \ r_m^2(\tan\alpha_1 + \tan\beta_1)} - \frac{U_1 r_1 \tan\alpha_1}{2\pi \ N \ r_m^2(\tan\alpha_1 + \tan\beta_1)}\right] \qquad (2.24)$$

In the above equation, the explicit dependence on the flow coefficient has been removed. However, its effect is still present through the $\tan\alpha_1 + \tan\beta_1$ terms in the denominators.

The pressure coefficient is related to the temperature coefficient through the efficiency. For an ideal stage, the stage's pressure ratio can be calculated from the temperature ratio by:

$$\frac{P_{o2}}{P_{o1}} = \left(\frac{T_{o2}}{T_{o1}}\right)^{\frac{\gamma}{\gamma-1}} \qquad (2.25)$$

Putting (2.25) in terms of temperature and pressure changes:

$$\frac{\Delta P_{os}}{P_{o1}} + 1 = \left(\frac{\Delta T_{os}}{T_{o1}} + 1\right)^{\frac{\gamma}{\gamma-1}} \qquad (2.26)$$

Since there are losses in the compression process, not all of the temperature rise results in a rise in pressure. This is accounted for by the isentropic efficiency. Including the efficiency:

$$\frac{\Delta P_{os}}{P_{o1}} + 1 = \left(\frac{\eta \ \Delta T_{os}}{T_{o1}} + 1 \right)^{\frac{\gamma}{\gamma-1}}$$

(2.27)

Finally, putting the temperature and pressure changes in terms of Ψ^P (2.3) and Ψ^T (2.2) and using the ideal gas law:

$$\Psi^P = \frac{T_{o1} R}{(2\pi \ Nr_m)^2} \left\{ \left[1 + \frac{\eta \ \Psi^T (2\pi \ Nr_m)^2}{C_P T_{o1}} \right]^{\frac{\gamma}{\gamma-1}} - 1 \right\}$$

(2.28)

When determining the pressure coefficient, it will be initially assumed that the efficiency is constant over the whole range of flow coefficient. In the pre-stall case where the flow coefficient is close to the design point, the efficiency changes very little from the maximum. However, as seen in Figure 1.1, the efficiency changes dramatically as the flow coefficient moves away from the design point and into the off-design portion of the curve.

2.3.2 Changes in the Performance Coefficients

The basic equations describing the relationships between the performance coefficients are given in equations (2.23), (2.24) and (2.28) and account for rotor speed and geometry. The change in the performance coefficients due to a change in the IGV or stator outlet angle, α_1, can be determined from those equations. When determining the change in a multivariate function due to a change in its variables, the

2-8

differential can be used as an approximation of that change. Given a function $z = f(x,y)$, this can be mathematically stated as (Ref. 9):

$$\Delta z = \frac{\partial z}{\partial x} \Delta x + \frac{\partial z}{\partial y} \Delta y \qquad (2.29)$$

where $\partial z/\partial x$ and $\partial z/\partial y$ are the partial derivatives of z with respect to x and y respectively. This concept is used to determine the changes in the temperature and flow coefficients. For constant rotor speed and fixed geometry functional relationships of (2.24) and (2.23):

$$\Psi^T = f(\alpha_1, \beta_2) \qquad (2.30)$$

$$\Phi = f(\alpha_1, \beta_1) \qquad (2.31)$$

For ease in calculating the derivatives, both functions are put in terms of the same flow angles. Thus, the relationship:

$$\beta_2 = \beta_1 - \varepsilon \qquad (2.32)$$

is substituted in (2.30) to remove the β_2 dependence.

$$\Psi^T = f(\alpha_1, \beta_1, \varepsilon) \qquad (2.33)$$

In general, the change in temperature and flow coefficients due to a change in angles is:

$$\Delta \Psi^T = (\partial \Psi^T/\partial \alpha_1) \Delta \alpha_1 + (\partial \Psi^T/\partial \beta_1) \Delta \beta_1 + (\partial \Psi^T/\partial \varepsilon_1) \Delta \varepsilon \qquad (2.34)$$

$$\Delta \Phi = (\partial \Phi/\partial \alpha_1) \Delta \alpha_1 + (\partial \Phi/\partial \beta_1) \Delta \beta_1 \qquad (2.35)$$

When determining the changes in the flow and temperature coefficients, a change in the temperature coefficient will be computed along a line of constant flow coefficient, and a change in the flow coefficient will be computed along a line of

constant temperature coefficient. Thus, for the derivative of Ψ^T (2.24), Φ is kept constant. Similarly, Ψ^T is kept constant for the derivative of Φ (2.23). In either case, β_1 and ε depend only on α_1, and the functions in (2.30) and (2.31) can be cast in terms of the single variable, α_1. The changes in the performance coefficients due to a change in α_1 are then:

$$\Delta\Psi^T = (\partial\Psi^T/\partial\alpha_1)\,\Delta\alpha_1 \tag{2.36}$$

$$\Delta\Phi = (\partial\Phi/\partial\alpha_1)\,\Delta\alpha_1 \tag{2.37}$$

The change in $\Psi_P^{\,P}$ is related to the change in $\Psi_P^{\,T}$ and the efficiency by (2.28).

2.3.2.1 Change in the Temperature Coefficient for Constant Φ

Starting with (2.33) and expanding the partial derivative where the variables β_1 and ε are dependent upon α_1 (through the constant flow coefficient in (2.23)):

$$\partial\Psi^T/\partial\alpha_1 = \partial\Psi^T/\partial\alpha_1 + (\partial\Psi^T/\partial\beta_1)\,(\partial\beta_1/\partial\alpha_1) + (\partial\Psi^T/\partial\varepsilon)\,(\partial\varepsilon/\partial\beta_1)\,(\partial\beta_1/\partial\alpha_1) \tag{2.38}$$

Using (2.24):

$$\frac{\partial\,\Psi^T}{\partial\,\alpha_1} = \frac{r_1\sec^2\alpha_1}{2\pi\,Nr_m^2(\tan\alpha_1 + \tan\beta_1)^2}\left(\frac{U_2A_1}{A_2}\tan(\beta_1 - \varepsilon) - U_1\tan\beta_1\right) \tag{2.39}$$

$$\frac{\partial\,\Psi^T}{\partial\,\beta_1} = \frac{r_1}{2\pi\,Nr_m^2(\tan\alpha_1 + \tan\beta_1)^2}$$

$$\left(-\frac{U_2A_1}{A_2}(\sec^2(\beta_1 - \varepsilon)(\tan\alpha_1 + \tan\beta_1) - \tan(\beta_1 - \varepsilon)\sec^2\beta_1) + U_1\tan\alpha_1\sec^2\beta_1\right)$$

$$\tag{2.40}$$

$$\frac{\partial\,\Psi^T}{\partial\,\varepsilon} = \frac{U_2A_1r_1}{A_2\,2\pi\,Nr_m^2(\tan\alpha_1 + \tan\beta_1)}\left(\sec^2(\beta_1 - \varepsilon)\right) \tag{2.41}$$

In order to determine the changes in β_1 and ε with respect to α_1, the flow coefficient (2.23) is used. Solving (2.23) for β_1 and taking the derivative with respect to α_1 holding Φ constant:

$$\beta_1 = \operatorname{atan}((A_1 r_1 / A_m r_m \Phi) - \tan \alpha_1) \qquad (2.42)$$

$$\frac{\partial \beta_1}{\partial \alpha_1} = \frac{-\sec^2 \alpha_1}{1 + \left(\dfrac{A_1 r_1}{A_m r_m \Phi} - \tan \alpha_1\right)^2} \qquad (2.43)$$

The change in ε is functionally given by:

$$\partial \varepsilon / \partial \alpha_1 = (\partial \varepsilon / \partial \beta_1)(\partial \beta_1 / \partial \alpha_1) \qquad (2.44)$$

For two-dimensional and free vortex flow, it can be shown that the deflection angle, ε, is a function of only β_1. Thus, the first term in (2.44) is an ordinary derivative, $d\varepsilon/d\beta_1$. This derivative can be estimated using the approximately linear relationship between the incidence and deflection angles as shown in the pre-stall portion of the curve in Figure 2.2. The "*" values are fixed and denote a design point value for the cascade. The variable incidence is related to β_1 through the fixed blade angle, β_1', as follows:

$$i = \beta_1 - \beta' \qquad (2.45)$$

$$i^* = \beta_1^* - \beta_1' \qquad (2.46)$$

$$i - i^* = \beta_1 - \beta_1^* \qquad (2.47)$$

Taking the derivative of both sides:

$$d(i - i^*) = d\beta_1 \qquad (2.48)$$

$$d[\varepsilon/\varepsilon^*] \, /d[(i - i^*)/\varepsilon^*] = d\varepsilon/d\beta_1 \qquad (2.49)$$

The right hand side of (2.49) will be designated ε' throughout the rest of this paper and is a source term used in determining the changes in the temperature characteristic. Putting this all together:

$$\partial\varepsilon/\partial\alpha_1 = \varepsilon' \, (\partial\beta_1/\partial\alpha_1) \qquad (2.50)$$

For a constant ε', the above relationship is true only for the pre-stall case. As the stage moves into and past stall, the relationship between the deflection angle and the inlet flow angle is no longer linear. As seen in Figure 2.2, the slope of the deflection curve may be zero or negative as flow through the stage approaches and moves past stall.

2.3.2.2 Change in the Flow Coefficient for Constant Ψ^T

The change in the temperature coefficient due to a change in α_1 has been determined. The change in the flow coefficient along a line of constant temperature coefficient is derived similarly from (2.31) noting that β_1 depends on α_1 via (2.24) with Ψ^T constant.

$$\partial\Phi/\partial\alpha_1 = \partial\Phi/\partial\alpha_1 + (\partial\Phi/\partial\beta_1) \, (\partial\beta_1/\partial\alpha_1) \qquad (2.51)$$

Starting with (2.23) to get the partial derivatives of Φ with respect to the angles:

$$\frac{\partial \Phi}{\partial \alpha_1} = \left(\frac{-\sec^2 \alpha_1}{\left(\tan\alpha_1 + \tan\beta_1 \right)^2} \right) \frac{A_1 r_1}{A_m \, r_m} \qquad (2.52)$$

$$\frac{\partial \Phi}{\partial \beta_1} = \left(\frac{-\sec^2\beta_1}{(\tan\alpha_1 + \tan\beta_1)^2}\right)\frac{A_1 r_1}{A_m \ r_m} \tag{2.53}$$

In order to get $\partial\beta_1/\partial\alpha_1$, solve (2.24) for β_1 and take the derivative holding Ψ^T constant.

$$\tan\beta_1 = \frac{\left[\dfrac{U_2 A_1 r_1 \tan(\beta_1 - \varepsilon)}{A_2 2\pi \ N \ r_m^2} + \dfrac{U_1 r_1 \tan\alpha_1}{2\pi \ N \ r_m^2}\right]}{\dfrac{U_2^2}{(2\pi \ Nr_m)^2} - \Psi^T} \tag{2.54}$$

$$\frac{\partial \beta_1}{\partial \alpha_1} = \frac{\left[\dfrac{U_1 r_1}{2\pi \ N \ r_m^2\left(\dfrac{U_2^2}{(2\pi \ Nr_m)^2} - \Psi^T\right)} - 1\right]\sec^2\alpha_1}{\sec^2\beta_1 - \dfrac{(1-\varepsilon\,')U_2 A_1 r_1}{\left(\dfrac{U_2^2}{(2\pi \ Nr_m)^2} - \Psi^T\right)A_2 2\pi \ N \ r_m^2}\sec^2(\beta_1 - \varepsilon)} \tag{2.55}$$

2.3.3 Calculating the Reference Curve Angles

The previous sections demonstrate how an initial reference curve may be adjusted by a change in α_1. The reference curve is a general temperature characteristic used in determining the new temperature characteristic through the test flow and temperature coefficients (Φ_T, $\Psi_T{}^T$). Once the differences in geometry or flow angles between the reference curve and the test point have been calculated, the new temperature curve can be generated from the reference curve. The reference curve is based either on the temperature characteristic from the stage to be tested, other scaled models, or other compressor stages in the same compressor. The angles are

2-13

determined through a single reference data point, and the full curve is developed through iteration of ε' which will be discussed in section 3.3.3.

For evaluation of the partial derivatives in equations (2.39-41, 2.43, 2.50, 2.52-53, and 2.55), reference curve values are required for the determination of $\partial\Phi/\partial\alpha$ and $\partial\Psi/\partial\alpha$, and this involves knowing the angles (α_1, β_1, and ε) for the reference stage at the particular reference point which maps to the new curve. Not only do we want to determine the change in the stator outlet angle, $\Delta\alpha_1$, we need to know α_1 for the reference curve. α_1 is constant for the entire reference curve because it is assumed that the stator blade is fixed for a given rotor speed. However, on the reference characteristic, β_1 and ε will change with the flow coefficient, and they may be calculated using the reference curve performance points (Φ_R, Ψ_R^T) if α_1 is known for the reference curve. A method to determine an appropriate α_1 was devised based on common design principles of diffusion factor, degree of reaction, and relative inlet Mach number.

The diffusion factor (DF) is a measure of the blade loading, with common values ranging from 0.4-0.6. It is defined in Ref. 3 as follows:

$$DF = 1 - \frac{V_2}{V_1} + \frac{\Delta C_w}{2\sigma V_1} \tag{2.56}$$

where σ = solidity (chord length/spacing) and is assumed to be 1.2 for the three stages in this study; values below 1.2 significantly increase the diffusion factor beyond the general design limit of 0.6. From the velocity triangles in Figure 2.1, the relative velocities are given by:

2-14

$$V_1 = C_{a1}/\cos \beta_1 \qquad (2.57)$$

$$V_2 = C_{a2}/\cos \beta_2 \qquad (2.58)$$

Using the velocity triangles, the change in the tangential velocity is given by:

$$\Delta C_w = U_2 - C_{a2} \tan \beta_2 - U_1 + C_{a1} \tan \beta_1 \qquad (2.59)$$

Substituting (2.57-2.59) into (2.56):

$$DF = 1 - \frac{C_{a2}}{C_{a1}} \frac{\cos\beta_1}{\cos\beta_2} + \frac{\cos\beta_1}{2\sigma C_{a1}} \left(U_2 - U_1 - C_{a2} \tan\beta_2 + C_{a1} \tan\beta_1 \right) \qquad (2.60)$$

The axial velocities in terms of the mass flow rate are given by (2.14 and 2.15):

$$C_{a1} = m_1/\rho_1 A_1 \qquad (2.14)$$

$$C_{a2} = m_2/\rho_2 A_2 \qquad (2.15)$$

Substituting in the flow coefficient for the mass flow rate (2.1) and simplifying with the incompressible flow assumption:

$$C_{a1} = 2 \pi N r_m A_m \Phi/A_1 \qquad (2.61)$$

$$C_{a2} = 2 \pi N r_m A_m \Phi/A_2 \qquad (2.62)$$

The blade speeds, U_1 and U_2, can be determined by the radii, r_1 and r_2, and the rotor rotational speed, N:

$$U_1 = 2 \pi N r_1 \qquad (2.63)$$

$$U_2 = 2 \pi N r_2 \qquad (2.64)$$

Substituting (2.61-64) into (2.60) and simplifying:

$$DF = 1 - \frac{A_1}{A_2} \frac{\cos\beta_1}{\cos\beta_2} + \frac{A_1 \cos\beta_1}{2\sigma} \left(\frac{r_2 - r_1}{\Phi A_m r_m} + \frac{\tan\beta_1}{A_1} - \frac{\tan\beta_2}{A_2} \right) \qquad (2.65)$$

2-15

A second design parameter is the degree of reaction, Λ. It is a measure of the rotor's contribution to the overall static enthalpy rise of the stage. Typical on-design values range from 0.4-0.6 at the mean radius. It is defined in Ref. 3 as follows:

$$\Lambda = \Delta h_r / \Delta h_s \qquad (2.66)$$

where Δh is the change in the static enthalpy, the subscript r denotes the rotor and the subscript s denotes the stage. The enthalpy is related to the static temperature change by the specific heat of the fluid:

$$\Delta h = C_p \Delta T \qquad (2.67)$$

Substituting (2.67):

$$\Lambda = C_p \Delta T_r / C_p \Delta T_s \qquad (2.68)$$

The work input to the stage is given by the change in the stagnation temperature:

$$W = C_p \Delta T_{os} \qquad (2.69)$$

using (2.11-12) and the velocity triangles the work input is given by:

$$W = U_2 C_{a2} \tan \alpha_2 - U_1 C_{a1} \tan \alpha_1 \qquad (2.70)$$

Substituting in (2.61-62) for the axial velocities and simplifying:

$$W = \Phi 2\pi \, Nr_m A_m \left(\frac{U_2}{A_2} \tan \alpha_2 - \frac{U_1}{A_1} \tan \alpha_1 \right) \qquad (2.71)$$

The work can also be determined by the change in the static temperature across the rotor and the change in the absolute velocities, C_1 and C_2.

$$W = C_p \Delta T_r + (C_2{}^2 - C_1{}^2)/2 \qquad (2.72)$$

Setting (2.71) equal to (2.72) and solving for the enthalpy rise across the rotor:

$$C_p \Delta T_r = 2\pi \ Nr_m A_m \Phi \left(\frac{U_2}{A_2} \tan\alpha_2 - \frac{U_1}{A_1} \tan\alpha_1 \right) - \frac{1}{2}\left(C_2^2 - C_1^2 \right) \qquad (2.73)$$

Using the velocity triangles, the absolute velocities are given by:

$$C_1 = C_{a1} \sec \alpha_1 \qquad (2.74)$$

$$C_2 = C_{a2} \sec \alpha_2 \qquad (2.75)$$

Substituting in (2.61-62) for the axial velocities:

$$C_1 = 2 \ \pi Nr_m A_m \Phi \sec \alpha_1 / A_1 \qquad (2.76)$$

$$C_2 = 2 \ \pi Nr_m A_m \Phi \sec \alpha_2 / A_2 \qquad (2.77)$$

Substituting (2.76-77) into (2.73) and simplifying:

$$C_p \Delta T_r = 2\Phi\pi \ Nr_m A_m \left(\frac{U_2}{A_2} \tan\alpha_2 - \frac{U_1}{A_1} \tan\alpha_1 \right) - 2\left(\Phi\pi \ Nr_m A_m \right)^2 \left(\frac{\sec^2 \alpha_2}{A_2^2} - \frac{\sec^2 \alpha_1}{A_1^2} \right)$$
$$(2.78)$$

It is common for compressors to be designed such that the absolute velocity entering the stage is equal to the absolute velocity leaving the stage (Ref. 3). In this case, the stagnation temperature rise over the stage is equal to the static temperature rise over the stage. Thus,

$$C_p \Delta T_s = C_p \Delta T_{os} \qquad (2.79)$$

and substituting (2.71):

$$C_p \Delta T_s = \Phi 2\pi \ Nr_m A_m \left(\frac{U_2}{A_2} \tan\alpha_2 - \frac{U_1}{A_1} \tan\alpha_1 \right) \qquad (2.80)$$

Substituting (2.78) and (2.80) into (2.68) and simplifying:

$$\Lambda = 1 - \frac{\Phi\pi \, Nr_m A_m \left(\dfrac{\sec^2 \alpha_2}{A_2^2} - \dfrac{\sec^2 \alpha_1}{A_1^2} \right)}{\dfrac{U_2}{A_2}\tan\alpha_2 - \dfrac{U_1}{A_1}\tan\alpha_1} \tag{2.81}$$

The final design parameter is the relative Mach number at the tip, inlet to the rotor (M_{rel}). When looking at the distribution of the velocity along the rotor blade, hub to tip, the highest relative velocity is at the tip of the rotor blade. The relative Mach number at this point must be limited in order to limit the aerodynamic losses due to shock waves. Its value is generally limited to 1.1 - 1.2. The relative Mach number can be calculated as follows:

$$M_{rel} = V_{1t} / \sqrt{\gamma \, RT_1} \tag{2.82}$$

where V_{1t} is the relative tip velocity.

In order to determine an appropriate value for α_1, the diffusion factor, degree of reaction and relative Mach number are calculated for a range of α_1. The inlet absolute flow angle, α_1, is chosen such that the calculated design parameters (DF, Λ, and M_{rel}) fall into the acceptable ranges stated above.

Once α_1 for the reference curve is determined, the variation of β_1 and ε over the reference curve may be calculated. For a given reference curve data set, a primary reference point (Φ_R, Ψ_R^T) is selected from the data. For this analysis, the midpoint of the reference curve data set was selected. Using the primary reference point and α_1, a reference inlet flow angle is calculated from (2.42) as follows:

$$\beta_{1REF} = atan((A_1 r_1 / A_m r_m \Phi_R) - \tan\alpha_1) \tag{2.42}$$

2-18

Solving (2.24) for β_2 with the primary reference point gives the reference outlet flow angle:

$$\beta_{2REF} = a\tan\left\{\frac{2\pi\ Nr_m A_2}{U_2 \Phi_R A_m} * \left[\left(\frac{U_2}{2\pi\ Nr_m}\right)^2 - \Psi_R\right] - \frac{U_1 A_2}{U_2 A_1}\tan\ \alpha_z\right\} \qquad (2.83)$$

From the definition of the deflection angle, ε, the reference deflection angle is calculated as follows:

$$\varepsilon_{REF} = \beta_{1REF} - \beta_{2REF} \qquad (2.84)$$

The inlet flow angles for the rest of the curve are determined from the reference angles (β_{1REF}, ε_{REF}), α_1, and the reference curve flow coefficients using (2.42). The linear relationship between ε and β_1, derived in section 2.3.2.1, yields the deflection angle, given by:

$$\varepsilon = \varepsilon_{REF} + \varepsilon'\ (\beta_1 - \beta_{1\ REF}) \qquad (2.85)$$

Up to this point, the temperature coefficients, Ψ^T, have not been involved in the determination of the reference curve angles other than for β_{1REF} and ε_{REF}. In order to check the accuracy of the reference curve angles, the temperature coefficients related to these angles are calculated using (2.24). These calculated values are compared to reference curve data using the mean sum square of the errors as follows (Ref. 8):

$$MSE = \frac{\displaystyle\sum_{j=1,N}\left(\Psi_{Rj}{}^T - \Psi_{Cj}{}^T\right)^2}{N} \qquad (2.86)$$

where j denotes the data point, R denotes the value of Ψ^T from the reference data set, C denotes the calculated Ψ^T, and N is total number of data points. ε' is adjusted in order to minimize the MSE. This adjustment of ε' will be presented in section 3.3.3.

2.4 Solution Algorithms

The theory needed to solve the stage characteristic generation problem has been presented. The reference curve and test performance data have been nondimensionalized; the reference curve angles are known; and the theoretical relationships detailing the changes in the performance parameters from the reference curve due to a change in α_1 have been derived. The algorithm determining the adjustment parameters, $\Delta\alpha_1$ and (Φ_R, Ψ_R^T), between the performance point and the reference curve is covered below in section 2.4.1.1. Section 2.4.1.2 outlines the process to generate the new temperature and pressure curves given $\Delta\alpha_1$ and (Φ_R, Ψ_R^T).

2.4.1 Predicting the New Characteristics from One Performance Point

2.4.1.1 Determination of $\Delta\alpha_1$ and the Reference Curve Mapping Point(Φ_R, Ψ_R^T)

There are two unknowns involved in the prediction of the new characteristics -- the change in α_1 between the reference characteristic and the new characteristic and the point on the reference curve (Φ_R, Ψ_R^T) that maps to the given performance point. The determination of these values parameters requires an iterative approach. First, an initial (i.e., guessed) reference point is chosen by setting the reference flow coefficient,

Φ_R, equal to the test data flow coefficient, Φ_T. The reference temperature coefficient, Ψ_R^T, is already determined as a function of Φ_R. $\Delta\alpha_1$ is calculated using Ψ_R^T and the given temperature coefficient, Ψ_T^T. The calculated $\Delta\alpha_1$ is then checked by first calculating a new flow coefficient, Φ_{calc}, using $\Delta\alpha_1$ and the reference flow coefficient, Φ_R. Φ_{calc} is compared to Φ_R, and if the two values are not equal, new Φ_R and Ψ_R^T are chosen, and the iteration is repeated. The method of solution is outlined below:

1. Assume a reference point on the reference curve such that the flow coefficients of the reference (Φ_R) and test (Φ_T) points are equal.

$$\Phi_R = \Phi_T \qquad (2.87)$$

Calculate the angles (β_1 and ϵ) using (2.42) and (2.85) and the previously selected value of α_1. Calculate the reference temperature coefficient using the angles, (α_1, β_1, and ϵ), and Φ_R in (2.24)

2. Calculate $\Delta\Psi^T$.

$$\Delta\Psi^T = \Psi_T^T - \Psi_R^T \qquad (2.88)$$

3. Calculate $\partial\Psi^T/\partial\alpha_1$ along a line of constant flow coefficient using (2.38-41), (2.43) and (2.50).

4. Determine $\Delta\alpha_1$ approximating the differential as the ratio of the total differences.

$$\Delta\alpha_1 = \Delta\Psi^T/(\partial\Psi^T/\partial\alpha_1) \qquad (2.89)$$

5. Compute $\partial\Phi/\partial\alpha_1$ along a line of constant temperature coefficient using (2.51-53) and (2.55).

6. Calculate $\Delta\Phi$.

$$\Delta\Phi = (\partial\Phi/\partial\alpha_1)^*\Delta\alpha_1 \qquad (2.90)$$

7. Calculate Φ_{calc} that is associated with the choice of (Φ_R, Ψ_R^T) and the calculation of $\Delta\alpha_1$.

$$\Phi_{calc} = \Phi_R + \Delta\Phi \qquad (2.91)$$

8. If the proper reference point has been chosen, $\Phi_{calc} = \Phi_T$. Otherwise, check to see if the calculated and test flow coefficients agree to within a chosen tolerance.

$$\upsilon = \left|\frac{\Phi_T - \Phi_{calc}}{\Phi_T}\right| \le 0.0002 \qquad (2.92)$$

9. If υ is not within the specified tolerance, select another reference point and restart calculations at step 2. The selection of another reference point requires some explanation. If it is not chosen correctly, the iteration algorithm will diverge. The method used in choosing the new reference flow coefficient is commonly referred to as the "shooting method" (Ref. 15). The new Φ_R is determined by minimizing the error, ν, at each iteration step. Essentially, if the error and the selected Φ_R were to be plotted, the x-axis intercept for a straight line connecting the previous estimate and the current estimate would approximate a zero error as shown in Figure 2.3. The equation for the intercept point is as follows:

$$\Phi_R = \Phi_{R_{j-1}} - \upsilon_{j-1}\left(\frac{\Phi_{R_j} - \Phi_{R_{j-1}}}{\upsilon_j - \upsilon_{j-1}}\right) \qquad (2.93)$$

where j and j-1 refer to the current and previous iteration step respectively. It is evident that this iteration requires two previous guesses of the reference point before

the shooting method can be applied. The second value in the iteration is determined by setting that iteration's new reference point equal to the calculated flow coefficient from Step 7.

$$\Phi_{R(j=2)} = \Phi_{calc} \qquad (2.94)$$

10. After the iteration has converged, the efficiency for the test point is calculated by solving (2.28) for the efficiency:

$$\eta = \frac{T_{o\,1} C_P}{\Psi_T^T (2\pi\,Nr_m)^2} \left\{ \left[1 + \frac{\Psi_T^P (2\pi\,Nr_m)^2}{RT_{o\,1}} \right]^{\frac{\gamma-1}{\gamma}} - 1 \right\} \qquad (2.95)$$

2.4.1.2 Generating the New Curve

Once the change in α_1 and the reference mapping point are known, the new stage characteristics can be generated. The difference vector $(\Delta\Phi, \Delta\Psi^T)$ at each reference point is calculated and added vectorally to the reference point resulting in the new characteristic coefficients. The solution is as follows:

1. Starting at the leftmost point on the reference curve, the changes, $\Delta\Phi$ and $\Delta\Psi^T$, are calculated from (Φ_R, Ψ_R^T) using (2.38-41), (2.43), (2.50), (2.52-53) and (2.55).

$$\Delta\Phi = (\partial\Phi/\partial\alpha_1)*\Delta\alpha_1 \qquad (2.96)$$

$$\Delta\Psi^T = (\partial\Psi^T/\partial\alpha_1)*\Delta\alpha_1 \qquad (2.97)$$

2. The new flow, Φ_G, and temperature, Ψ_G^T, coefficients are determined from:

$$\Phi_G = \Phi_R + \Delta\Phi \qquad (2.98)$$

$$\Psi_G{}^T = \Psi_R{}^T + \Delta\Psi \qquad\qquad (2.99)$$

3. From the efficiency (2.95), the new temperature coefficient, $\Psi_G{}^T$, and (2.28) the new pressure coefficient, $\Psi_G{}^P$ are determined assuming that the efficiency is constant over the curve.

4. To complete the generation of the temperature and pressure curves, the calculations are repeated over the whole range of the reference curve flow coefficients.

2.4.2 Refinement of the New Characteristic Curves

2.4.2.1 Non-Linear Least Squares Estimation of New $\Delta\alpha_1$

Once a new stage characteristic has been generated, additional test data may be used to improve that estimate. This may be accomplished through a non-linear least squares estimation method developed in Ref. 14. What is basically involved is finding the value of $\Delta\alpha_1$ that minimizes the sum of the squared deviations of the data points from the values predicted by the algorithm.

During the one-point solution process described in section 2.4.1.1, we determined the value of $\Delta\alpha_1$ using the initial given data point. Once this was accomplished, the rest of the data on the curve was generated using the estimated $\Delta\alpha_1$ and the algorithm outlined in section 2.4.1.2. The new temperature coefficient curve may be functionally represented as follows:

$$\Psi_{j\,calc}{}^T = G(\Delta\alpha_1) \qquad\qquad (2.100)$$

where j denotes a particular data point and G represents the non-linear relationship between the calculated temperature coefficients, $\Psi_{calc}{}^T$, and $\Delta\alpha_1$, as given by the

algorithm outlined in section 2.4.1.2. Equation (2.100) is known as the observation relation (Ref. 14). In a non-linear least squares analysis, the observation relation must be linearized. If the initial test data point (Φ_T, $\Psi_T{}^T$) had been a perfect measurement, the iteration in section 2.4.1.1 would have yielded the true value of $\Delta\alpha_1$. True values are denoted by the subscript "o". Since this is not the case, set:

$$\Delta\alpha_1 = \Delta\alpha_{1o} + \delta\Delta\alpha_1 \tag{2.101}$$

where $\Delta\alpha_1$ is the iterated value, $\Delta\alpha_{1o}$ is the true value, and $\delta\Delta\alpha_1$ is some deviation from the true value. The true error vector is given by:

$$e = \Psi^T - \Psi_o{}^T \tag{2.102}$$

where Ψ^T and $\Psi_o{}^T$ are matrices containing the measured temperature coefficients and the true value of the temperature coefficients, respectively. The true values would be those obtained if an instrument with no measurement error were used to record the data. Replacing the temperature coefficients with the observation relation:

$$e = G(\Delta\alpha_1) - G(\Delta\alpha_{1o}) \tag{2.103}$$

Substituting in the value of $\Delta\alpha_1$ (2.101):

$$e = G(\Delta\alpha_{1o} + \delta\Delta\alpha_1) - G(\Delta\alpha_{1o}) \tag{2.104}$$

A Taylor series expansion of the first term on the right hand side yields:

$$e = G(\Delta\alpha_{1o}) + \left.\frac{\partial G}{\partial \Delta\alpha_{1o}}\right|_{\Delta\alpha_{1o}} \delta\Delta\alpha_1 - G(\Delta\alpha_{1o}) \tag{2.105}$$

or:

$$e \cong \left. \frac{\partial G}{\partial \Delta\alpha_{1o}} \right|_{\Delta\alpha_{1o}} \delta\Delta\alpha_1 \tag{2.106}$$

Equation (2.106) is the relationship between the true error in the matrix of the temperature coefficients Ψ^T and the error in $\Delta\alpha_1$. Since the true error can never really be obtained, it is approximated by the residual vector, which is the difference between the measured data and the estimate of that data calculated in section 2.4.1.2:

$$r = \Psi^T - \Psi_{calc}{}^T \tag{2.107}$$

Substituting in the observation relation (2.100) where $\Delta\alpha_1$ is the iterated value:

$$r = \Psi^T - G(\Delta\alpha_1) \tag{2.108}$$

The residual is approximately equal to the true error if the calculated $\Delta\alpha_1$ is nearly equal to $\Delta\alpha_{1o}$, or $\delta\Delta\alpha_1$ is small. Linearizing the error by setting E equal to the difference between the residual and the true error and replacing the true error with (2.106):

$$E = r - \left. \frac{\partial G}{\partial \Delta\alpha_1} \right|_{\Delta\alpha_{1o}} \delta\Delta\alpha_1 \tag{2.109}$$

Defining $H \equiv \left. \dfrac{\partial G}{\partial \Delta\alpha_1} \right|_{\Delta\alpha_{1o}}$:

$$E = r - H \, \delta\Delta\alpha_1 \tag{2.110}$$

From gaussian error statistics, the probability of obtaining a particular data set is given by:

$$P = (2\pi)^{-N^*/2} |Q|^{-1/2} \exp(-\frac{1}{2}S) \tag{2.111}$$

2-26

where P is the probability of obtaining the data set, N^* is the number of data points, Q is the instrumental covariance matrix (the error in the data due to the measuring instrument), and S is a scalar quantity. For non-linear estimation:

$$S = E^T Q^{-1} E \qquad (2.112)$$

Here the superscript "T" refers to the transpose of the matrix and "-1" refers to the inverse of a matrix. Substituting in (2.110)

$$S = (r^T - H \, \delta\Delta\alpha_1)^T Q^{-1} (r^T - H \, \delta\Delta\alpha_1) \qquad (2.113)$$

Multiplying out the matrix quantity:

$$S = r^T Q^{-1} r - r^T Q^{-1} H \, \delta\Delta\alpha_1 + (\delta\Delta\alpha_1^T H^T Q^{-1} H)^T + H^T Q^{-1} H \, \delta\Delta\alpha_1 \quad (2.114)$$

Using the Principle of Maximum Likelihood (Ref. 14), the most probable data set is obtained when (2.111) is at a maximum. This is determined by taking the derivative of S (2.114) with respect to the estimated $\Delta\alpha_1$ and setting it equal to zero:[1]

$$\partial S / \partial(\delta\Delta\alpha_1) = -(r^T Q^{-1} H)^T - H^T Q^{-1} r + (\delta\Delta\alpha_1^T H^T Q^{-1} H)^T + H^T Q^{-1} H \, \delta\Delta\alpha_1 = 0$$

$$(2.115)$$

Simplifying:

$$-2 H^T Q^{-1} r + 2 H^T Q^{-1} H \, \delta\Delta\alpha_1 = 0 \qquad (2.116)$$

Which gives the change in the calculated $\delta\Delta\alpha_1$

$$\delta\Delta\alpha_1 = (H^T Q^{-1} H)^{-1} H^T Q^{-1} r \qquad (2.117)$$

---

1 The gradient of an inner product obeys the identity:

$$\frac{\partial}{\partial x}(a^T x) = \frac{\partial}{\partial x}(x^T a) = a$$

where a is a constant with respect to x.

The new value of $\Delta\alpha_1$ which minimizes the error between the estimated and measured temperature coefficients is given by:

$$\Delta\alpha_{1new} = \Delta\alpha_1 + \delta\Delta\alpha_1 \qquad (2.118)$$

2.4.2.2 Updating the Temperature Characteristics with the New $\Delta\alpha_1$

At this point, the $\Delta\alpha_1$ used in calculating the temperature curve has been computed. The temperature characteristic using one performance point has been generated. As additional test data on the new curve are acquired, they are integrated into a new estimate of $\Delta\alpha_1$, and the temperature characteristic is updated. It has been assumed that the best fit is attained through adjusting the originally calculated $\Delta\alpha_1$ by minimizing the errors between the estimated and actual Ψ^T values. The theory for obtaining the change in $\Delta\alpha_1$ was outlined in the previous section. The implementation of that theory is as follows:

For each test data point (Φ_j, Ψ_j^T)

1. Calculate the estimated $\Psi_{j\,est}^T$ using the acquired Φ_j and the algorithm described in 2.4.1.2.

2. Compare the predicted $\Psi_{j\,est}^T$ values with the actual Ψ_j^T data by calculating the residuals:

$$r_j = \Psi_j^T - \Psi_{j\,est}^T \qquad (2.119)$$

3. Numerically estimate $H_j = \partial G/\partial(\Delta\alpha_1)$ by incrementing $\Delta\alpha_1$ by some small value κ and re-calculating $\Psi_{j\,est2}^T$ using the algorithm in 2.4.1.2.

$$H_j \cong (\Psi_{j\,est2}^T - \Psi_{j\,est}^T)/\kappa \qquad (2.120)$$

2-28

4. Determine the new $\Delta\alpha_1$ using (2.117) and (2.118), calculating the matrices as a running sum.

$$\delta\Delta\alpha_1 = \frac{\sum \dfrac{H_j r_j}{Q}}{\sum \dfrac{H_j^2}{Q}} \qquad (2.121)$$

When calculated as a running sum, the instrumental covariance matrix, Q, cancels out of Equation (2.121) resulting in:

$$\delta\alpha_1 = \sum (H_j \, r_j) \, / \sum (H_j)^2 \qquad (2.122)$$

5. Calculate the change in $\Delta\alpha_1$ using (2.118). Check the convergence of the algorithm, by comparing $\Delta\alpha_{1\,new}$ to the previous $\Delta\alpha_1$.

$$\left| \frac{\Delta\alpha_{1new} - \Delta\alpha_1}{\Delta\alpha_1} \right| \leq \varsigma \qquad (2.123)$$

If they are not equal within some tolerance, ς, redo calculations starting at Step 1 by setting $\Delta\alpha_1 = \Delta\alpha_{1new}$.

2.4.2.3 Determining the Updated Pressure Characteristic for Additional Data

The pressure and temperature curves are related by the efficiency (η) of the stage as seen in (2.28). In general, η is not a constant over the possible range of flow coefficients. Given a curve representing η as a function of Φ, it is generally parabolic as seen in Figure 1.1. If additional points are available, an alternate, more accurate, method to estimate the pressure curve may be used. Once the temperature characteristic has been modified with additional data to minimize the error between the

data and the estimate of the data, the efficiency model can also be modified. The temperature curve can be updated with as little as two points; however, a minimum of three points are required to determine a parabolic efficiency model.

The efficiency is computed for the additional points using (2.95), and a parabola of negative curvature is fit through the calculated data. The least squares curve fitting algorithm in Ref. 11 is commonly used to curve fit parabolic data. However, least squares does not necessarily determine a parabola of negative curvature, particularly for data with experimental scatter. With the efficiency model, the pressure curve can be updated using (2.28) with Φ and Ψ^T.

In order to understand how the efficiency model was developed, a brief overview of parabolic equations will be presented. Any parabola, as shown in Figure 2.4, may be described by:

$$y = A\,x^2 + B\,x + C \qquad\qquad (2.124)$$

where A, B, and C are constants. The slope of the parabola at some point is given by:

$$dy/dx = 2\,A\,x + B \qquad\qquad (2.125)$$

For negative curvature, at the maximum y on the curve, $dy/dx = 0$. This location on the x-axis is denoted x_o.

$$2\,A\,x_o + B = 0 \qquad\qquad (2.126)$$

Solving for B:

$$B = -2\,A\,x_o \qquad\qquad (2.127)$$

At two points on the curve, the slope may be linearly approximated if the points are sufficiently close:

2-30

$$m = (y_2 - y_1)/(x_2 - x_1) \qquad (2.128)$$

The subscripted values in this case represent values of η and Φ determined from two test data points. Setting (2.125) equal to (2.128):

$$2 A x + B = m \qquad (2.129)$$

Substituting in (2.127) for B and solving for A.

$$A = m/(2 (x - x_o)) \qquad (2.130)$$

Thus if x_o and m are known, A and B are immediately determined. Given some data set, x_o occurs at the maximum value of y.

The slope, m, in (2.130) is determined by examining the slopes to the left and the right of x_o. If there is scatter in the data, the calculated slopes may not have the proper sign. In Figure 2.5, the third slope is negative when it should be positive. By searching through the calculated slopes, the median slope of correct sign is used to calculate A in order to avoid zero or infinite slopes. B is determined by (2.127). With A and B calculated, C is determined from the value that minimizes the error between the data points (η_j) and the values predicted by the parabolic curvefit. This value, C, is computed using non-linear least squares.

The curvefit algorithm just described is outlined below:

1. Calculate the efficiency for the additional data points using (2.95).

$$\eta_j = \frac{T_{o\,1} C_P}{\Psi_j^T (2\pi\, Nr_m)^2} \left\{ \left[1 + \frac{\Psi_j^P (2\pi\, Nr_m)^2}{RT_{o\,1}} \right]^{\frac{\gamma-1}{\gamma}} - 1 \right\} \qquad (2.131)$$

2. Given the data (Φ, η) points, determine the straight line slope between them:

$$m_j = (\eta_{j+1} - \eta_j)/(\Phi_{j+1} - \Phi_j) \qquad (2.132)$$

3. Determine the flow coefficient corresponding to the maximum efficiency, Φ_o, by checking the calculated efficiencies for the maximum value. The associated flow coefficient is set equal to Φ_o.

$$\eta_{max} = max(\eta_1, \eta_2, \eta_3, \ldots \eta_j, \ldots \eta_N) \qquad (2.133)$$

$$\eta_{max} = f(\Phi_o) \qquad (2.134)$$

4. Determine the slope, m_A, used to calculate A. First, check the signs of the slopes to the left and right of Φ_o to be sure they are positive and negative, respectively. Second, remove the slopes from further examination if they are not of the correct sign. Third, select m_A from the remaining slope values by choosing the median value.

$$m_A = median(m_1, m_2, m_3, \ldots m_j, \ldots m_N) \qquad (2.135)$$

5. Given m_A, the corresponding flow coefficient, Φ_A, and Φ_o, calculate A and B.

$$A = m_A/(2(\Phi_A - \Phi_o)) \qquad (2.136)$$

$$B = -2\,A\,\Phi_o \qquad (2.137)$$

6. Calculate the first approximation for C.

$$C = \eta_1 - A\,\Phi_1^2 - B\,\Phi_1 \qquad (2.138)$$

7. Calculate the estimated efficiencies.

$$\eta_j = A\,\Phi_j^2 + B\,\Phi_j + C \qquad (2.139)$$

8. Calculate the residuals between the estimated values and the actual values:

$$r_j = \eta_{jact} - \eta_j \qquad (2.140)$$

9. Estimate H_j for each point by incrementing C by some small value ξ and evaluating the efficiency, η_{j2} at that point using (2.139).

$$H_j \cong (\eta_{j2} - \eta_j)/\xi \qquad (2.141)$$

10. Determine the change in C and its new value:

$$\delta C = \Sigma (H_j \ r_j) /\Sigma (H_j)^2 \qquad (2.142)$$

$$C_{new} = C_{old} + \delta C \qquad (2.143)$$

11. Check the value of C_{new} against the old value to see if C has converged within some tolerance μ.

$$\left| \frac{C_{new} - C_{old}}{C_{old}} \right| \leq \mu \qquad (2.144)$$

12. If the iteration has not converged, go to Step 6 and repeat the calculations.

As more pressure rise data is acquired, C is further adjusted to minimize the errors. With a new efficiency model determined and the temperature curve, the updated pressure characteristic can be determined using (2.28).

III. DATA ANALYSIS

3.1 Description of Validation Data Set

The data used to validate the characteristic curve generation algorithm was obtained from the DYNTECC testcase data files. Partial listings of the data may be found in Ref. 13. The testcase data file is from the three stage High-Stage Loading/Low Aspect Ratio Compressor (HSL/LARC) described in Ref. 1. The file contains mass flow rate, pressure ratio, and temperature ratio data for each of the three stages and seven rotor speeds. The rotor speeds are designated 1 through 7 in the following order: 100, 95, 90, 80, 70, 60, and 50 % of design speed (227 rps). Figures 3.1-3.6 show the given characteristic curve data for stages 1-3. The flow, temperature and pressure coefficients shown in these figures are defined according to:

$$\Phi_D = \frac{m\sqrt{T_{o1}/T_{oref}}}{P_{o1}/P_{oref}} * NRcor \tag{3.1}$$

$$\Psi_D^T = \left(\frac{T_{o2}}{T_{o1}} - 1\right) * NRcor^2 \tag{3.2}$$

$$\Psi_D^P = \left(\frac{P_{o2}}{P_{o1}} - 1\right) * NRcor^2 \tag{3.3}$$

where the subscript "D" denotes DYNTECC data, T_{oref} and P_{oref} are the reference total temperature and pressure at sea level standard, and NRcor = (Design Speed/Actual Speed)/$(T_{o1}/T_{oref})^{1/2}$. As seen in Figures 3.1-6, Stages 1-2 exhibit orderly pressure and

temperature curves. The data for Stage 3 are more scattered which is problematic for a prediction scheme that uses a smooth, continuous reference curve to generate new characteristics.

3.2 Transformation to Classical Definition

The flow coefficient given in (3.1) is dimensional with units of lbm/s. The temperature and pressure data in (3.2) and (3.3), however, are nondimensional but have not been scaled for speed and stage geometry. Therefore, each data point was transformed to the coefficients defined in Chapter 2 (2.1-3) resulting in:

$$\Phi = \frac{\Phi_D \dfrac{P_{o1}}{P_{oref}}}{2\rho_m A_m \, N \, r_m \, \pi \, NRcor \sqrt{\dfrac{T_{o1}}{T_{oref}}}} \qquad (3.4)$$

$$\Psi^T = \frac{C_p \, T_{o1} \, \Psi_D^T}{NRcor^2 (2\pi \, N \, r_m)^2} \qquad (3.5)$$

$$\Psi^P = \frac{R \, T_{o1} \, \Psi_D^P}{NRcor^2 (2\pi \, N \, r_m)^2} \qquad (3.6)$$

where R is the Universal Gas Constant for air. Figures 3.7-3.12 show the shift in characteristic curves from Figures 3.1-3.6 when transformed to the classical definitions of (3.4-6).

3.3 Analysis and Determination of the Reference Curve

Before the curve generation method may be executed, an appropriate reference curve must be identified. The angles associated with that curve, α_1, $\beta_1(\Phi)$, and $\varepsilon(\Phi)$, must

be determined (if not already known from a measurement of the reference stage angles) in order to calculate the partial derivatives needed to generate the new temperature characteristic. α_1 may be determined from design principles as demonstrated in section 2.3.3. Once α_1 is known, β_1 can be calculated from the flow coefficient and ε (a linear function of β_1) as given in (2.42) and (2.85).

3.3.1 Selection of the Reference Curves

For this study, the speed 3 characteristics were selected as reference curves for each stage because of their continuous, smooth nature and the fact that the data were in a pre-stall region. (The curve generation algorithm is based on pre-stall theory and assumptions.) Since the characteristic data were obtained from DYNTECC testcase input files, blade angle data were unavailable as was the gas angle, α_1. The determination of an appropriate α_1 was accomplished in accordance with section 2.3.3. The results of that analysis are presented in the next section.

3.3.2 Determination of α_1 for the Reference Curve

A method to select appropriate values of α_1 for the reference curves was based on an analysis of the diffusion factor (DF), degree of reaction (Λ), and relative inlet Mach number (M_{rel}). (Recall that common values for DF are 0.4-0.6, 0.4-0.6 for Λ, and 1.1-1.2 for M_{rel}.) Figures 3.13-15 show values of DF, Λ, and M_{rel} for a range of α_1's for the three reference curves, respectively. In Figure 3.13, for most values of α_1 below 40 degrees, the diffusion factor is fairly constant and on the high end of that commonly seen, 0.583 -

0.605. Reference curve 2 (Figure 3.14) shows diffusion factors of 0.560-0.575. As for the third curve (Figure 3.15), the diffusion factor ranges from 0.534-0.567.

The degree of reaction for all three curves is within reasonable design limits for α_1 values less than 30 degrees; M_{rel}, however, is low for higher values of α_1. In choosing α_1, larger angles, above 60 degrees for all three reference curves, are improbable because of a negative degree of reaction. The most probable values for α_1 lie at the low end where M_{rel} is near unity and degree of reaction is roughly 0.5. For example, for α_1 equal to 10 degrees, $\Lambda = 0.47$, and $M_{rel} = 1.03$ for curve 1. For reference curve 2, $\Lambda = 0.5$, and $M_{rel} = 0.975$. For reference curve 3, $\Lambda = 0.534$, and $M_{rel} = 0.945$. With an appropriate value of α_1 established (10 degrees for all curves), the reference curve angles, β_1 and ε, with an assumed value of ε', are calculated using the method outlined in section 2.3.3. The value of ε', however, must be iterated, as mentioned in section 2.3.3, in order to establish a good curvefit. This is discussed next.

3.3.3 Fitting a Reference Curve to Stage Data through Iteration of ε'

The curvefit algorithm is highly dependent upon the validity of the reference curve. As discussed in section 2.3.3, the development of the reference characteristic requires an iteration of ε'. A parabolic fit (obtained using PACFIT) was available, but it was not always in accord with the physics involved in stage characteristics. In the course of determining the reference curve angles, as discussed in the previous section, the temperature coefficients associated with those angles were also calculated and these provided a means to secure a good curvefit through the data. To achieve a best fit for the

reference curve data (Φ_R, Ψ_R^T), ε' was used as a source term and adjusted to minimize the deviation between the calculated and given stage temperature data as follows:

For each reference curve data point:

1. Calculate the estimated $\Psi_{j\,est}^T$ using the given Φ_j, the calculated angles, β_1 and ε, a guessed ε', and (2.24).

2. Compare the estimated $\Psi_{j\,est}^T$ values with the given Ψ_j^T data by calculating the residuals:

$$r_j = \Psi_j^T - \Psi_{j\,est}^T \tag{2.119}$$

3. Calculate $H_j = \partial G / \partial(\varepsilon')$. For this case the observation relation, G, is equal to Ψ^T given in (2.19). And since

$$\beta_2 = \beta_1 - (\varepsilon_{REF} + \varepsilon'\,(\beta_1 - \beta_{1REF})) \tag{3.7}$$

Then

$$G = \frac{U_2^2}{\left(2\pi\,Nr_m\right)^2} - \frac{U_2 A_m \Phi \tan\left[\beta_1 - \varepsilon_{REF} - \varepsilon'(\beta_1 - \beta_{1REF})\right]}{A_2\,2\pi Nr_m} - \frac{U_1 A_m \Phi \tan\alpha_1}{A_1\,2\pi\,Nr_m} \tag{3.8}$$

The derivative of G with respect to ε', H, is given by:

$$H_j = \frac{\Phi_j A_m U_2}{2\pi Nr_m A_2}(\beta_1 - \beta_{1REF})\sec^2\left[\beta_1 - \varepsilon_{REF} - \varepsilon'(\beta_1 - \beta_{1REF})\right] \tag{3.9}$$

4. Determine the change in ε' as a running sum.

$$\delta\varepsilon' = \Sigma\,(H_j\,r_j)\,/\Sigma\,(H_j)^2 \tag{3.10}$$

5. Calculate the new ε' as follows:

$$\varepsilon'_{new} = \varepsilon' + \delta\varepsilon' \tag{3.11}$$

6. Check the convergence of the algorithm, by comparing ε'_{new} to the previous ε'.

$$\left| \frac{\varepsilon'_{new} - \varepsilon'}{\varepsilon'} \right| \leq \tau \tag{3.12}$$

If the error is not smaller than τ, redo calculations starting at Step 1 by setting $\varepsilon' = \varepsilon'_{new}$. The minimum error for reference curve 1 was achieved when $\varepsilon' = 3.205$. For curve 2, $\varepsilon' = 3.072$. For curve 3, the algorithm did not converge properly because the stage data were near stall. For this case, a value of ε' equal to 1.0 gave the minimum error and negative curvature of the reference curve. (Values of ε' less than 1 resulted in a parabolic curve of positive curvature, opposite to that required of pre-stall characteristics.) Note that since ε' does not occur in the formulations of Φ_R and Ψ_R^T, DF, Λ and M_{rel} are not affected.

Figures 3.16-18 show a comparison between the parabolic curvefits determined from PACFIT and the reference curves developed using the physics-based approach. The pre-stall portions of the new reference curves extend beyond the parabolic curves. For reference curve 1 (Figure 3.16), the line matches the data and does not indicate a definite stall like that of the parabolic fit. Curve 2 (Figure 3.17) is similar in shape. The curve 3 (Figure 3.18) fit is not as good as the fit given by PACFIT. The data for curve 3 are near the stall region, and since the new fit method assumes pre-stall with constant ε', the fit temperature coefficients do not capture the curvature as well.

IV. <u>RESULTS AND DISCUSSION</u>

4.1 Validation of Stage Characteristic Generation Algorithm

This chapter presents the analyses of the stage characteristic generation algorithms. The data that were used as inputs to the algorithms were taken from the DYNTECC testcase input files. For the one-point generation algorithm in section 2.4.1, a point was arbitrarily selected from the data set to simulate results from an in-progress compressor test. For the non-linear least squares algorithm in section 2.4.2, additional data required for the algorithm were also taken from the DYNTECC testcase data set. The following items were accomplished in validating the characteristic prediction algorithm:

1. New stage characteristics were predicted using a reference curve from the same stage and one data point.

2. Characteristics for stages 2 and 3 were predicted using reference curve 1 and the one-point algorithm.

3. The assumed value of α_1 (determined in section 3.3.2) was varied to check the sensitivity of the curve generation method to α_1.

4. Different data points (from the DYNTECC testcase data set) were input to the one-point algorithm in order to study changes in the generated stage characteristics.

5. Additional data points, using the algorithm of section 2.4.2, were used to improve the initial curve prediction generated using the one-point algorithm.

A summary of the results for each of these items is given in the summary section at the end of the chapter.

4-1

For each generated stage characteristic, the generated curves were compared to the given data (from the DYNTECC testcase data files) by calculating the square root of the mean sum-squared-deviation of the predicted performance coefficients from the given performance coefficients:

$$\sigma^T = \frac{1}{N}\sqrt{\sum_{j=1,N} \frac{\left(\Psi_{Tj}^{\ T} - \Psi_{Gj}^{\ T}\right)^2}{\left(\Psi_{Tj}^{\ T}\right)^2}} \qquad (4.1)$$

$$\sigma^P = \frac{1}{N}\sqrt{\sum_{j=1,N} \frac{\left(\Psi_{Tj}^{\ P} - \Psi_{Gj}^{\ P}\right)^2}{\left(\Psi_{Tj}^{\ P}\right)^2}} \qquad (4.2)$$

where the subscript "j" denotes the data point index, subscript G's denote values from the generated curve, subscript T's denote testcase data, N is the total number of data points, σ^T is the deviation for the temperature coefficients and σ^P is the deviation for the pressure coefficients. Values of σ^T and σ^P below 1.6 e-2 indicate that the generated curves represent the test data accurately. For the one-point generation algorithm, in order to avoid misrepresenting the goodness of the fit, the input data point was removed from the error calculations, σ^T and σ^P, since the error at that point would be zero. (The algorithm forces the generated curve to go through the input data point.)

The tables in this chapter summarize the results of the analyses. The tabulated values of Φ_R and Ψ_R^T are those points on the reference curve that transform to the tabulated test data points (Φ_T, Ψ_T^T) for an iterated $\Delta\alpha_1$. The tables also list the estimated change in the stator outlet angle from the reference curve to the predicted curve, $\Delta\alpha_1$, and the errors in the generated curves, σ^T (4.1) and σ^P (4.2).

4.2 Characteristics Generated for the Same Stage with One Data Point (Φ, Ψ^T, Ψ^P)

This section presents the results of the one-point generation method. For this case, the reference curves and the new data at a different speed are from the same stage. For example, reference curve 1 (the stage characteristic for Stage 1/Speed 3) is used to generate the temperature and pressure curves for the other stage 1 speeds, 1, 2, 4, 5, 6 and 7. Only a single test data point was input to the generation algorithm outlined in section 2.4.1.

Figures 4.1-4.6 show the results of same-stage, one-point predictions for the three stages running at rotor speeds 2, 4, 5 and 7 (95, 80, 70, and 50% design speed). (Speeds 1 and 6 are not shown in order to improve the figures' clarity.) The broken lines are the generated characteristics. The symbols represent data points taken from the DYNTECC testcase data files for the HSL/LARC compressor (Ref. 13). The thick solid lines shown on the temperature figures (Figures 4.1, 4.3, and 4.5) are the reference curves. A discussion for each stage follows.

4.2.1 Characteristics for Stage 1 Generated with Reference Curve 1

Figures 4.1 and 4.2 display the results of using reference curve 1 to generate four of the first stage's temperature and pressure characteristics. Table 4.1 is a summary of six computational results. In Figure 4.1, most of the data points fall on the generated temperature characteristics. There is some deviation at the left end of the speed 7 (50% of design speed) data set which is in the stall regime. In Table 4.1, σ^T for the speed 7 data is larger than any of the other speed line errors.

Table 4.1: Summary of Results for Stage 1

Speed Line	Φ_T	Ψ_T^{T}	Mapped Φ_R	Mapped Ψ_R^{T}	$\Delta\alpha_1$ (degrees)	Error σ^T	Error σ^P
1	0.5153	0.7266	0.4377	0.6518	-11.18	5.843 e-3	5.360 e-3
2	0.4834	0.6890	0.4385	0.6500	-6.453	2.053 e-3	7.894 e-3
4	0.3723	0.5918	0.4387	0.6495	9.547	5.908 e-3	1.567 e-2
5	0.3160	0.4267	0.4668	0.5741	22.93	7.310 e-3	9.942 e-3
6	0.3101	0.4995	0.4490	0.6247	20.27	8.111 e-3	9.777 e-3
7	0.3035	0.5267	0.4401	0.6461	19.70	1.646 e-2	4.845 e-2

Also of interest in Table 4.1 is the change in the stator outlet angle, $\Delta\alpha_1$. Speed data above the reference curve speed line (Speed 3, or 90% design speed) show a decrease in α_1 while speeds below the reference show an increase in α_1. This is in accord with the theory used in this analysis. The ideal equation for Ψ^T as a function of Φ (Ref. 3) is:

$$\Psi^T = 1 - \Phi(\tan\alpha_1 + \tan\beta_2) \qquad (4.3)$$

where for the ideal case, β_2 is constant over the entire flow coefficient range. It is evident that for fixed Φ, an increase in α_1 decreases the temperature coefficient.

In Table 4.1, the pressure errors, σ^P, are larger than the temperature error values, visually observable in Figure 4.2, where the discrepancy between test data and generated curves is apparent. Speed 7 has the largest deviation as is expected due to imminent stall. The speed 4 data also deviate from the generated curve; but in this case, the data are not

approaching stall and the deviation is more likely due to the constant efficiency assumption. In order to improve the generated pressure characteristic, a variable efficiency model is required, as will be discussed in section 4.6.

4.2.2 Characteristics for Stage 2 Generated with Reference Curve 2

In Figure 4.3, the data for speeds 4, 5 and 7 deviate from the generated temperature characteristic due to stall effects. Likewise, the deflection angle, ε, is no longer a linear function of β_1, as can be inferred from cascade results, particularly as seen on the right side of Figure 2.2. The visual discrepancy is quantified in Table 4.2 which shows an increase in the σ^T errors, particularly for speeds 5 and 7.

Table 4.2: <u>Summary of Results for Stage 2</u>

Speed Line	Φ_T	Ψ_T^T	Mapped Φ_R	Mapped Ψ_R^T	$\Delta\alpha_1$ (degrees)	Error σ^T	Error σ^P
1	0.4119	0.6460	0.3807	0.6114	-6.784	5.985 e-3	2.504 e-2
2	0.4019	0.6315	0.3817	0.6090	-4.404	4.744 e-3	1.120 e-2
4	0.3702	0.5929	0.3826	0.6067	2.695	1.402 e-2	2.116 e-2
5	0.3645	0.5443	0.3935	0.5779	6.376	2.057 e-2	3.185 e-2
6	0.3652	0.5682	0.3876	0.5936	4.899	2.869 e-2	1.494 e-2
7	0.3481	0.5837	0.3785	0.6712	6.598	5.019 e-2	6.135 e-2

Since Ψ^P is dependent upon Ψ^T, errors in the temperature curves will be propagated into the generated pressure characteristics, as is apparent for speeds 5 and 7 in

Figure 4.4. As for speeds 2 and 4, in Figure 4.4, the pressure curve deviations are due to the assumption of constant efficiency required when only one data point has been acquired.

4.2.3 Characteristics for Stage 3 Generated with Reference Curve 3

Stage 3's generated temperature characteristics, seen in Figure 4.5, were poor compared to the curves generated for stages 1 and 2 (Figures 4.1 and 4.3). Practically all of the data shown here are in the stall region except for a portion of the data for speed 4 where the fitted curve predicts well the pre-stall portion of the data set. The pressure curves for stage 3, shown in Figure 4.6, are also not very accurate, again due to the proximity of the data to stall. In Table 4.3, most of the $\Delta\alpha_1$'s are negative because the input data points lie above the reference curve.

Table 4.3: <u>Summary of Results for Stage 3</u>

Speed Line	Φ_T	Ψ_T^T	Mapped Φ_R	Mapped Ψ_R^T	$\Delta\alpha_1$ (degrees)	Error σ^T	Error σ^P
1	0.3649	0.5392	0.3620	0.5354	-0.7562	9.895 e-3	4.707 e-2
2	0.3597	0.5423	0.3583	0.5404	-0.3710	9.840 e-3	4.719 e-2
4	0.3824	0.4848	0.3911	0.4960	2.101	1.058 e-2	3.924 e-2
5	0.4000	0.5122	0.3893	0.4984	-2.590	1.823 e-2	2.352 e-2
6	0.4313	0.5230	0.4005	0.4832	-7.277	1.892 e-2	2.210 e-2
7	0.4315	0.5263	0.3994	0.4847	-7.620	2.798 e-2	3.068 e-2

4.3 Predicting Stage Characteristics for Stages 2 and 3 using Reference Curve 1

In this section, the temperature and pressure characteristics for stages 2 and 3 are shown for the performance point (Φ_T, Ψ_T^T, Ψ_T^P) previously used and the reference curve for stage 1, a stage of slightly different geometry and different inlet temperature and pressure than for stages 2 and 3 (The radii, temperatures and pressures are listed in Ref. 13). Figures 4.7-10 show the resulting characteristic curves.

The temperature curves for stage 2 shown in Figure 4.7 are similar to the curves using reference curve 2 in Figure 4.3. This is to be expected since the two reference curves are similar in curvature as shown in Figures 3.17 and 3.18. In fact, a review of Tables 4.2 and 4.4 indicates that the characteristics using reference curve 1 are slightly better than those using reference curve 2.

Table 4.4 Summary of Results for Stage 2 using Curve 1

Speed Line	Mapped Φ_R	Mapped Ψ_R^T	$\Delta\alpha_1$ (degrees)	Error σ^T	Error σ^P
1	0.4329	0.6630	2.913	6.105 e-3	2.530 e-2
2	0.4349	0.6584	4.600	3.801 e-3	1.163 e-2
3	0.4405	0.6452	7.439	9.349 e-3	2.142 e-2
4	0.4387	0.6495	9.612	1.093 e-2	1.753 e-2
5	0.4513	0.6191	12.39	1.608 e-2	2.689 e-2
6	0.4447	0.6352	11.24	2.252 e-2	3.656 e-2
7	0.4360	0.6557	12.29	3.948 e-2	5.041 e-2

As seen in Table 4.4, the calculated $\Delta\alpha_1$'s have changed from those in Table 4.2 due to placement of the stage data with respect to the reference curve; i.e., the positions of reference curves 1 and 2 relative to stage 2 data are quite different as can be seen from an examination of Figures 4.3 and 4.7. Hence, all of the $\Delta\alpha_1$'s, as shown in Table 4.4, are positive.

The pressure characteristics shown in Figure 4.8 are similar, in terms of curvature and placement, to those shown in Figure 4.4. The similarity in the generated pressure curves is expected since the predicted temperature characteristics are similar regardless of which stage reference characteristic (1 or 2) is used, and the calculated efficiencies remain unchanged. A comparison of the pressure errors in Tables 4.2 and 4.4, indicates that the errors are slightly lower for Table 4.4 which further illustrates the previous point. Improvement in the predicted temperature curve will always lead to improvement in the predicted pressure curve.

Figures 4.9-10 present the results of generating the temperature and pressure characteristics for stage 3 using reference curve 1. There is no improvement in the generated curves over that using a stage 3 reference curve. This can be seen more readily by comparing the σ^T's in Tables 4.4 and 4.5. A general increase in the deviations from reference curve 3 characteristics to reference curve 1 characteristics is apparent. This is an indication that perhaps a flatter reference curve, such as curve 3 (see Figure 3.19), may predict stall data better and improve the pressure curves; however, a flatter, stall reference

curve could not be developed since the methodologies presented in section 3.3 can only be used to develop pre-stall curves .

The $\Delta\alpha_1$'s for the stage 3/reference curve 1 (Table 4.5) have also changed from those computed using reference curve 3 (Table 4.3). As for the pressure characteristics, some of the curve 1 predictions are better. The poor temperature fit may in some cases offset the error due to the constant efficiency assumption.

Table 4.5: <u>Summary of Results for Stage 3 using Curve 1</u>

Speed Line	Mapped Φ_R	Mapped Ψ_R^T	$\Delta\alpha_1$ (degrees)	Error σ^T	Error σ^P
1	0.4544	0.6113	11.55	1.074 e-2	4.141 e-2
2	0.4524	0.6163	11.92	1.777 e-2	3.867 e-2
3	0.4576	0.6033	11.42	2.170 e-2	4.198 e-2
4	0.4731	0.5628	12.09	2.067 e-2	3.315 e-2
5	0.4698	0.5716	9.263	4.025 e-2	4.707 e-2
6	0.4742	0.5600	5.722	4.902 e-2	5.424 e-2
7	0.4714	0.5605	4.142	9.449 e-2	9.869 e-2

4.4 Effect of α_1 Selection on Predicted Characteristics

In this part of the analysis, the selected value of the reference curve α_1 (as discussed in section 3.3.2) was varied to demonstrate its effect on the generated stage

characteristic. The stage characteristics for stage 1, speed 4 generated using reference curve 1 and varying α_1 are shown in Figure 4.11. As seen in the figure, the generated curves are practically indistinguishable from one another. Table 4.6 summarizes the results for a range of α_1's ranging from 0 to 30 degrees. In the table, it is evident just how similar the curves are, as the values of σ^T and σ^P are approximately the same regardless of the input α_1. However, the selection of α_1 does affect the value of $\Delta\alpha_1$ and the reference curve ε'. The value of ε' determined during the development of the reference curve (section 3.3) decreases to account for increases in the reference curve α_1. Increases in the selected α_1 also lead to a decrease in $\Delta\alpha_1$, suggesting that the characteristic generation method is insensitive to the selection of the reference curve α_1, as stated earlier.

**Table 4.6: <u>Summary of Results for Stage 1/Speed 4
Characteristic Generation using Curve 1 and Changing α_1</u>**

α_1 degrees	Mapped Φ_R	Mapped Ψ_R^T	$\Delta\alpha_1$ (degrees)	Error σ^T	Error σ^P	ε'
0	0.4386	0.6496	9.843	5.828 e-3	1.561 e-2	3.258
10	0.4387	0.6496	9.547	5.908 e-3	1.567 e-2	3.205
15	0.4386	0.6496	9.181	5.902 e-3	1.567 e-2	3.167
20	0.4387	0.6496	8.686	5.905 e-3	1.566 e-2	3.118
25	0.4387	0.6496	8.074	5.891 e-3	1.565 e-2	3.055
30	0.4388	0.6496	7.367	5.898 e-3	1.565 e-2	2.975

4.5 Changing the Given Data Point

When testing the compressor, there is no way to know a priori which input data point for the curve generation algorithm will occur. In the validation phase of the algorithm, as has been previously discussed, midpoints of the known data were arbitrarily selected as the single input data points for the curves generated in the previous figures. Figure 4.12 shows the effect on the generated temperature curves with changing input data. This figure shows the temperature curvefits for the stage 1, speed 4 curve using reference curve 1 (speed 3) and different selected starting data points from the given set. Table 4.7 lists the input data points, mapped reference points, $\Delta\alpha_1$, and the deviations, σ^T and σ^P, for the generated curves.

Table 4.7: Effect of Changing Data Point

Data Point $(\Phi_T, \Psi_T{}^T, \Psi_T{}^P)$	Mapped Φ_R	Mapped $\Psi_R{}^T$	$\Delta\alpha_1$ (degrees)	Error σ^T	Error σ^P
(0.3561, 0.6278, 0.6691)	0.4238	0.6836	9.536	5.742 e-3	2.517 e-2
(0.3663, 0.6139, 0.6642)	0.4306	0.6683	9.149	3.966 e-3	1.388 e-2
(0.3723, 0.5918, 0.6432)	0.4387	0.6495	9.547	5.908 e-3	1.567 e-2
(0.3797, 0.5825, 0.6416)	0.4432	0.6386	9.201	3.518 e-3	1.508 e-2
(0.3835, 0.5737, 0.6367)	0.4467	0.6302	9.193	3.575 e-3	1.813 e-2
(0.3864, 0.5692, 0.6351)	0.4488	0.6253	9.089	4.672 e-3	2.224 e-2

While the temperature errors, σ^T, for all input data in Table 4.7, fall into acceptable ranges (less than 1.6 e-2), the generated temperature curves, shown in Figure 4.12, using the first and third data points do not predict the rest of the data set as well as the curves generated using the second, fourth, fifth and sixth data points. The deviations, σ^T and σ^P, indicate that some input points result in more accurate curves. Obviously, a scheme is required to optimize the generated curve to minimize the deviation with respect to all of the data.

4.6 Increased Accuracy of Prediction using Additional Data Points

Figures 4.13 and 4.14 show the results of improving the prediction using the combination of additional test data and the non-linear least squares estimation algorithm discussed in section 2.4.2. Both figures compare the curves generated using one, three and six data points. The one-point curve used the section 2.4.1 algorithm, while the three and six data point curves used the algorithm from section 2.4.2. The steady improvement in the pressure curves is evident as more data points are included in the generation procedure. The final pressure curve, using all six data points, goes through the middle of the data set in comparison to the fits using one or three data points.

Values in Table 4.8 illustrate how the non-linear least squares algorithm adjusted the initial value of $\Delta\alpha_1$ (determined from the one-point algorithm) such that it minimized the deviations between the predicted data and given data. It also lists the data points that were used for each case. For the six-point case, all of the supplied data in the set were used.

**Table 4.8: Summary of Results for Stage 1/Speed 4
Characteristic Generation using Additional Data Points**

Number of Data Points	Data Points $(\Phi_T, \Psi_T^T, \Psi_T^P)$	$\Delta\alpha_1$ (degrees)	Error σ^T	Error σ^P
1	(0.3723, 0.5918, 0.6432)	9.547	5.908 e-3	1.567 e-2
3	(0.3561, 0.6278, 0.6691) (0.3663, 0.6139, 0.6642) (0.3723, 0.5918, 0.6432)	9.410	3.395 e-3	1.553 e-2
6	(0.3561, 0.6278, 0.6691) (0.3663, 0.6139, 0.6642) (0.3723, 0.5918, 0.6432) (0.3797, 0.5825, 0.6416) (0.3835, 0.5737, 0.6367) (0.3864, 0.5692, 0.6351)	9.282	2.712 e-3	4.704 e-3

As discussed in section 2.4.2., a method for improving the generated pressure characteristic includes improving the efficiency model. In the one-point method, efficiency was assumed constant, which is consistent with near-design flow coefficients. With additional data, a more realistic model of efficiency versus flow coefficient can be developed. The improved efficiency models for stage 1, speed 4 can be seen in Figure 4.15. In the figure, the three curves shown were developed using one, three, and six test data points. The function coefficients A, B and C are recalculated as additional data points are acquired. With the efficiencies and their respective flow coefficients, the algorithm discussed in 2.4.2.3 determined the constant coefficients for the following function of efficiency versus flow coefficient:

$$\eta = A\,\Phi^2 + B\,\Phi + C \tag{4.4}$$

4-13

For the one-point curve, A = B = 0 and C = 0.9273; for the three-point curve, A = -112.7, B = 83.89 and C = -14.69; for the six-point curve, A = -61.35, B = 47.41 and C = -8.211.

The section 2.4.2 algorithm can also be used to improve the stage characteristics generated using a reference curve from another stage. Figures 4.16 and 4.17 show how the temperature and pressure curves for stage 3, speed 7, generated with reference curve 1, can be moderately improved for near-stall regions using additional data. The new $\Delta\alpha_1$ from the section 2.4.2 algorithm is 2.380 degrees in comparison to 4.142 degrees using the one-point algorithm. In terms of the errors, σ^T and σ^P, an improvement was made. Using the section 2.4.2 algorithm, σ^T decreased from 9.449 e-2, using the one-point algorithm, to 6.791 e-2, and σ^P decreased from 9.869 e-2 to 6.742 e-2. The new calculated errors, however, do not fall below the acceptance range of 1.6 e-2. They are not even below the values calculated for the curves generated using reference curve 3 (Table 4.2). These large deviations can be seen in Figures 4.16 and 4.17 where the generated curves do not line up with the test data. Thus, using the section 2.4.2 algorithm to incorporate additional data into the curvefit is not sufficient to overcome the errors due to stall effects.

Stall effects can be accounted for by changing ε'. The curves generated in Figures 4.18 and 4.19 were developed using the $\Delta\alpha_1$ determined from the section 2.4.2 algorithm, 2.380 degrees, and the reference curve generation scheme outlined in section 3.3.3. The reference curve generation algorithm iterated ε' to best fit the given data and found ε' to be equal to -0.1718. This result for ε' is consistent with the stall portion of the deflection versus incidence curve shown in Figure 2.2 where, at stall, ε' approaches zero and

4-14

becomes negative. The reference temperature curve resulting from the section 3.3.3 algorithm is shown in Figure 4.18 and compared to the curves generated using one-point and non-linear least squares algorithms. Even though the fit for the data is good (σ^T for this case is 6.096 e-3), the negative curvature shown is not typical of stage characteristics. For this case, a variable ε' model as a function of flow coefficient would be of use in generating the new temperature characteristic.

The pressure curve shown in Figure 4.19 was developed using the new temperature curve from Figure 4.18, generated using a new ε', and an efficiency model developed using the section 2.4.2 algorithm. The curvefit has improved significantly for this case as well, $\sigma^P = 9.526$ e-3, and the curvature of the resulting characteristic is correct. Figures 4.18-19 and the results clearly demonstrate how a variable ε' versus flow coefficient model could be used to improve the generated curves.

4.7 Summary of Results

The one-point stage characteristic generation algorithm was shown to be accurate for the first stage of the compressor since the data for those curves were pre-stall; however, for post-stall data, such as stage 3, the generated curves were not as accurate. Curves generated for stage 2 using reference curve 1 were similar in curvature and placement to those generated using reference curve 2. However, the generated stage 3 characteristics using reference curve 1 showed a marked increase in the temperature deviation, σ^T, suggesting that a flatter reference curve would better predict data in the stall region. In comparison to the temperature curves, the generated pressure curves were not

as accurate using the one-point stage characteristic generation algorithm. This is due to the constant efficiency assumption, necessary with only one available performance point.

The generated stage characteristics were not sensitive to the selection of the reference curve α_1. A change in the input reference curve α_1 to the one-point generation algorithm changes the iterated value of $\Delta\alpha_1$ and ε' of the reference curve and generates the same curve. On the other hand, the generated characteristics were dependent upon the input data point. The generated curves shifted in order to go through the input point and depending upon that point, the deviation, σ^T, increased or decreased.

As additional data were acquired, the algorithm in section 2.4.2 could be implemented in order to determine a $\Delta\alpha_1$ that minimized the deviations between the generated curve and the testcase data. However, the section 2.4.2 algorithm could not be used to generate accurate stage characteristics for stall test data. In order to develop accurate curvefits for stall data, a variable ε' model would be required. Additional data could also be used to construct a more realistic, parabolic efficiency model. With the improved efficiency model and temperature curves, an improved pressure curve could be generated.

V. CONCLUSIONS AND RECOMMENDATIONS

5.1 Conclusions

1. The stage-characteristic curvefit method presented in this thesis is valid for the pre-stall portions of the stage characteristics as quantified by deviations, σ^T and σ^P, less than 1.6 e-2. The goodness of the curvefit, however, is dependent upon the choice of reference curve. Data in the high curvature stall or post-stall regimes will not be represented as accurately by reference curves chosen from pre-stall conditions, as seen in the flatter speed lines of all three stages, particularly for stage 3. Accurate fits were obtained for the first two stages (using a reference curve from stage 1) for data that followed a curvature similar to the reference. Flatter reference curves could be made to predict the stall data better, but this would require more work to be done in optimizing the parameter, ε'.

2. The accuracy of the curvefit in predicting the true characteristic from one point depends on the deviation of that point from the true operational characteristic; i.e., an invalid first data point will result in a skewed predicted curve not representative of the true characteristic. The deviation between the test data and the generated curve, σ^T, varies decidedly depending upon the input data point. In Table 4.7, σ^T varies from 4 e-3 to 7 e-3, and while these deviations are all within acceptable ranges, the lower the deviation, the better the fit. The best curvefit may be determined by the use of additional data in a non-linear, least-squares estimation algorithm. The non-linear least squares algorithm adjusts the estimated gas inlet angle for the stage, α_1, in order to minimize the errors. Using this

technique, the deviations for the stage 1, speed 4 curves, for example, are about half that of the one-point prediction as seen in the σ^T columns of Tables 4.1 and 4.8. The refinement algorithm of section 2.4.2 can be used to decrease errors in stage characteristics generated using a reference curve from another stage; however, it is not sufficient to predict the curvature due to stall effects. In order to account for stall effects, a variable ε' versus flow coefficient model is required.

3. The pressure characteristics are not predicted accurately using the one-point generation method. Accuracy may be improved by using additional data points to develop a parabolic model of efficiency versus flow coefficient. For example, when all of the data in the set are used, deviations in the pressure coefficient curvefit using the parabolic efficiency model for stage 1, speed 4 are only one third of those using the one-point algorithm.

4. It has also been shown that though the angles on the reference curve may be unknown, if the angles are derived based on common design and theoretical principles, valid characteristics can be generated. The one-point algorithm, from section 2.4.1, is not sensitive to the choice of the stator outlet angle, α_1, since an adjustment to the change in the stator outlet angle, $\Delta\alpha_1$ for the new data will occur and result in a nearly identical curve.

5.2 Recommendations

1. More research needs to be done in the following areas: post-stall regimes; the change in the slope of the deflection versus incidence curve as it relates to the flow

coefficient; the development of stall reference curves; efficiency modeling; and changes in other blade angles, β_1 and ε. The algorithms presented in this thesis are based on pre-stall theoretical behavior. Once the compressor stage enters the stall and post-stall regimes, the losses that have been assumed negligible become significant. Also, in the stall regions, the flow is separated and does not follow the contour of the rotor blades, and the linear function of ε versus β_1 used in this study is not accurate. As seen in Figure 2.2, ε' may decrease or become negative as stall is reached. An algorithm constructed to include the dependency of ε' on Φ would more adequately model stall and post-stall losses. Such a model could be used to develop a stall reference curve. Significant improvements were seen when using the flatter reference curve of stage 3 to predict the near-stall data as seen in Figure 4.5.

2. The pressure curves are dependent on both the temperature curve and the efficiency. Improvements in the efficiency model would greatly improve the pressure curve predictions. This could be done by developing a model of the efficiency as a function of flow coefficient to include effects due to changes in the blade angles. Such a model could be derived from cascade theory loss relationships described in Ref. 7.

3. Finally, the curve generation algorithms (section 2.4) mainly used changes in the IGV and stator outlet angles with the assumption that changes in other angles (β_1 and ε) were dependent upon changes in α_1. The algorithms' accuracy could be enhanced by including other blade angle changes, such as stagger, as independent quantities. A less constrained relationship, essentially with a nonzero $\Delta\beta_1$ or $\Delta\varepsilon$ in (2.34-35), could improve the prediction for curves that are not of the same stage as the reference, particularly in the

cases where in addition to the stator angle changes, the rotor blades angles have been changed as well.

VI. REFERENCES

(1)   Brent, J.A., et al. "High-Stage Loading/Low Aspect Ratio Compressor (HSL/LARC)." Final Report, AFWAL-TR-80-2075. September 1980.

(2)   Camp, T. R. and J. H. Horlock. "An Analytical Model of Axial Compressor Off-Design Performance." Journal of Turbomachinery. Vol 116. July 1994.

(3)   Cohen, H., G.F.C. Rogers, and H.I.H. Saravanamuttoo. Gas Turbine Theory, 3d ed. Longman Scientific & Technical, 1987.

(4)   Dixon, S.L. Fluid Mechanics, Thermodynamics of Turbomachinery 3d ed. Pergamon Press, 1978.

(5)   Gostelow, J.P. Cascade Aerodynamics. Pergamon Press, 1984.

(6)   Hale, A.A. and M.W. Davis. "DYNamic Turbine Engine Compressor Code DYNTECC--Theory and Capabilities." AIAA/SAE/ASME/ASEE 28th Joint Propulsion Conference and Exhibit. July 6-8, 1992. Nashville, TN.

(7)   Horlock, J.H. Axial Flow Compressors; Fluid Mechanics and Thermodynamics. Robert E. Krieger Publishing Company, 1985.

(8)   Mendenhall, William. Dennis D. Wackerly and Richard L. Scheaffer. Mathematical Statistics with Applications. Duxbury Press, 1990.

(9)   Mizrahi, Abe and Michael Sullivan. Calculus and Analytic Geometry. Wadsworth Publishing Company, 1986.

(10)   Muir, D.E. H.I.H. Saravanamuttoo, and D. J. Marshall. "Health Monitoring of Variable Geometry Gas Turbines for the Canadian Navy." Journal of Engineering for Gas Turbines and Power. Vol. 111, April 1989.

(11)   Nyhoff, Larry and Sanford Leestma. Fortran 77, for Engineers and Scientists 2nd ed. Macmillan Publishing Company, 1988.

(12)   Steinke, Ronald J. STGSTK; A Computer Code for Predicitng Multistage Axial-Flow Compressor Performance by a Meanline Stage-Stacking Method. NASA-TP-2020. May 1982.

(13)   Users Manual The DYNnamic Turbine Engine Compressor Code. Arnold Engineering Development Center, 1995.

(14)   Weisel, William E. "Chapter 3 Least Squares Estimation." <u>Modern Methods of
        Orbit Determination--Class Notes</u>. pp. 59-92. 1995.

(15)   Weisel, William E. "Chapter 5 Special Perturbations." <u>Advanced Astrodynamics--
        Class Notes</u>. pp. 115-150. 1994.
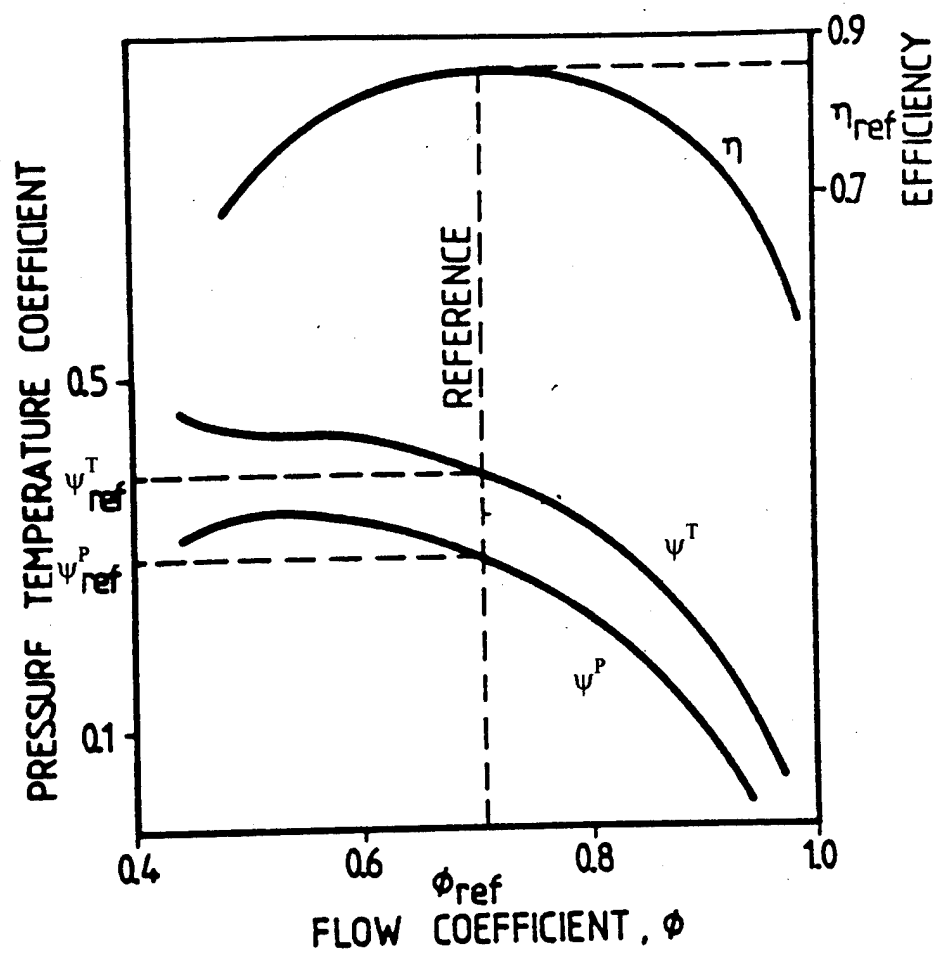
Figure 1.1 Example Compressor Stage Characteristic (Ref. 10)
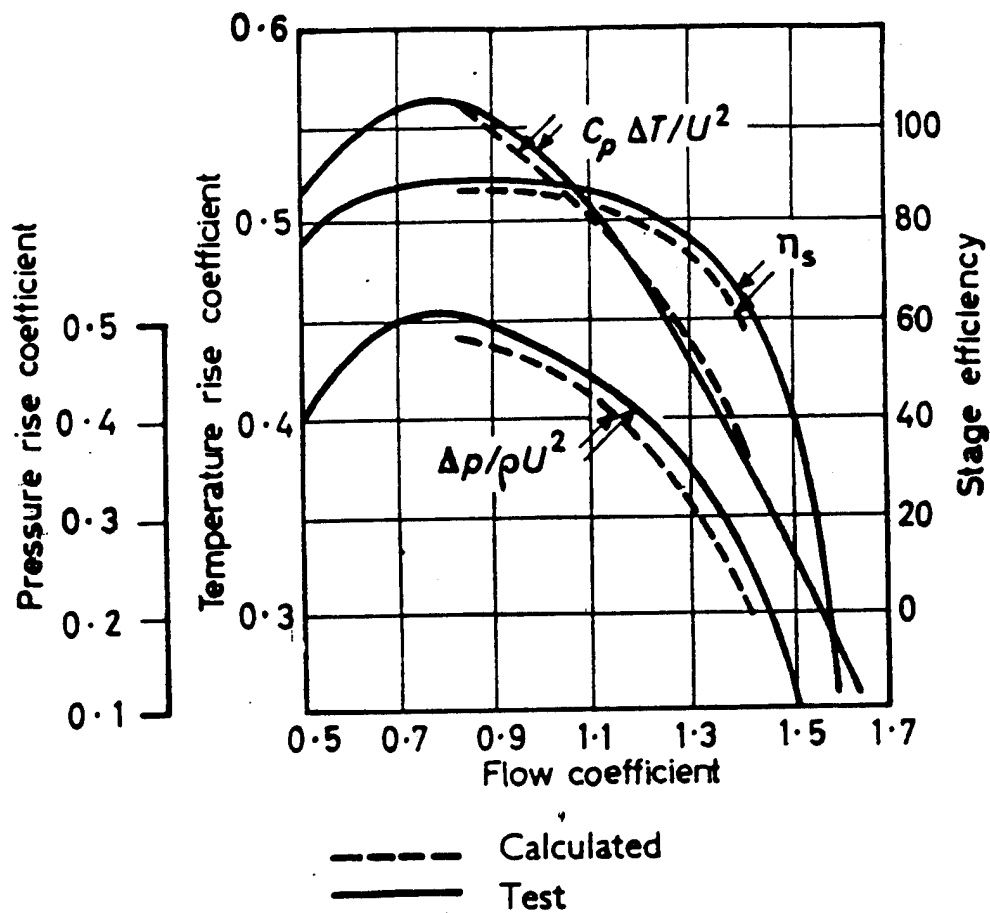
Figure 1.2 Comparison of Test and Calculated Stage Characteristics (Ref. 7)
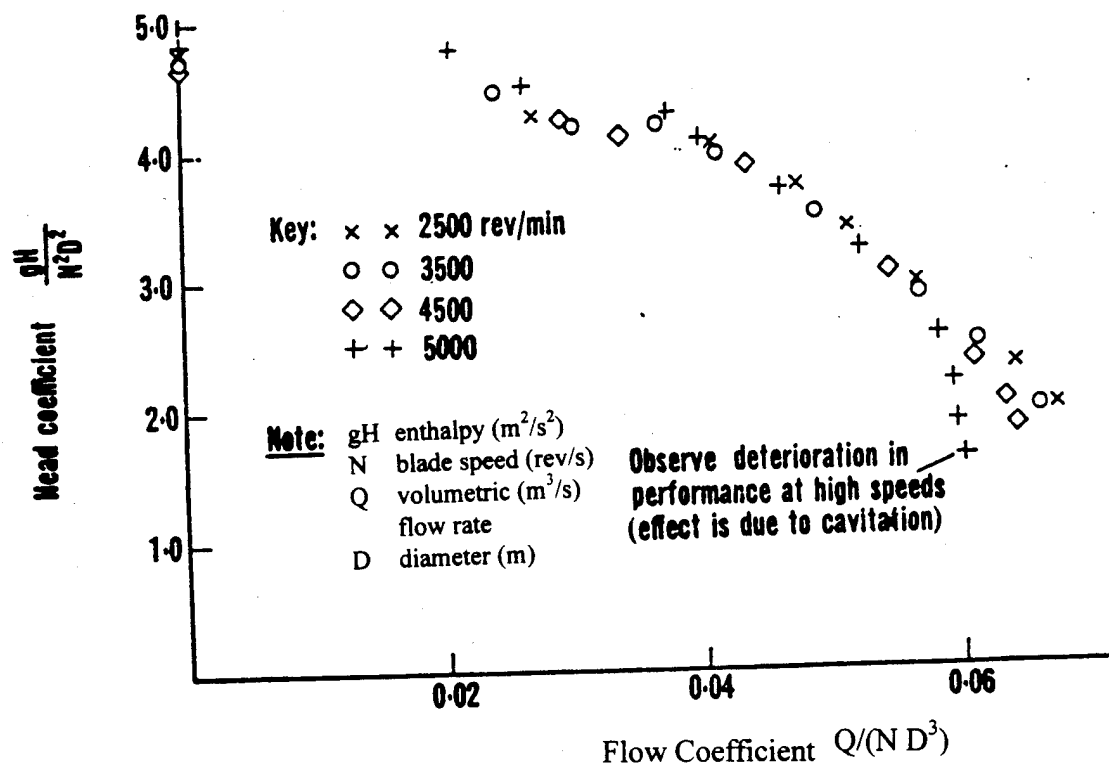
Figure 1.3 Dimensionless Head-Volume Characteristic of a
Centrifugal Pump (Ref. 4)
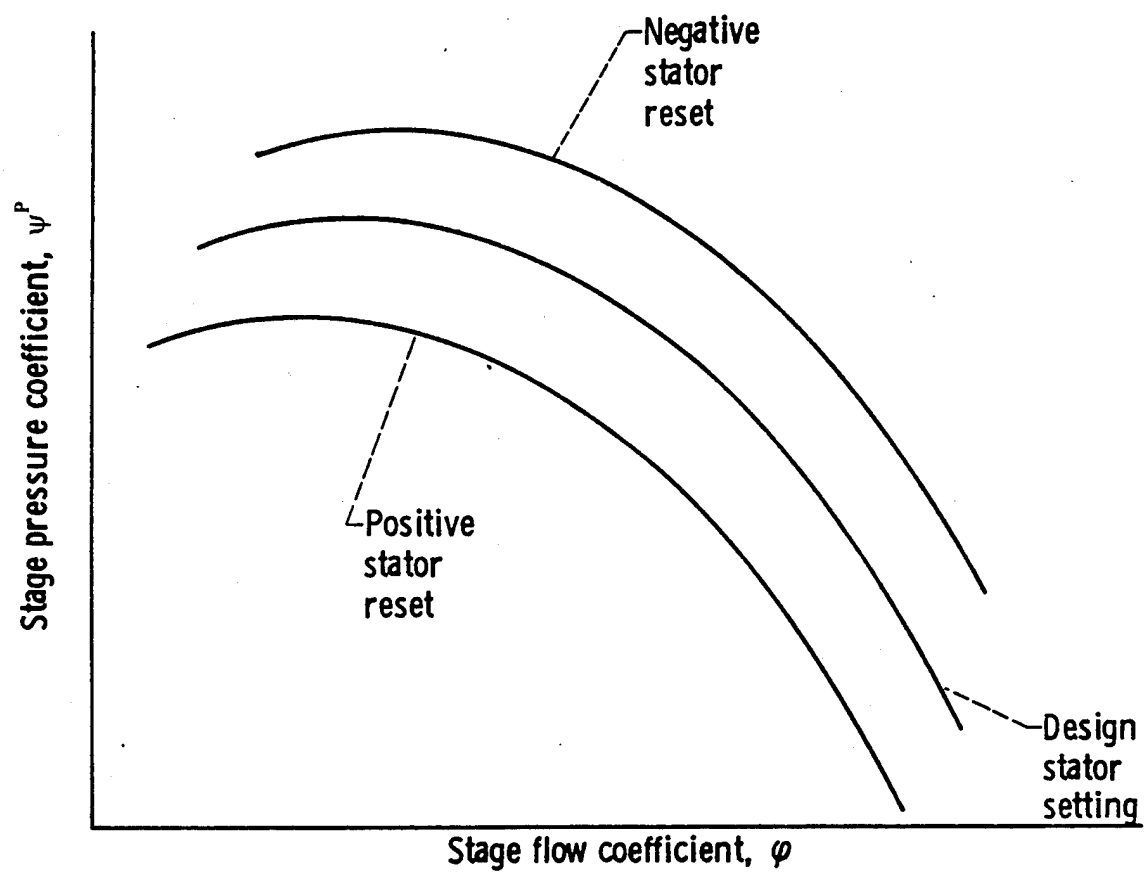
Figure 1.4 Change in Pressure Characteristic
Due to a Stator Reset (Ref. 12)
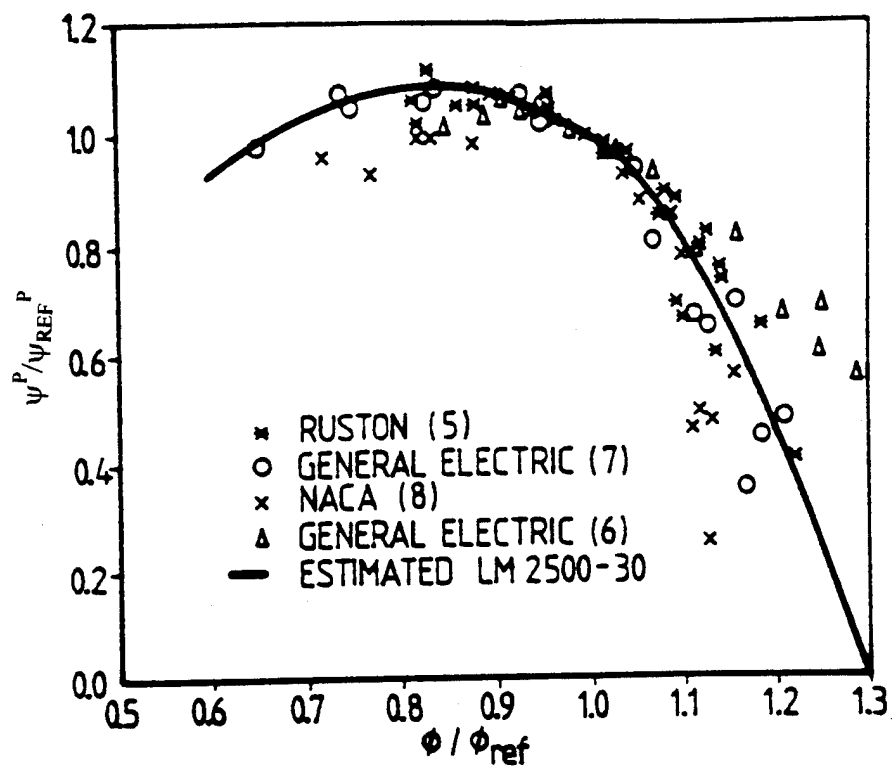
Figure 1.5 Generalized Stage Pressue Coefficient Curve (Ref. 10)
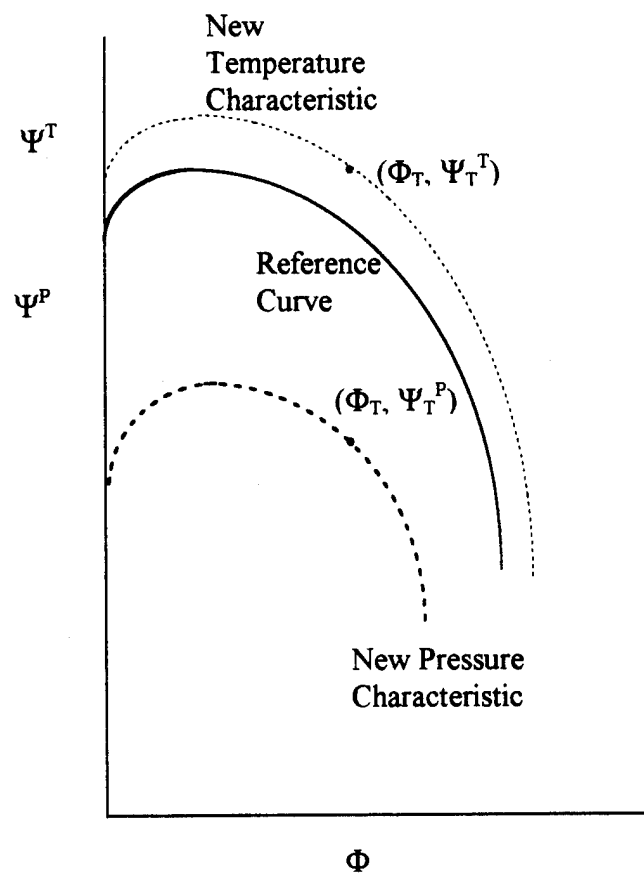
Figure 1.6 Problem Statement

β_1' = blade inlet angle
β_2' = blade outlet angle
θ = blade camber angle
  = $\beta_1' - \beta_2'$
ζ = setting or stagger angle
s = pitch (or space)
ϵ = deflection
  = $\beta_1 - \beta_2$
β_1 = air inlet angle
β_2 = air outlet angle
V_1 = air inlet velocity
V_2 = air outlet velocity
i = incidence angle
  = $\beta_1 - \beta_1'$
δ = deviation angle
  = $\beta_2 - \beta_2'$
c = chord

Point of maximum camber

Rotor

Stator
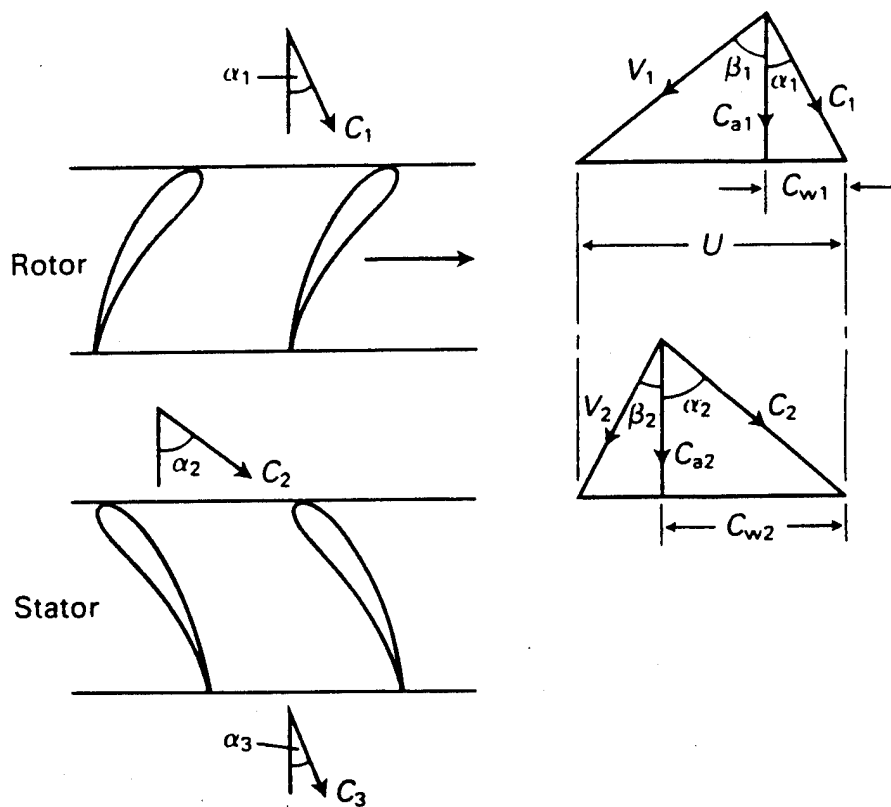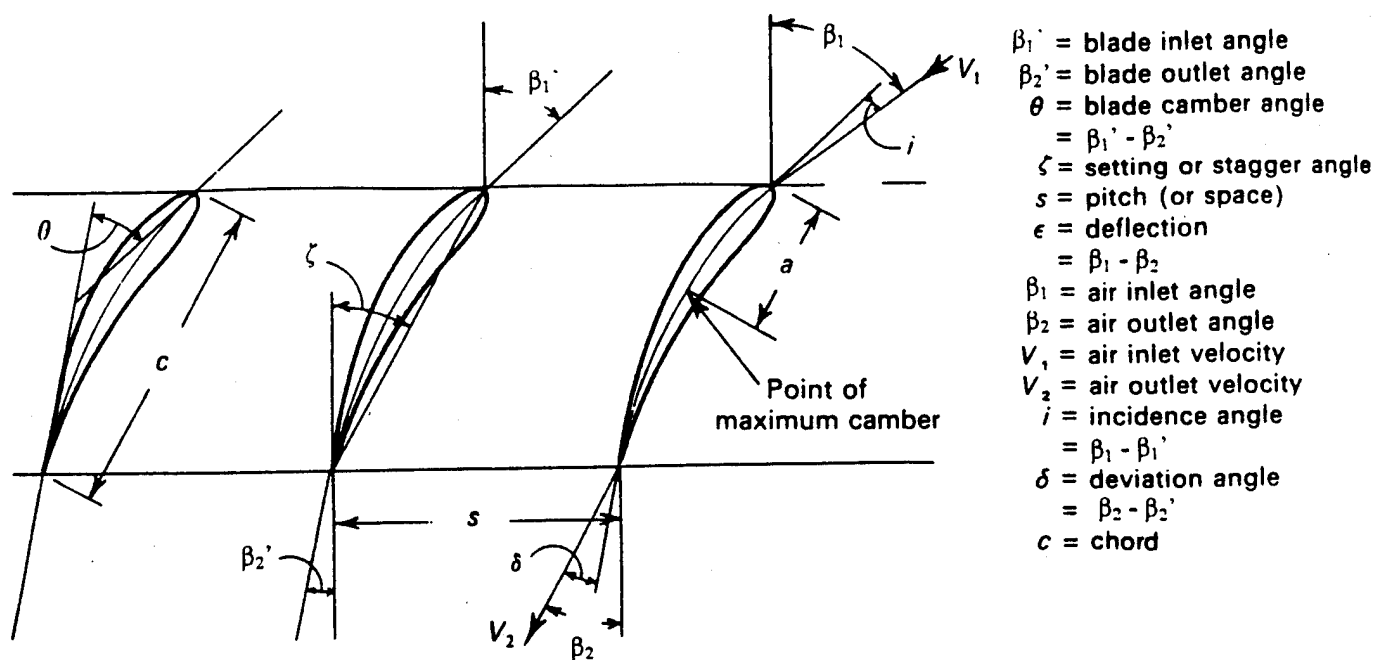
Figure 2.1 Compressor Cascade Terminology (Ref. 3)
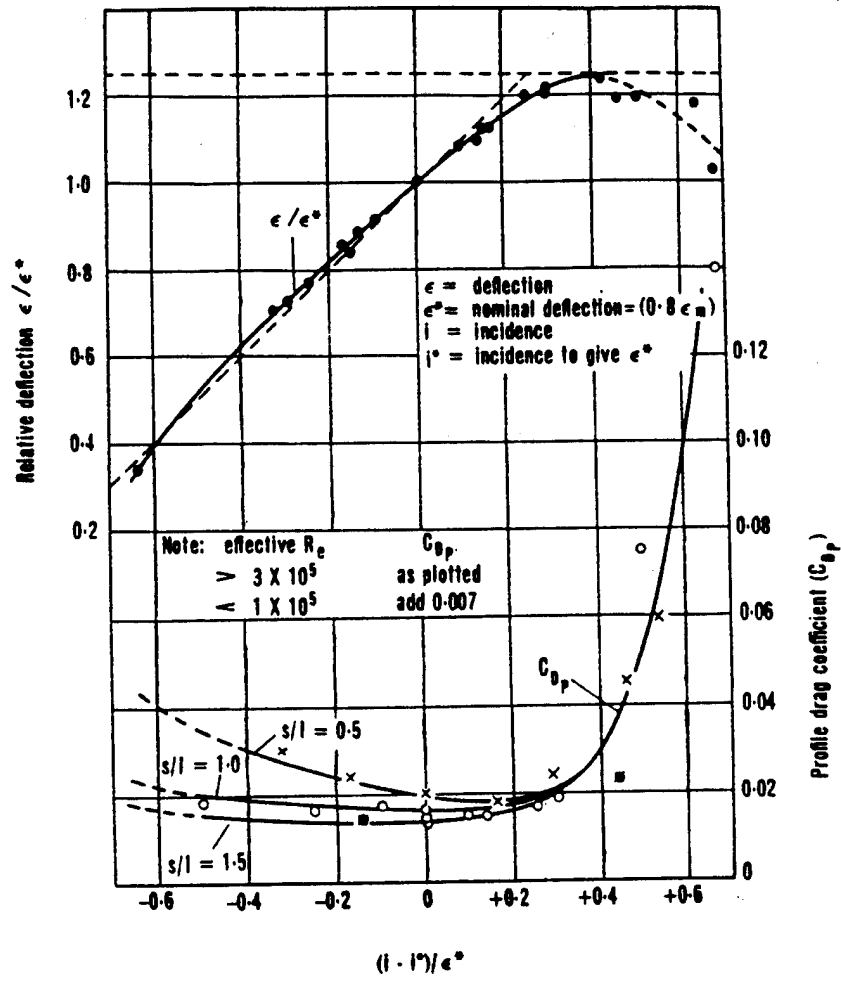
Figure 2.2 Off-Design Performance of a Compressor Cascade (Ref. 7)
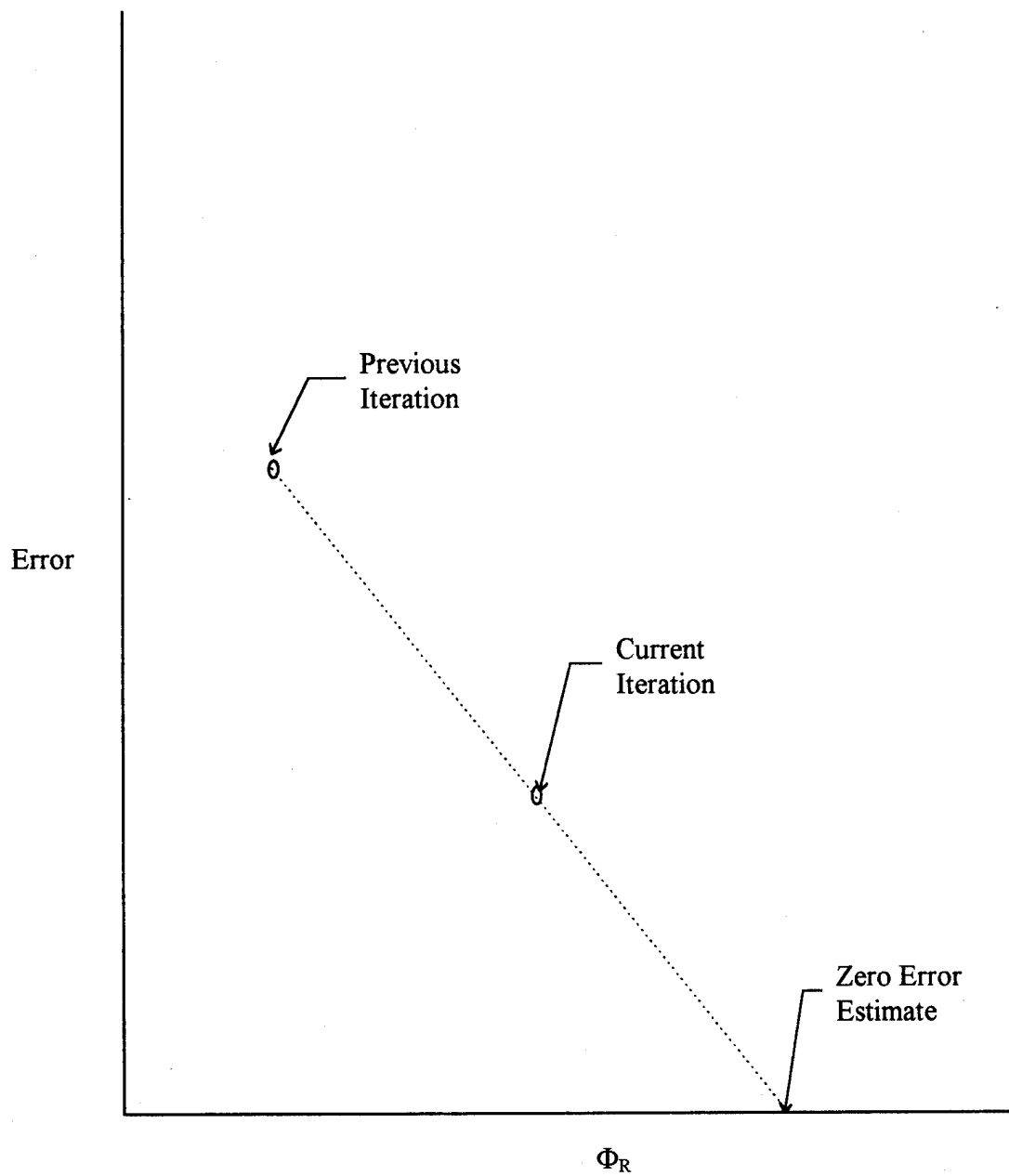
Figure 2.3 Plot of Error vs. Iterated Flow Coefficient
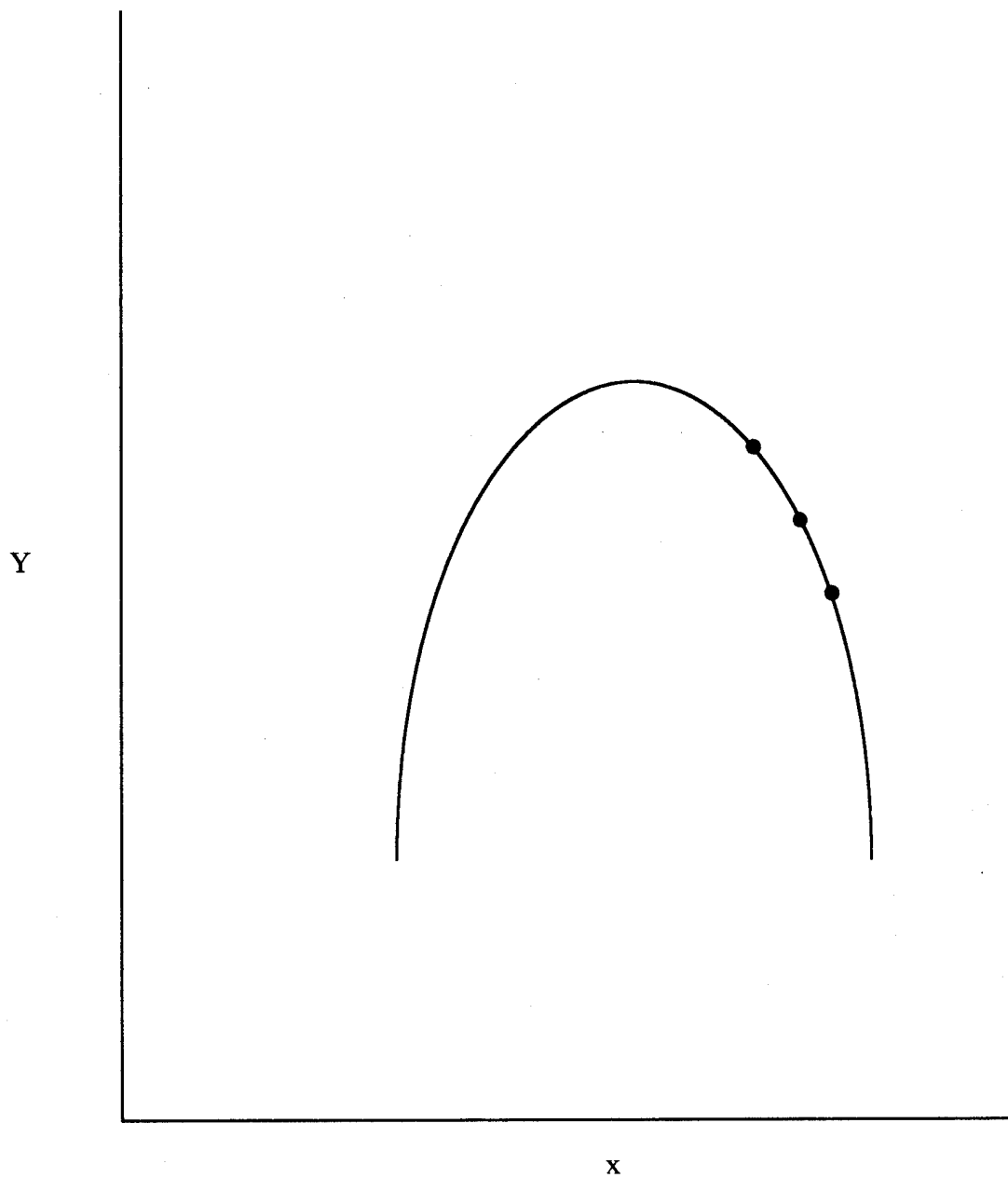
Figure 2.4 Example Parabola
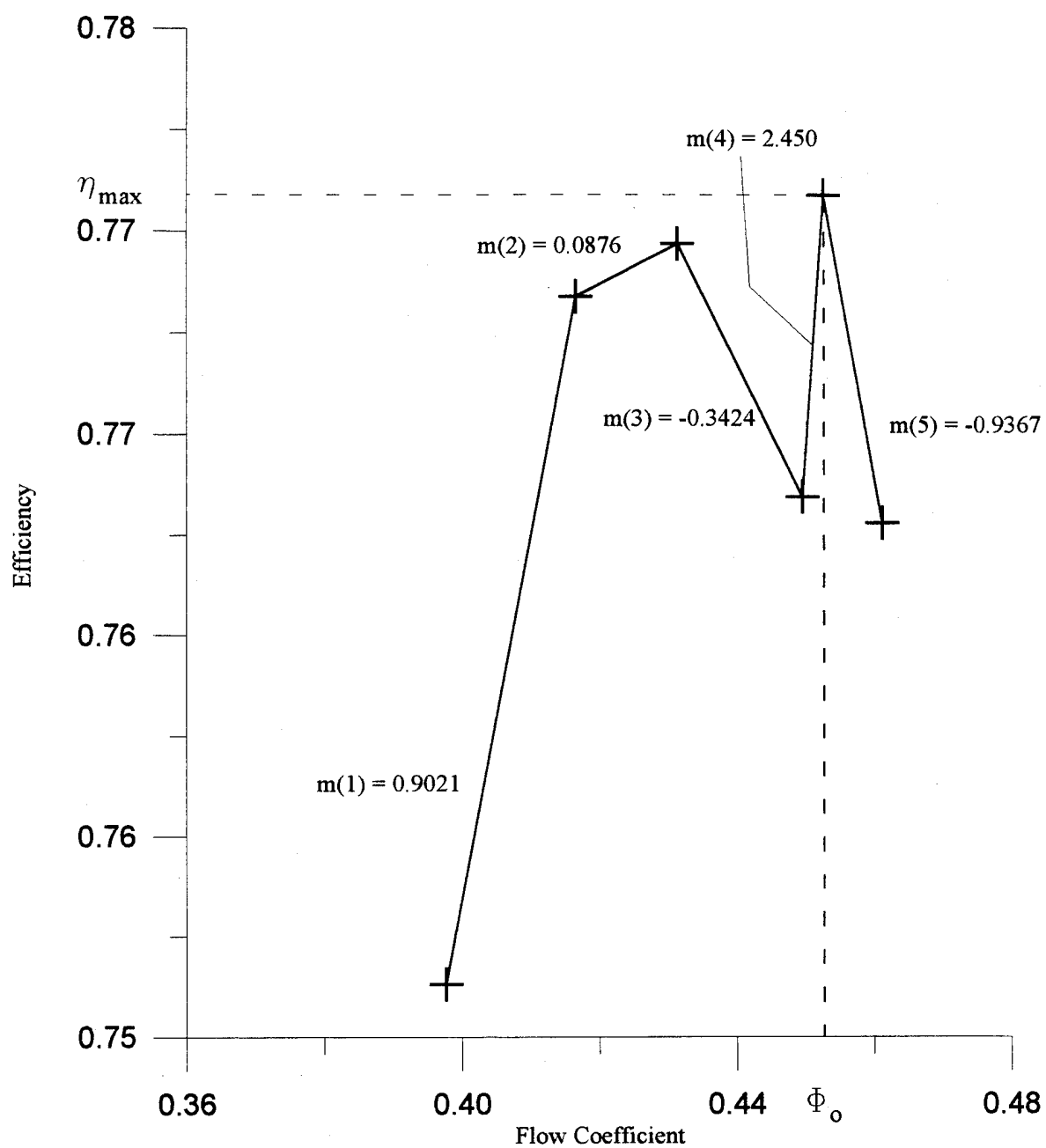
Figure 2.5 Efficiency vs. Flow Coefficient Data
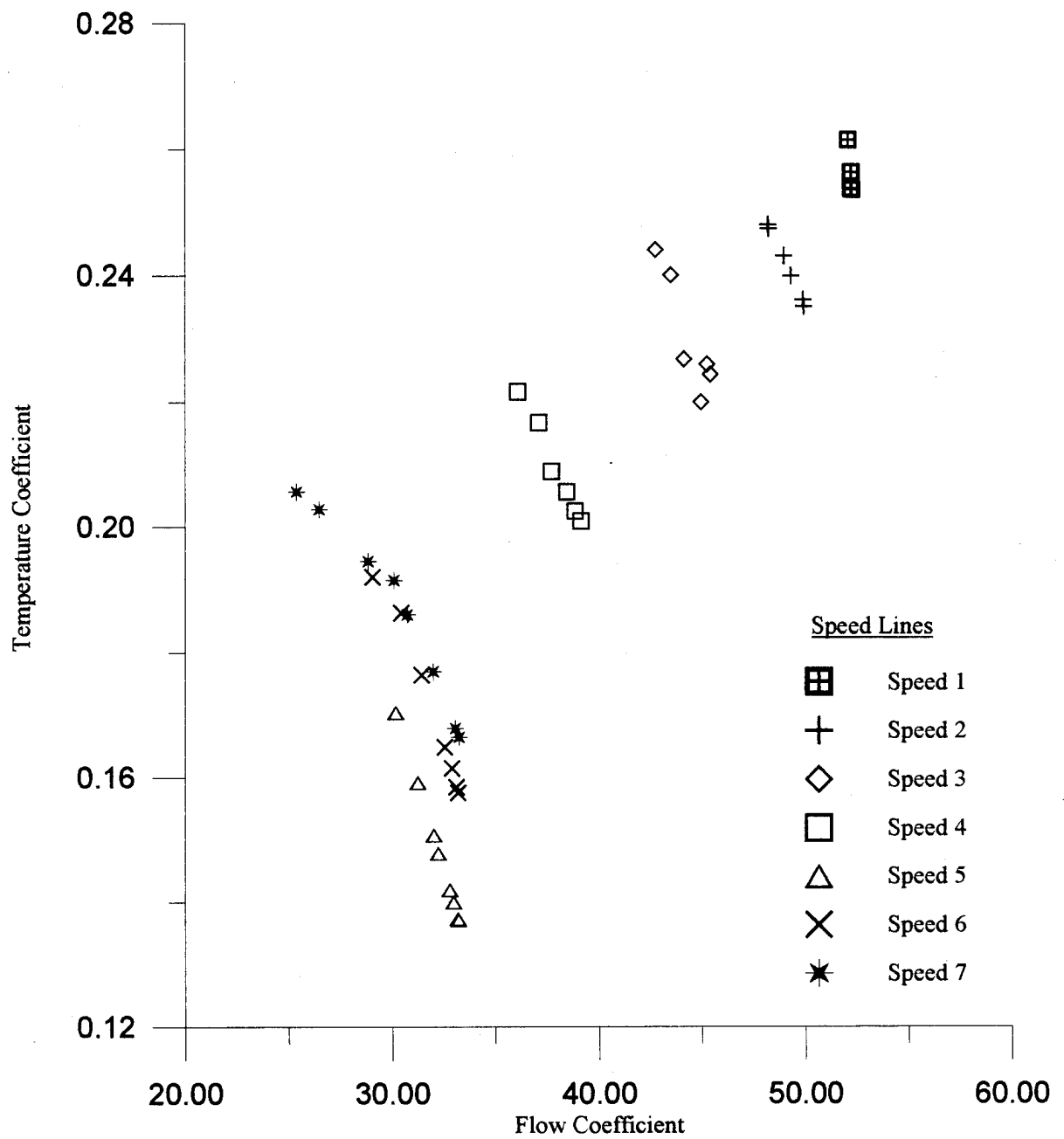
Figure 3.1 Stage 1 Temperature Characteristic
using DYNTECC Data
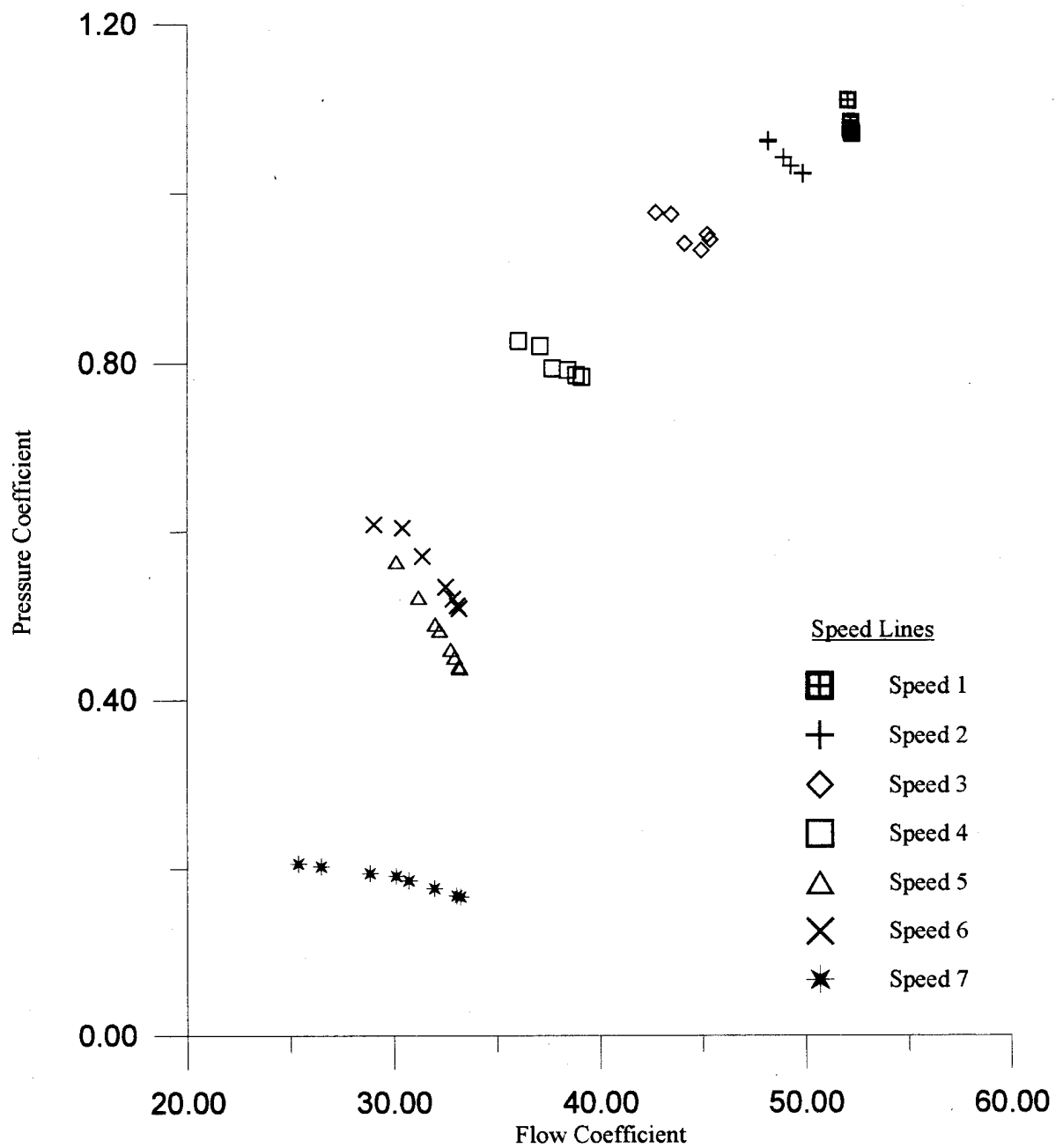
Figure 3.2 Stage 1 Pressure Characteristic
using DYNTECC Data
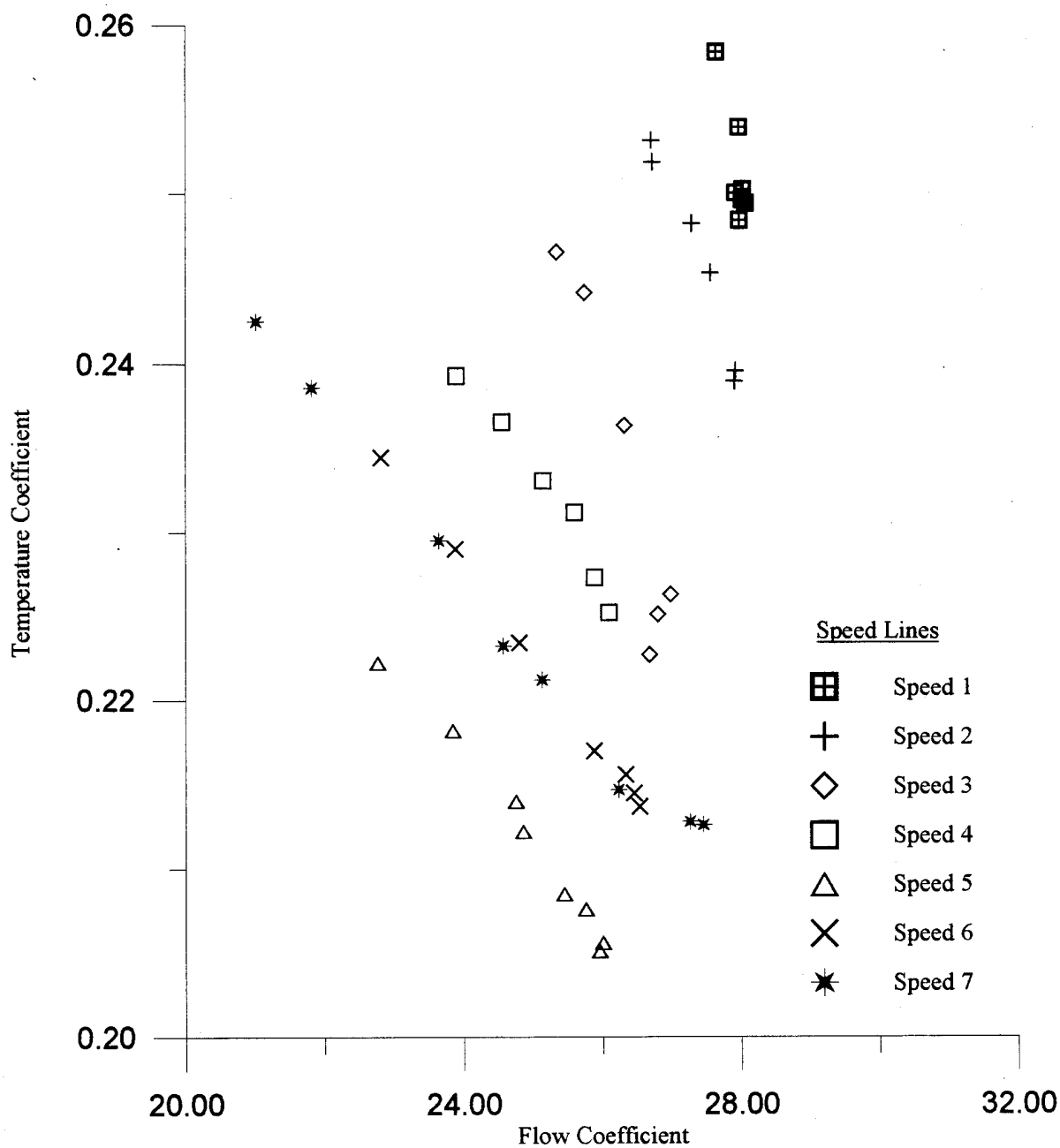
Figure 3.3 Stage 2 Temperature Characteristic
using DYNTECC Data
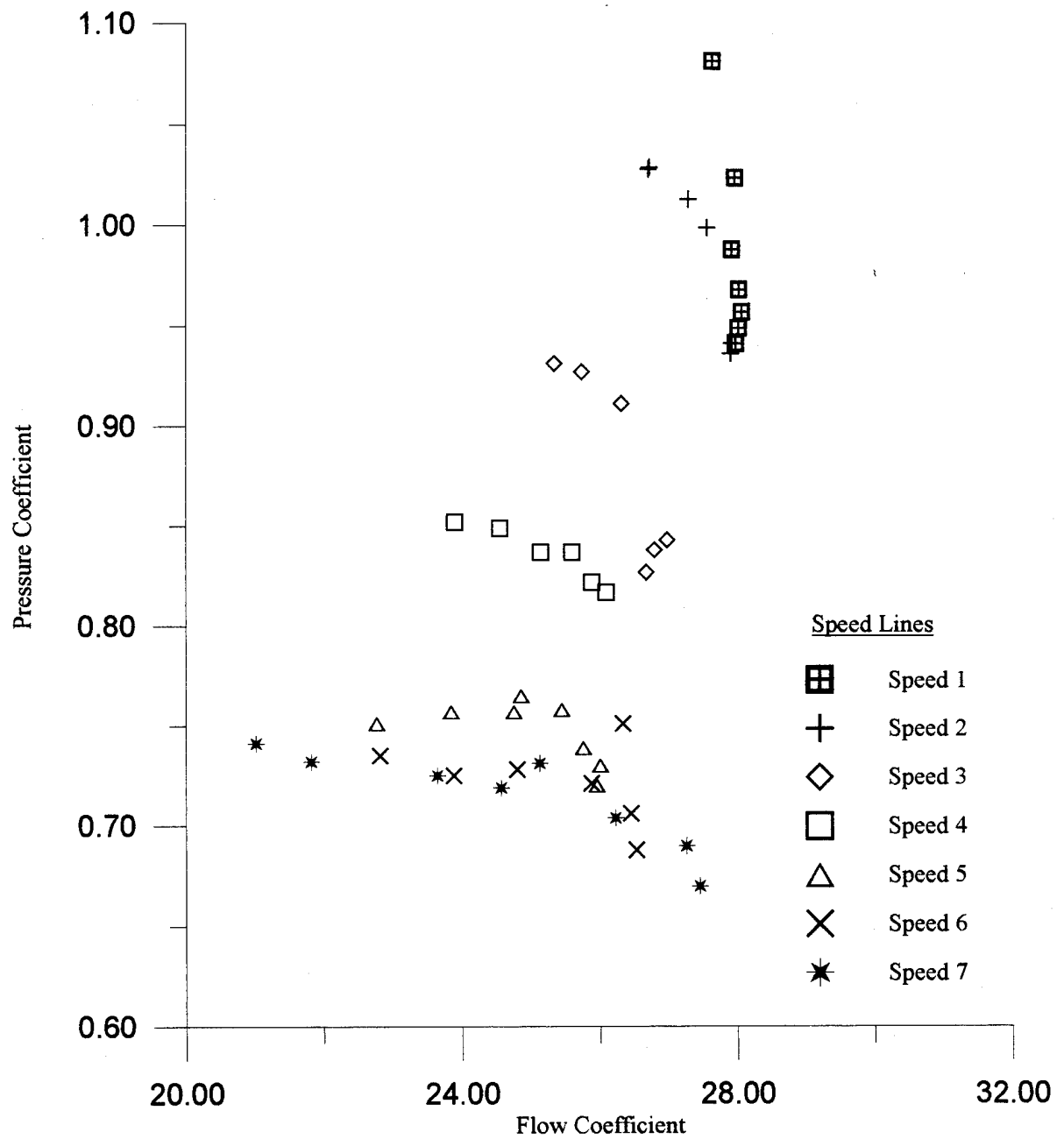
Figure 3.4 Stage 2 Pressure Characteristic
using DYNTECC Data
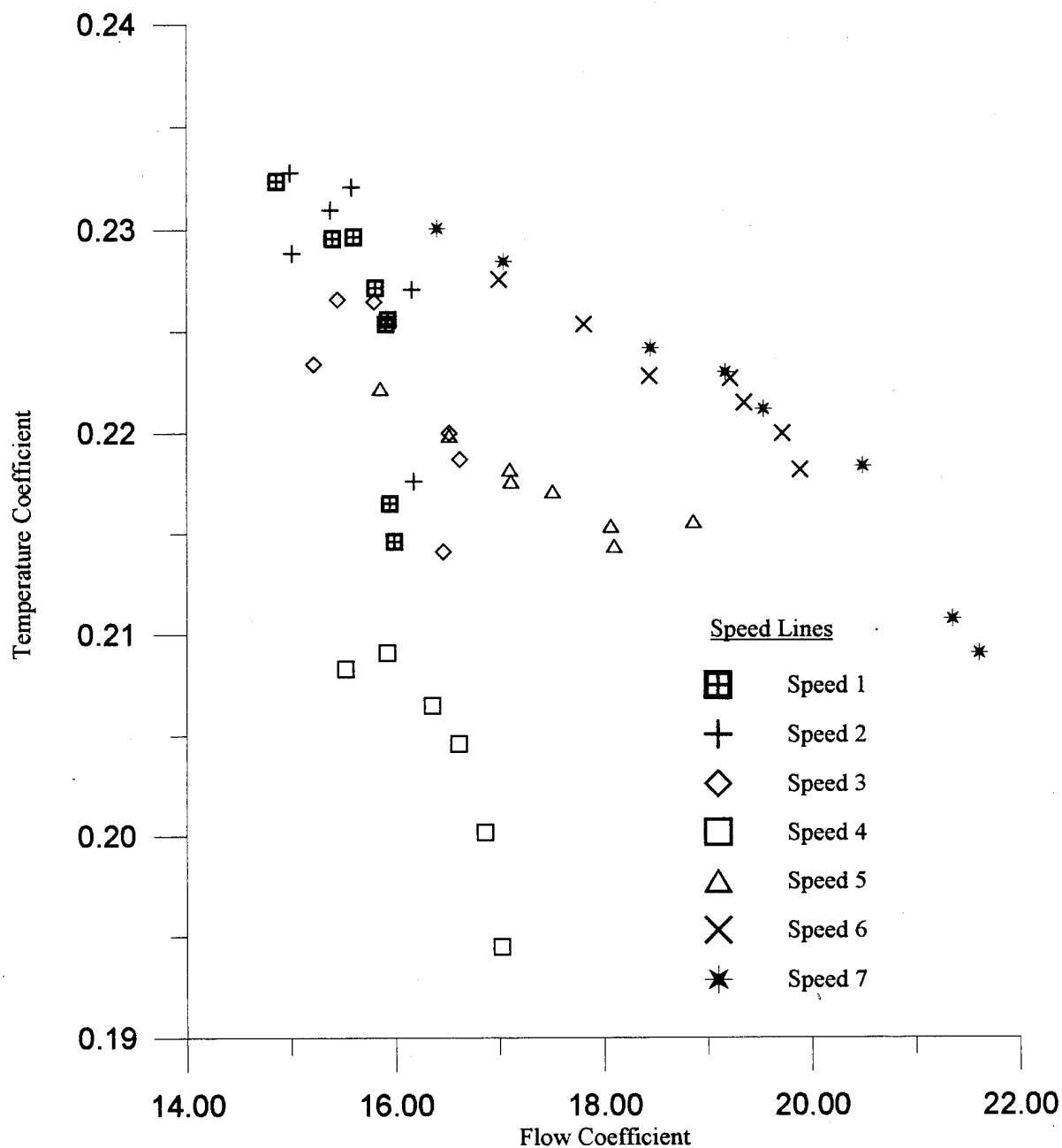
Figure 3.5 Stage 3 Temperature Characteristic
using DYNTECC Data
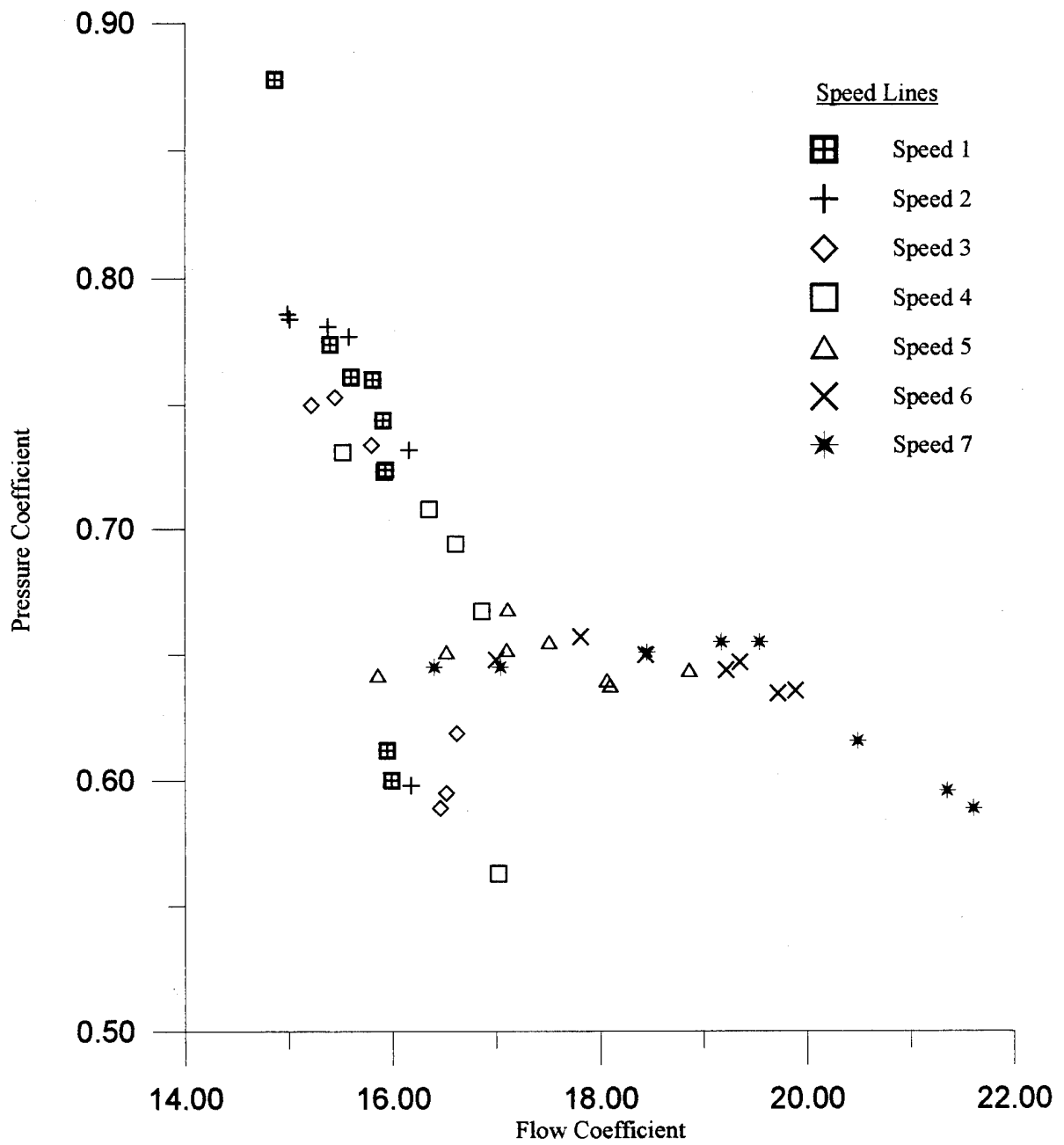
Figure 3.6 Stage 3 Pressure Characteristic
using DYNTECC Data
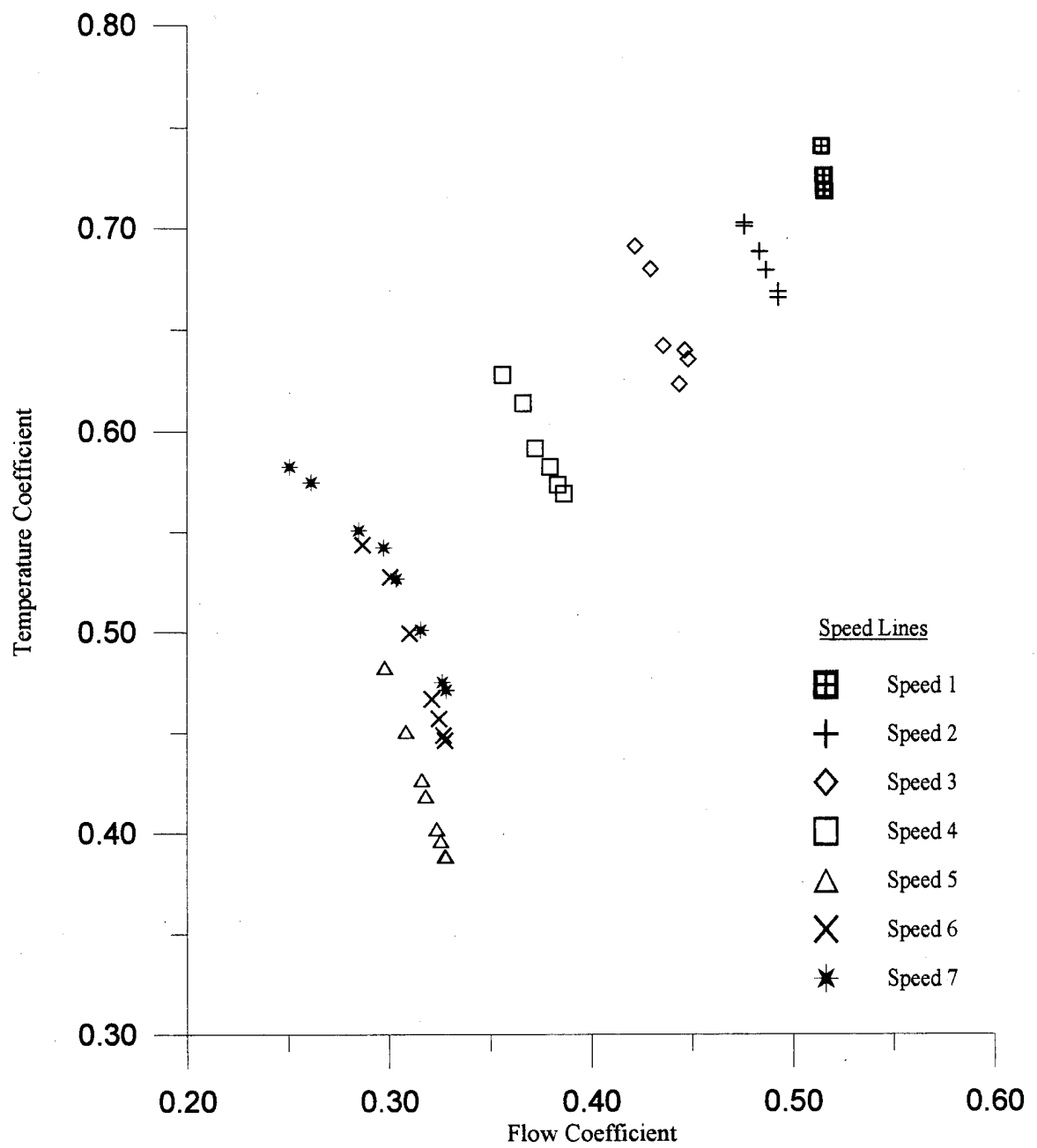
Fig. 3.7 Stage 1 Temperature Characteristic using
Non-Dimensionalized Coefficients
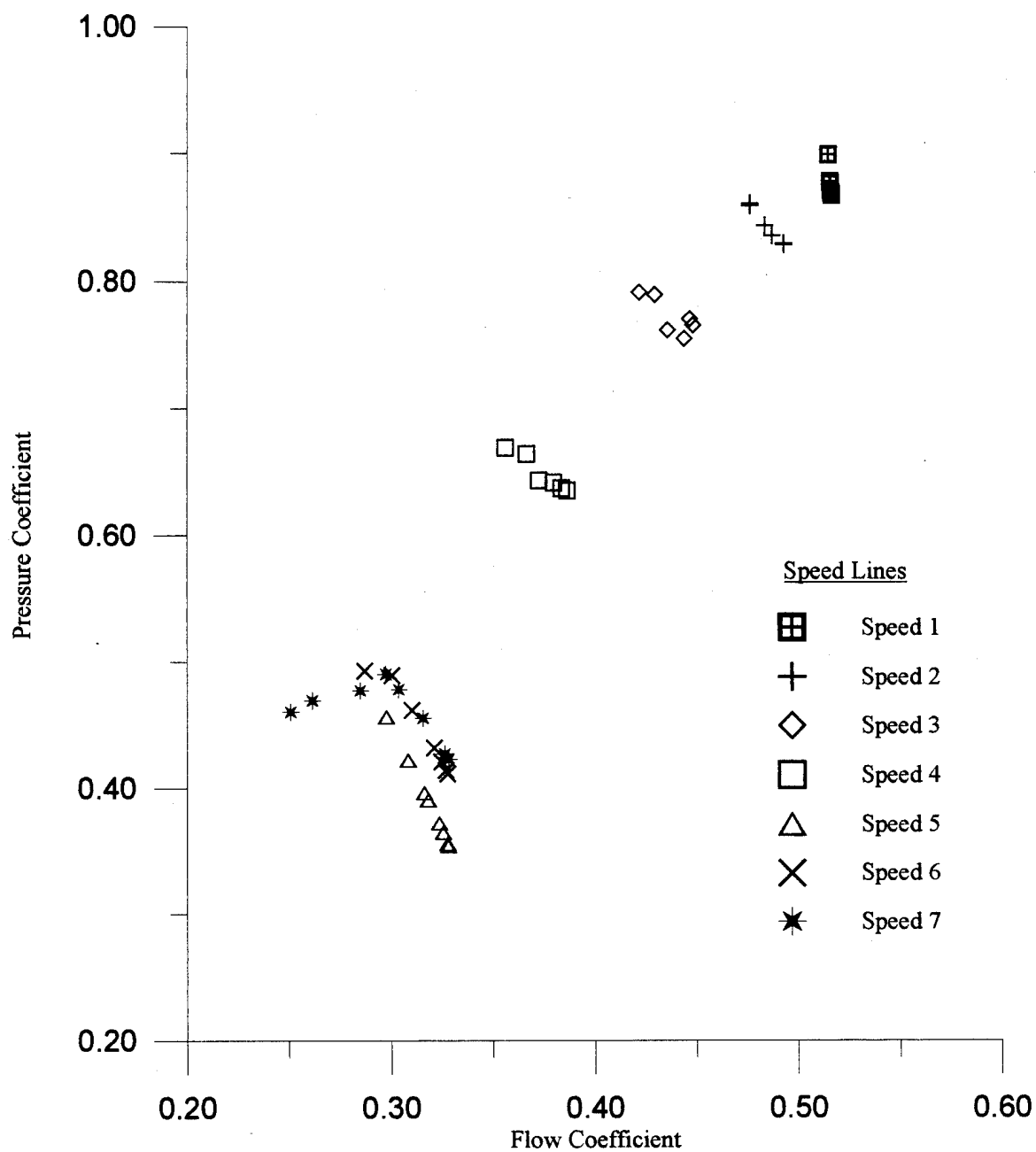
Figure 3.8 Stage 1 Pressure Characteristic using
Non-Dimensionalized Coefficients
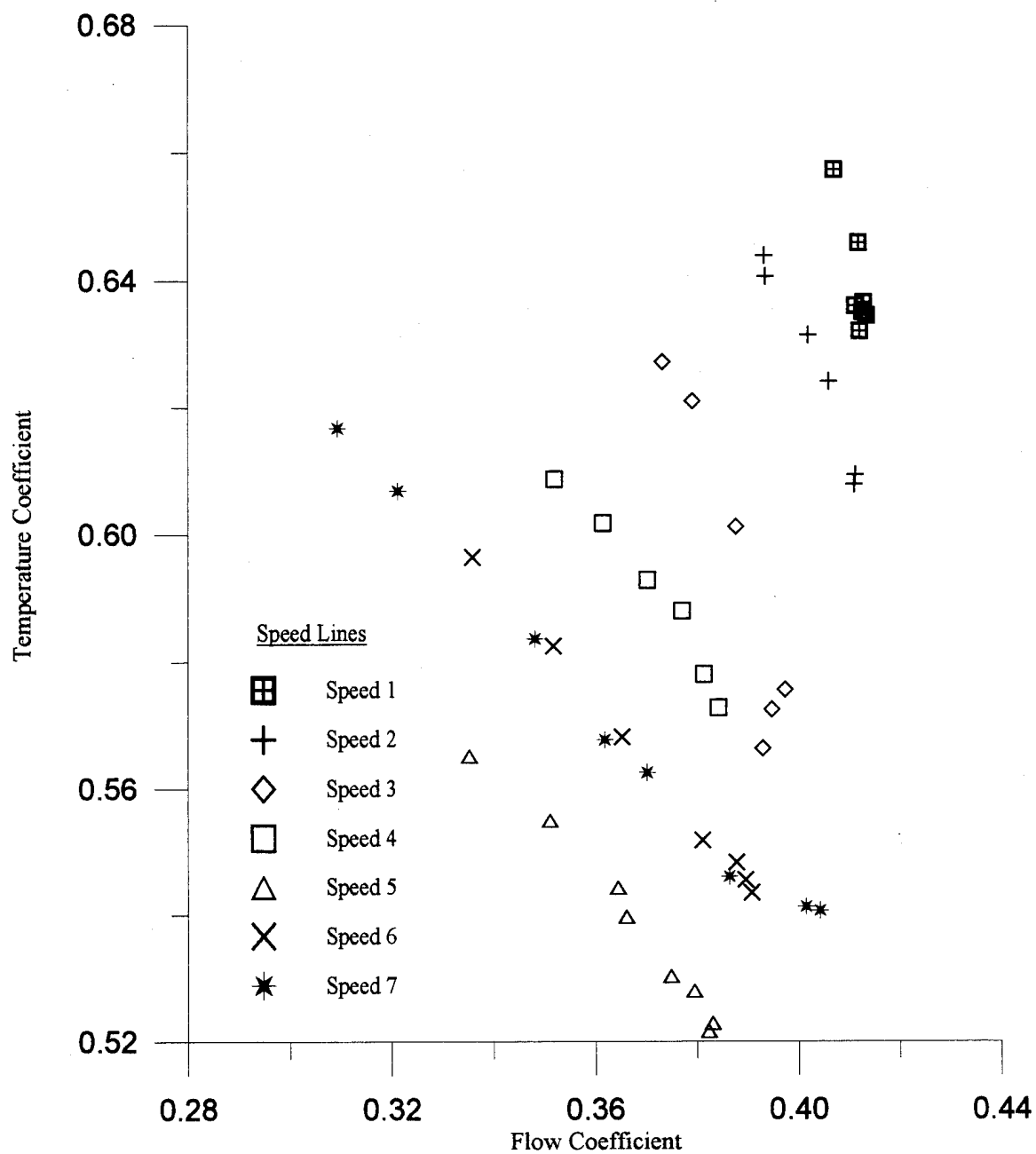
Fig. 3.9 Stage 2 Temperature Characteristic using
Non-Dimensionalized Coefficients
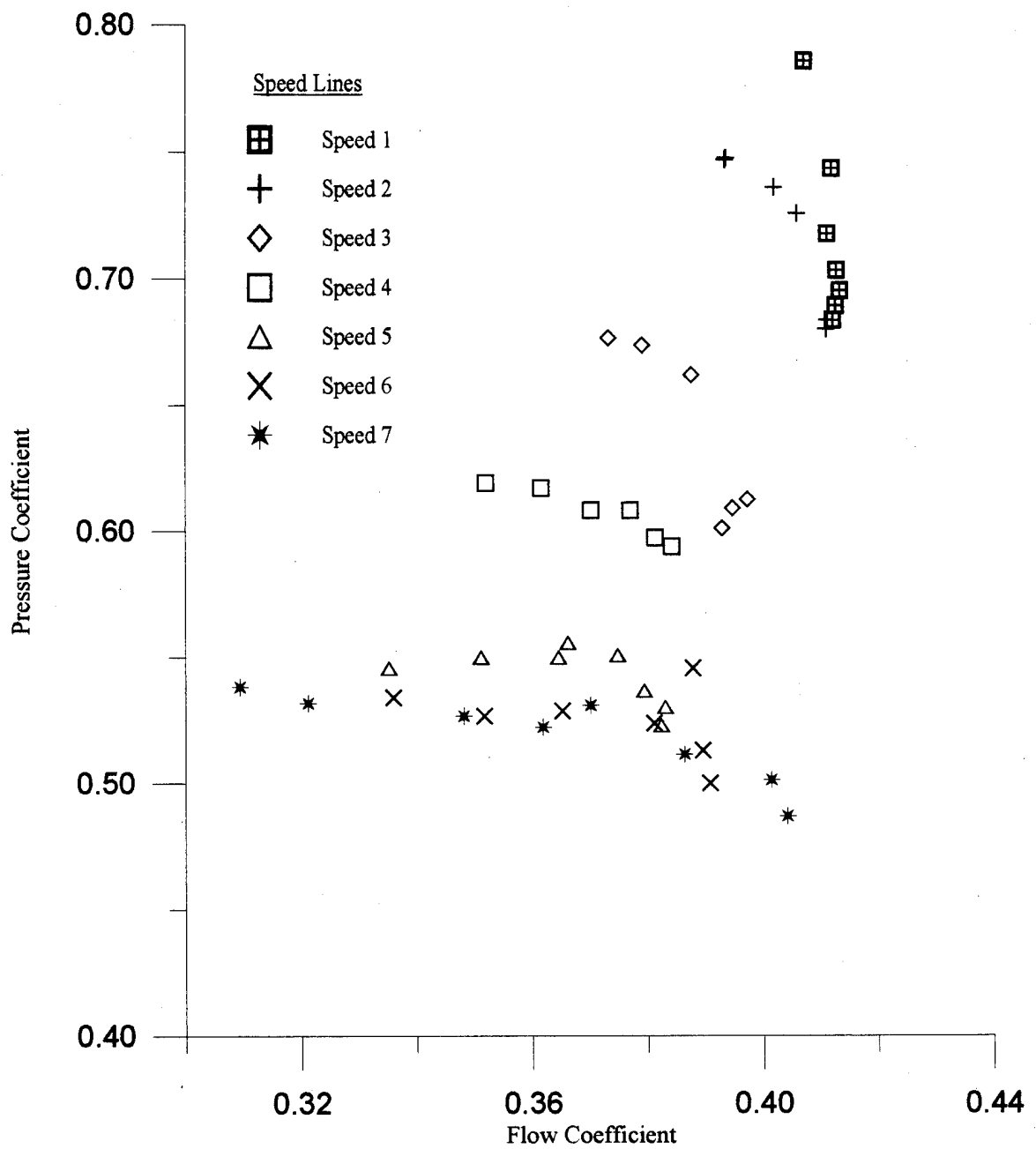
Fig. 3.10 Stage 2 Pressure Characteristic using
Non-Dimensionalized Coefficients
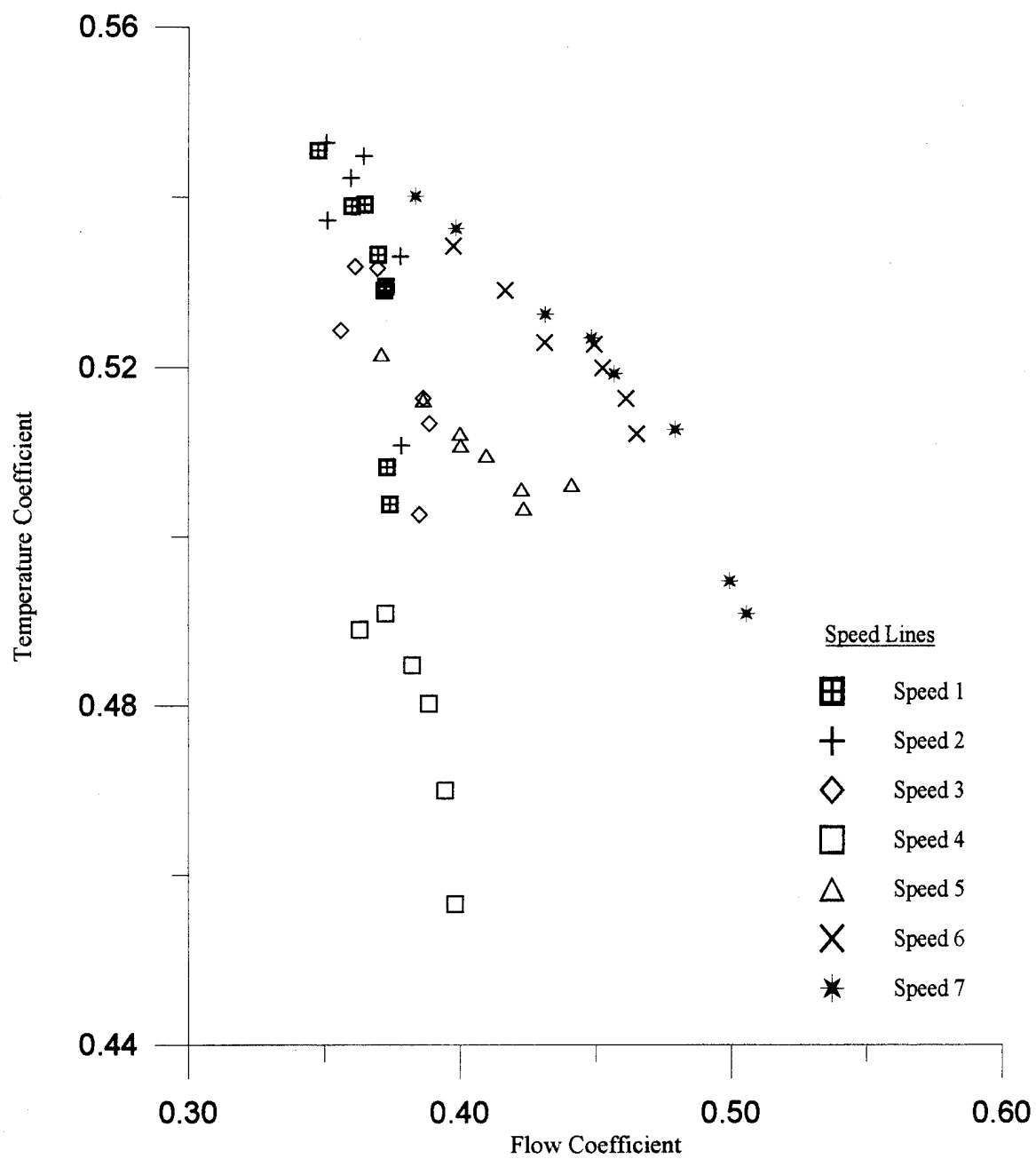
Fig. 3.11 Stage 3 Temperature Characteristic using
Non-Dimensionalized Coefficients
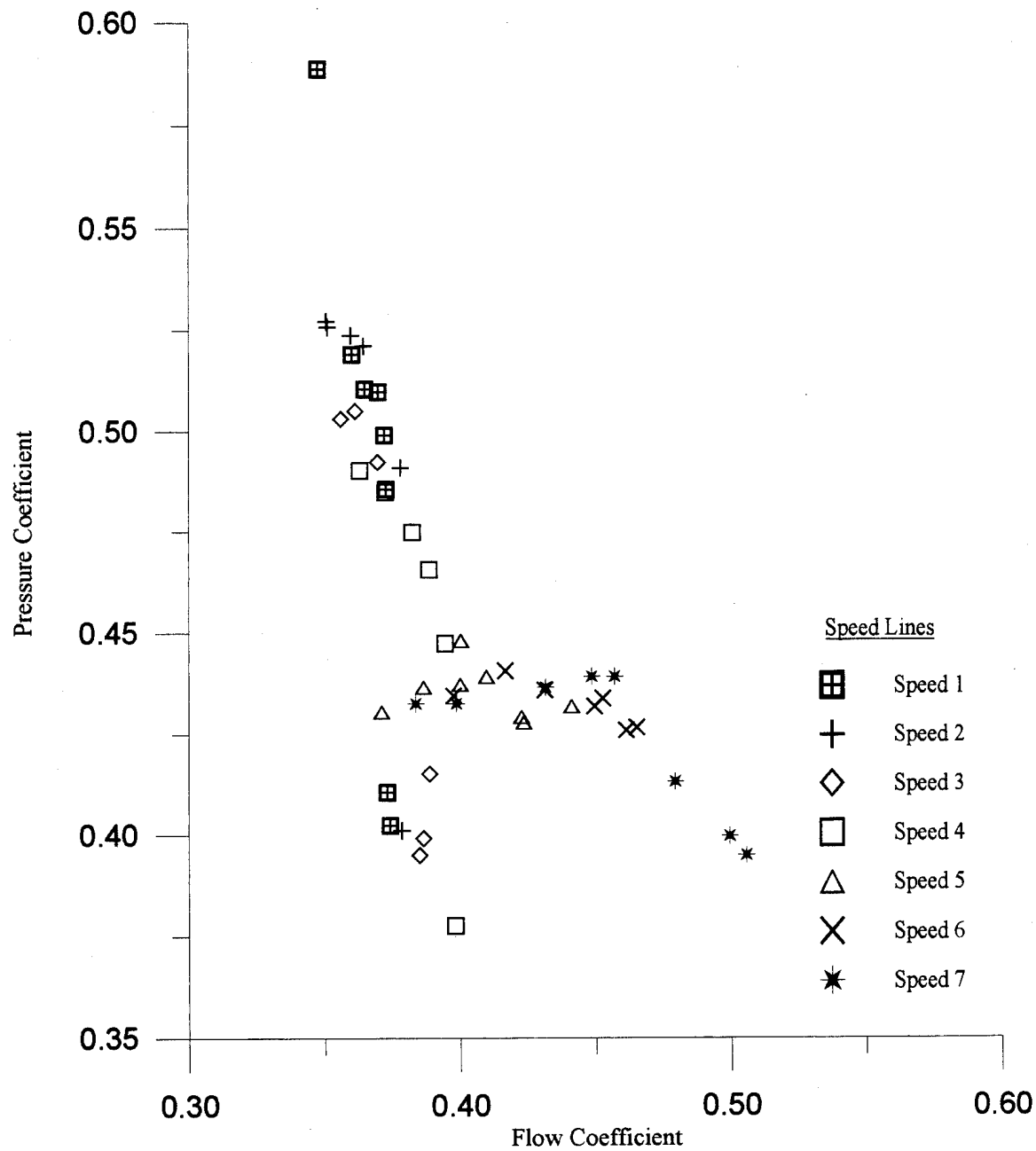
Fig. 3.12 Stage 3 Pressure Characteristic using
Non-Dimensionalized Coefficients
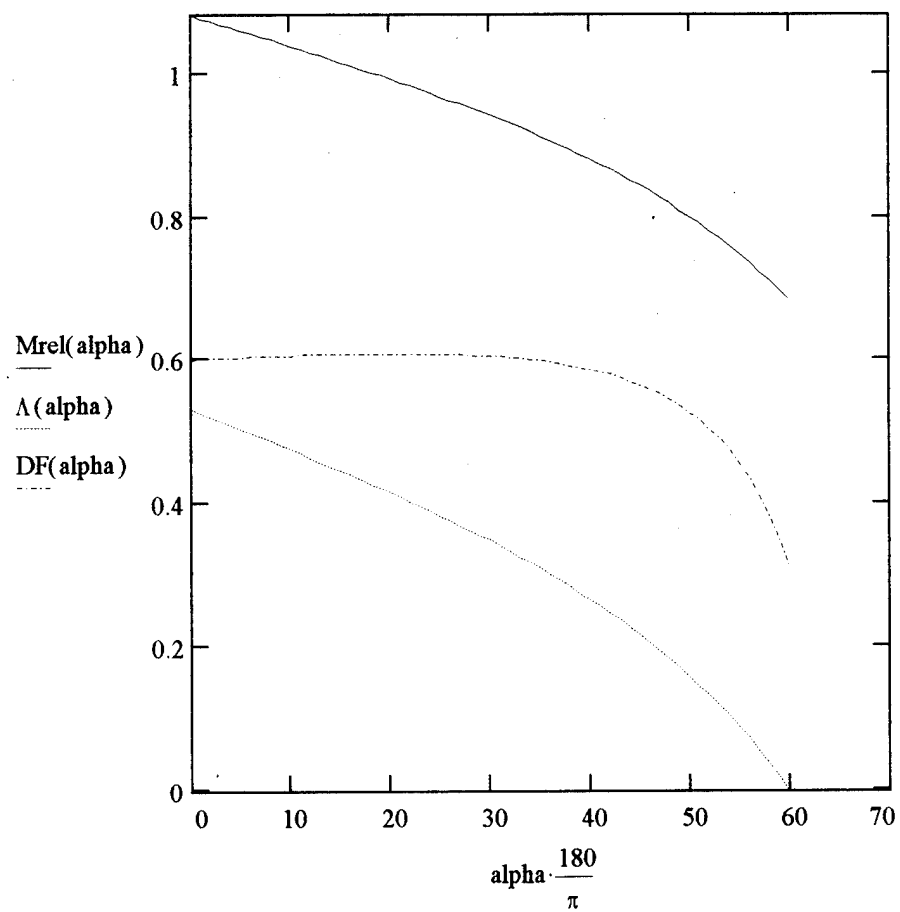
Figure 3.13 Diffusion Factor, Degree of Reaction, and Relative Mach Number vs. α_1 for Reference Curve 1
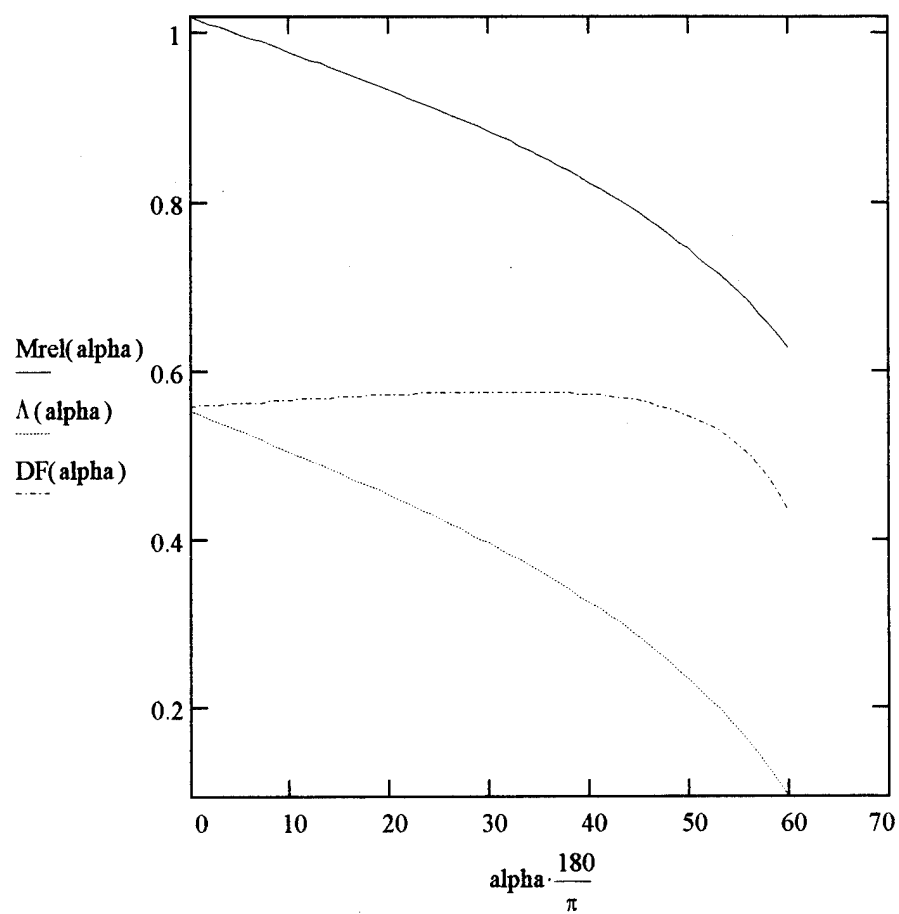
Figure 3.14 Diffusion Factor, Degree of Reaction, and Relative Mach
Number vs. α_1 for Reference Curve 2
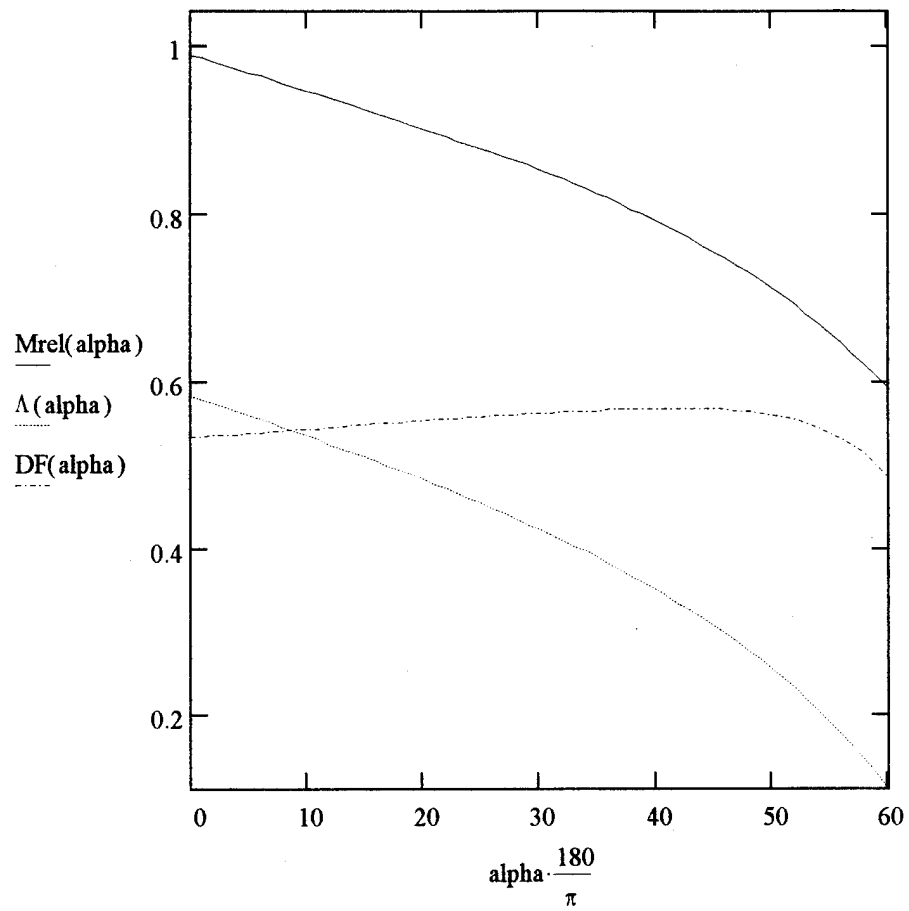
Figure 3.15 Diffusion Factor, Degree of Reaction, and Relative Mach
Number vs. α_1 for Reference Curve 3
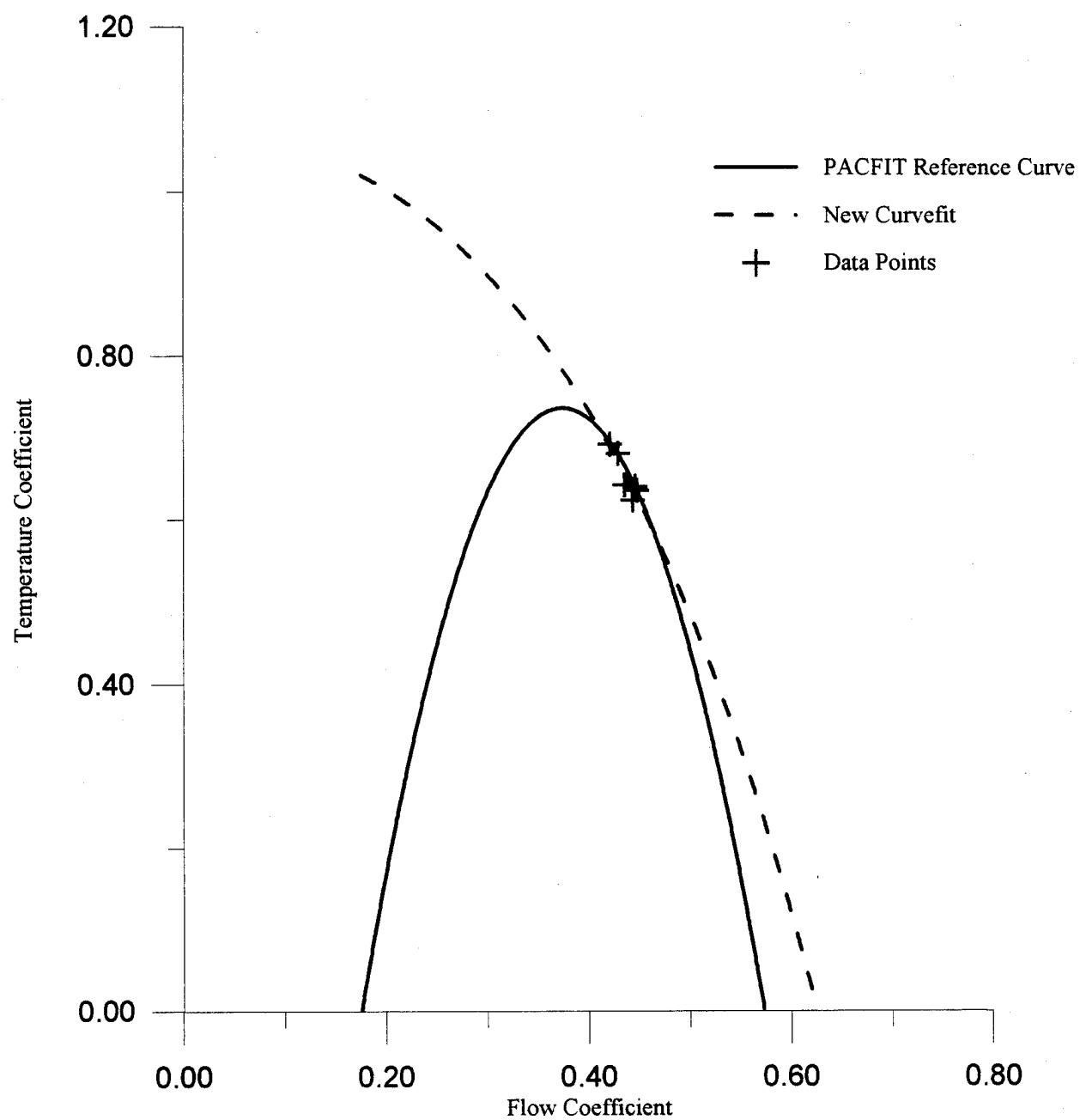
Figure 3.16 DYNTECC Reference Curve 1
versus New Curvefit
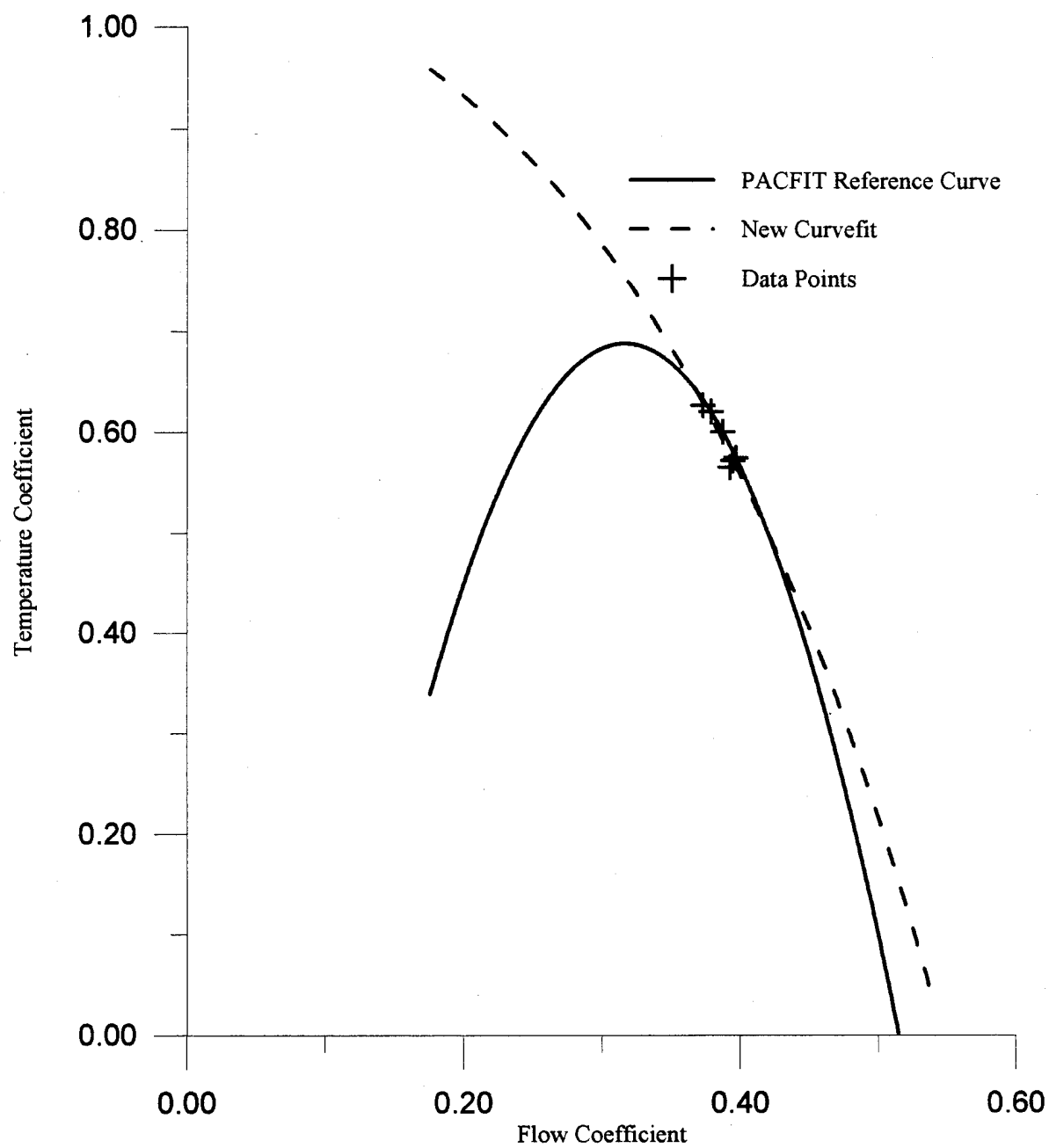
Figure 3.17 DYNTECC Reference Curve 2
versus New Curvefit
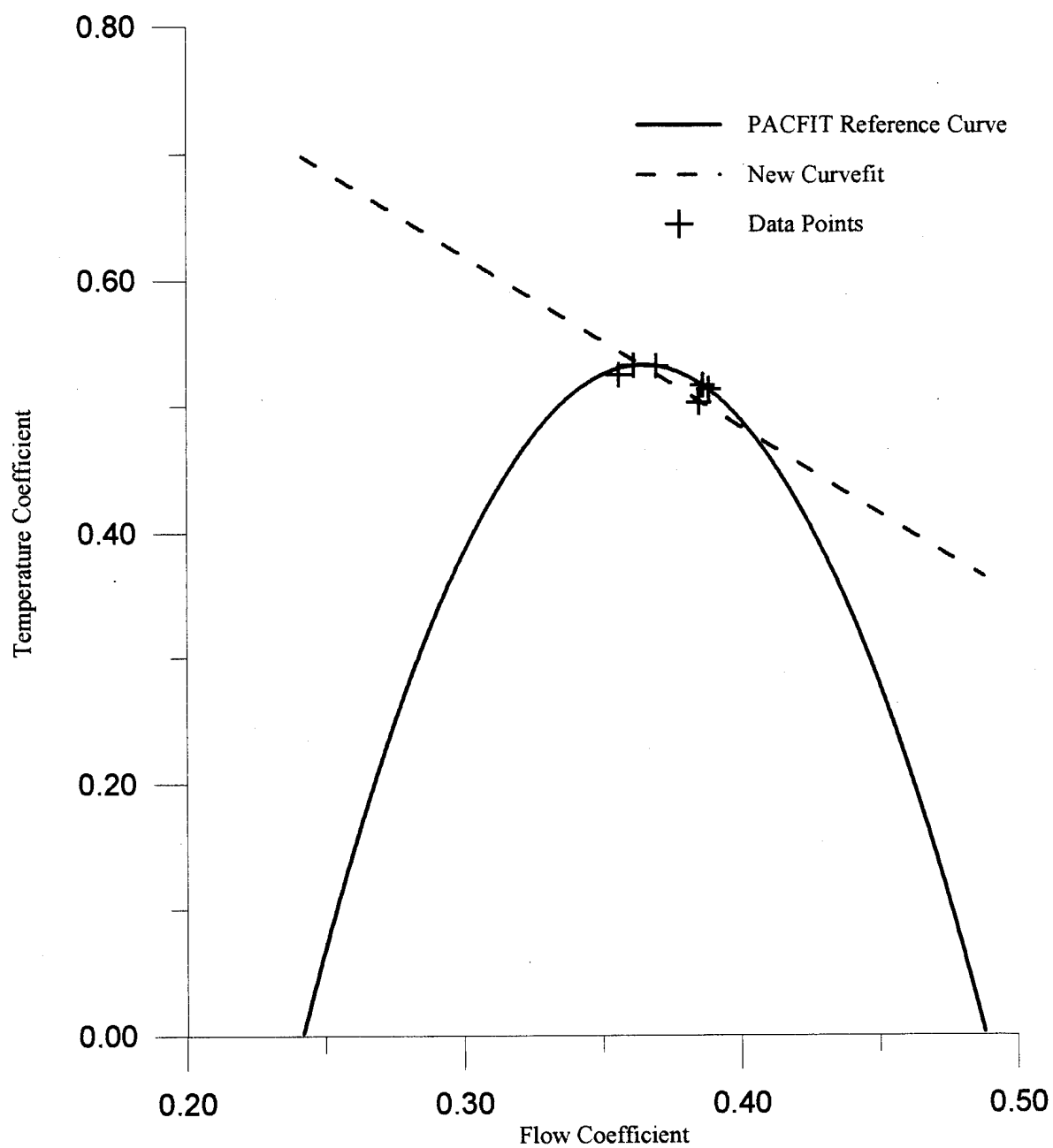
Figure 3.18 DYNTECC Reference Curve 3
versus New Curvefit
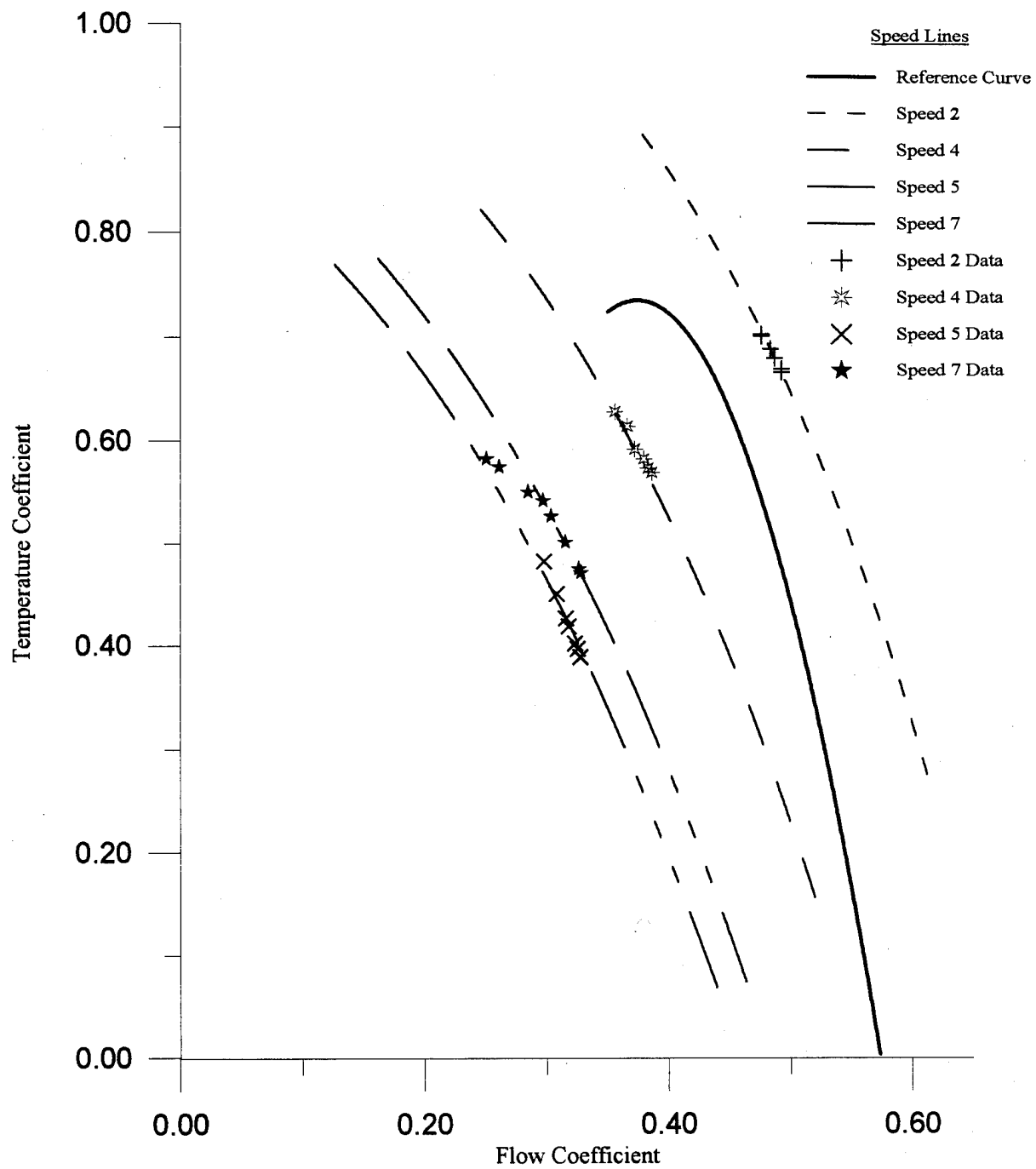
Figure 4.1 Stage 1 Temperature Characteristic
Prediction using Curve 1
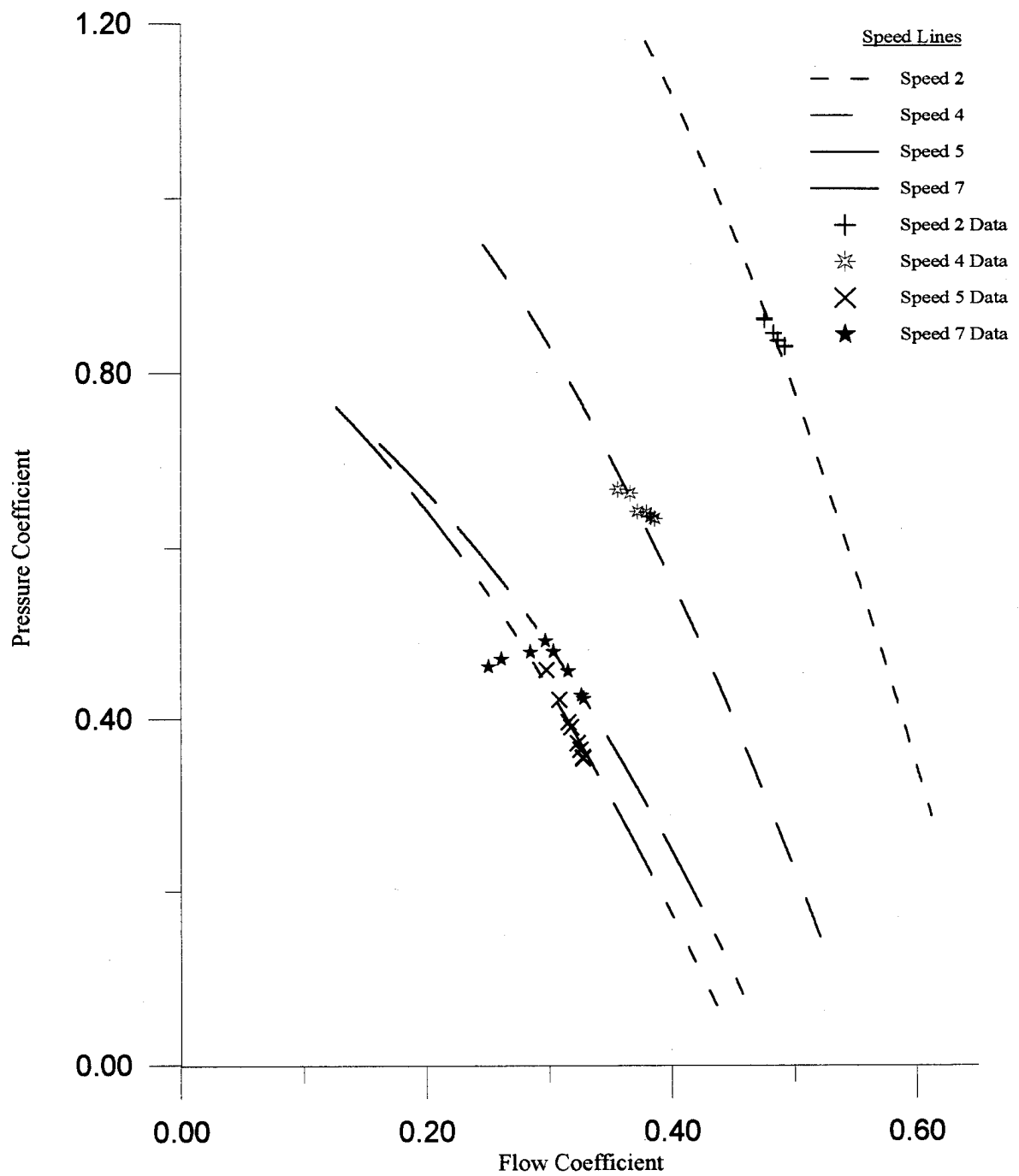
Figure 4.2 Stage 1 Pressure Characteristic
Prediction using Curve 1
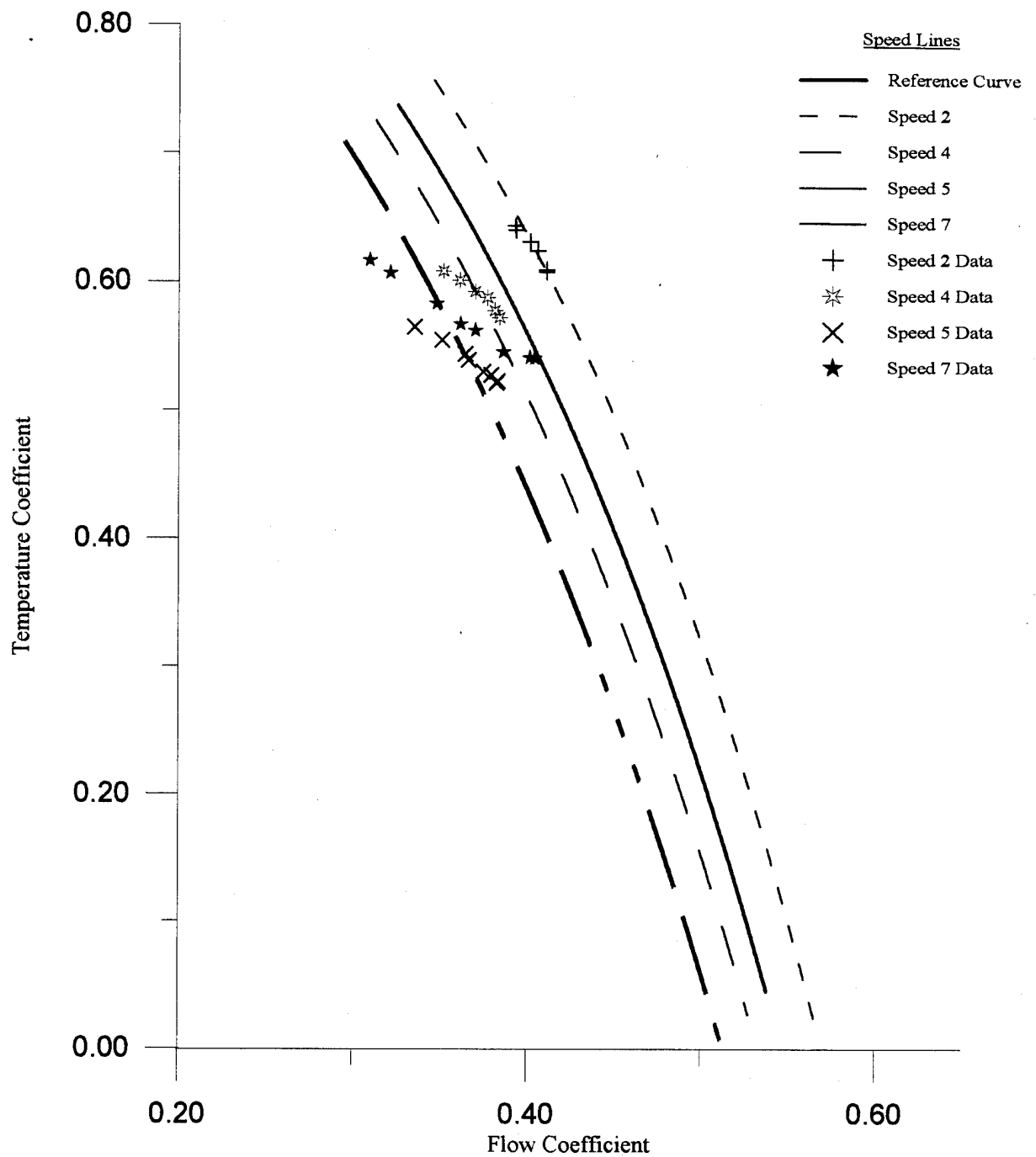
Figure 4.3 Stage 2 Temperature Characteristic
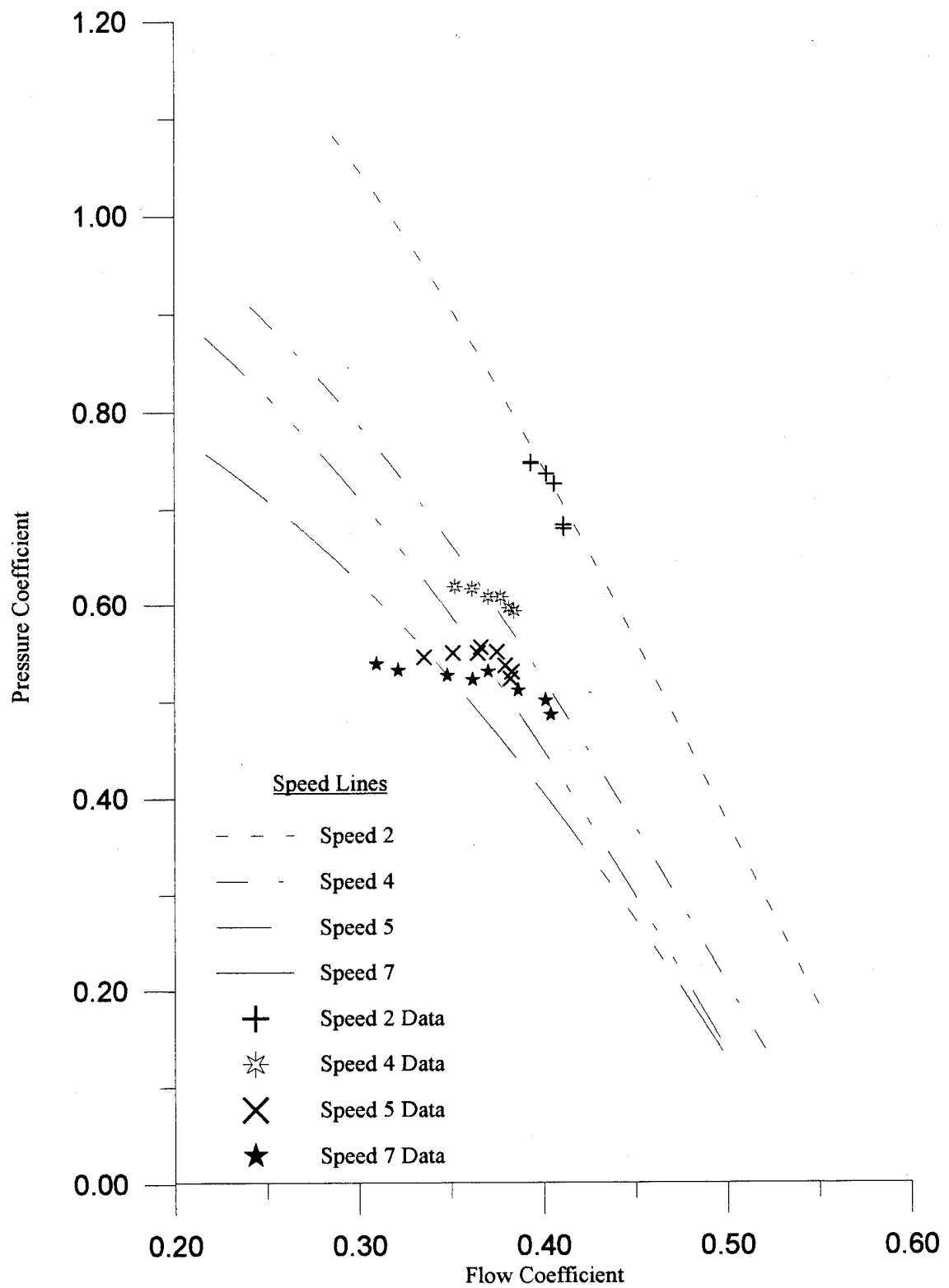Prediction using Curve 2
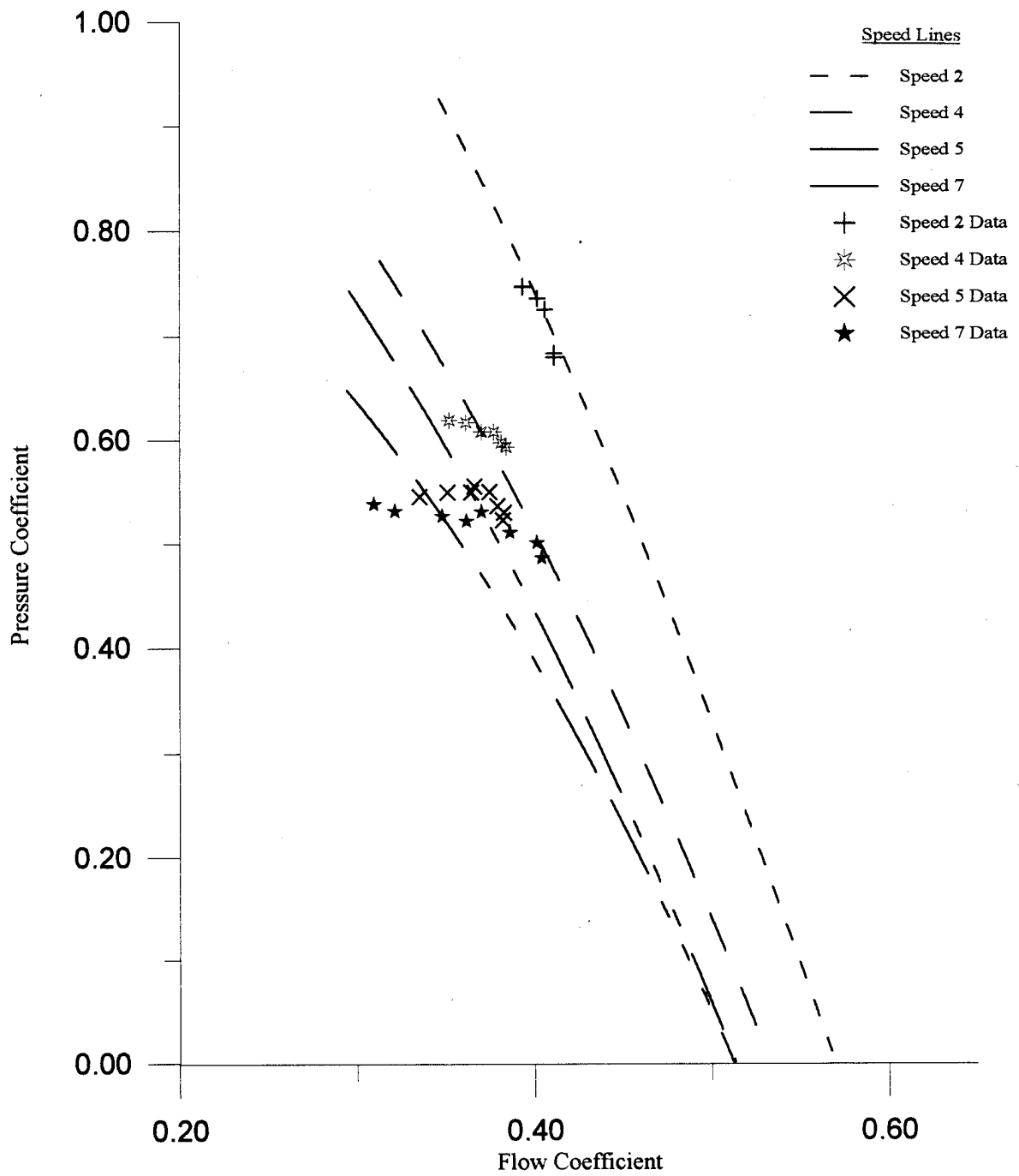
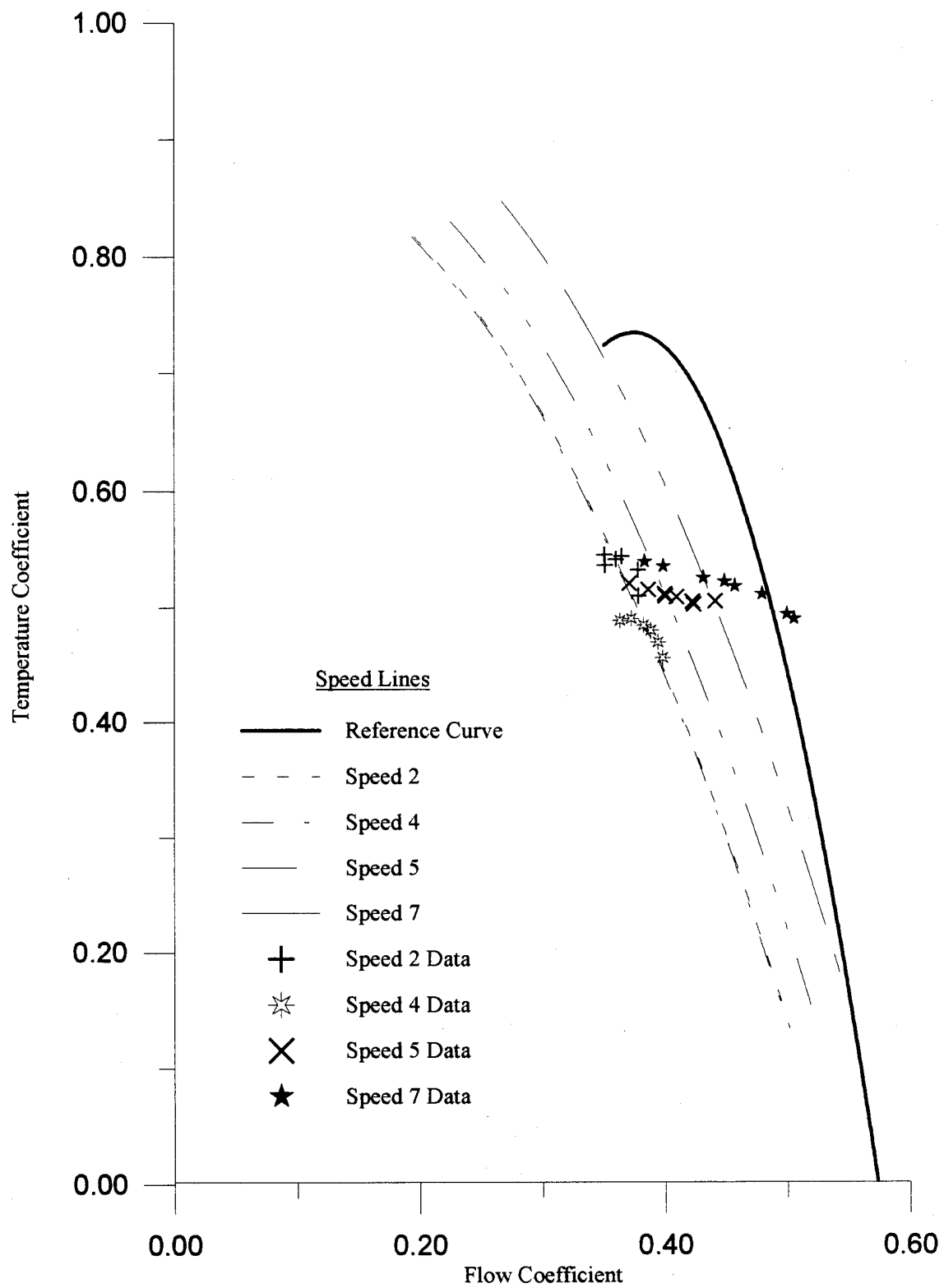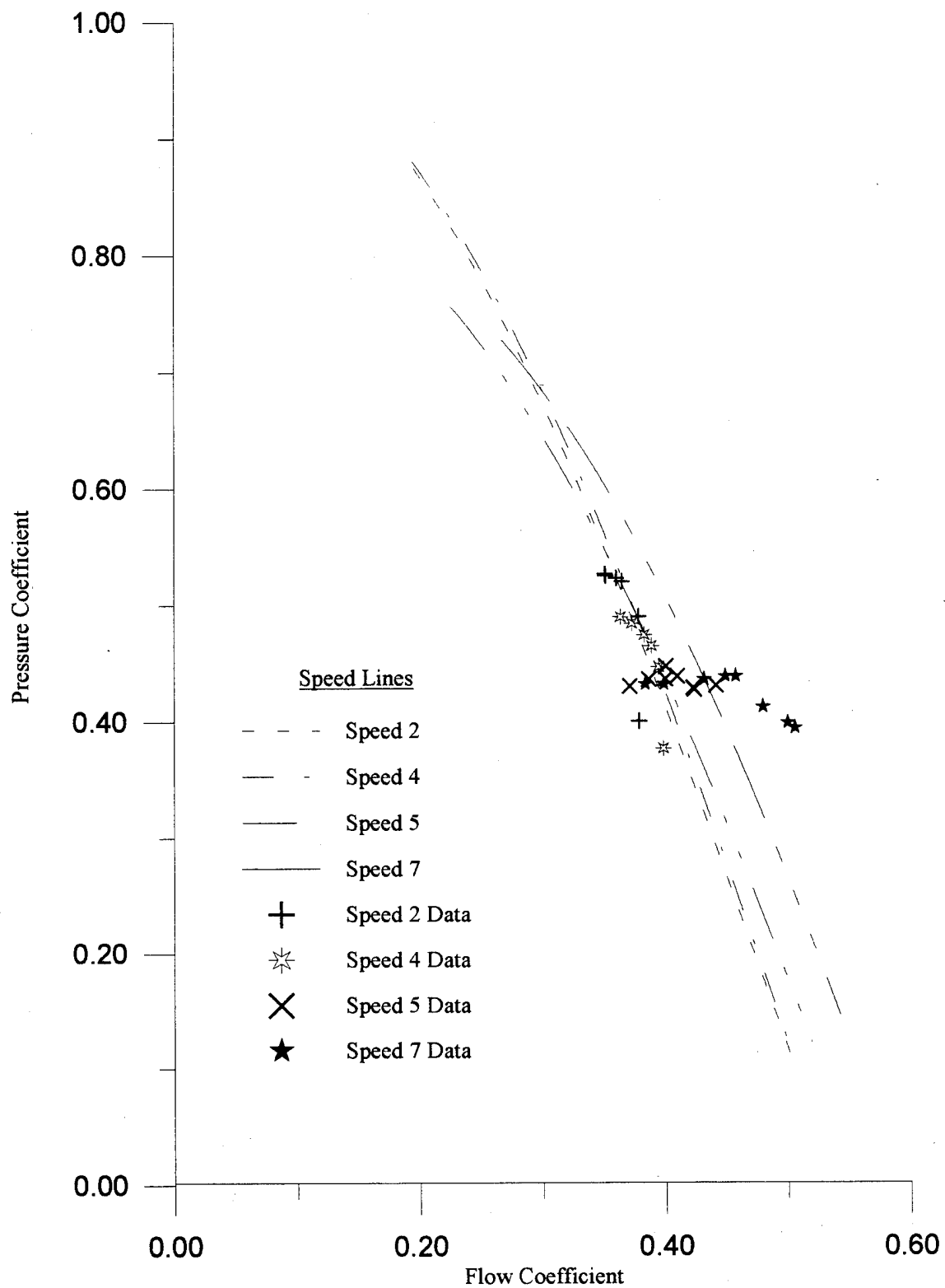Figure 4.4 Stage 2 Pressure Characteristic
Prediction using Curve 2
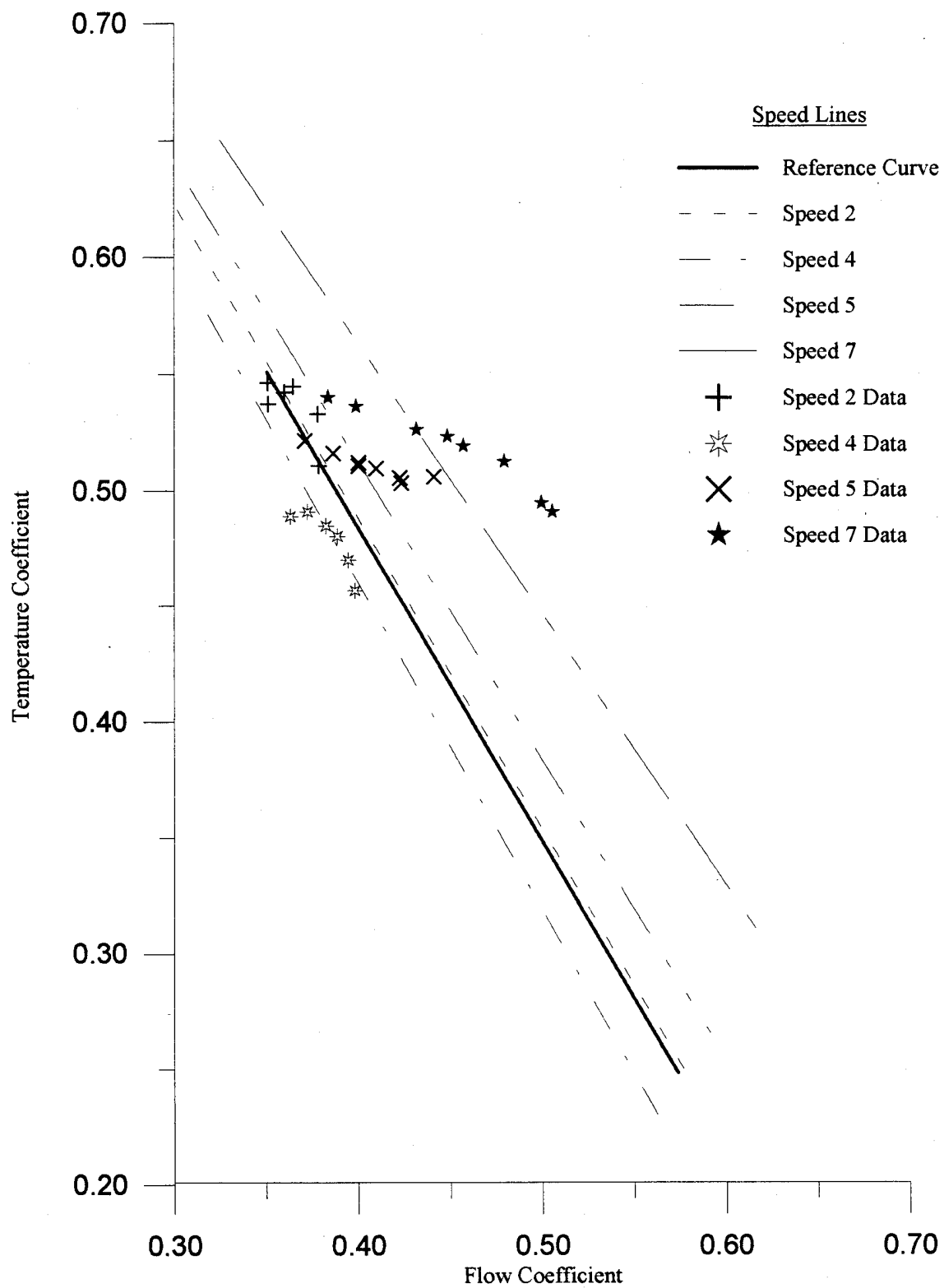
Figure 4.5 Stage 3 Temperature Characteristic
Prediction using Curve 3
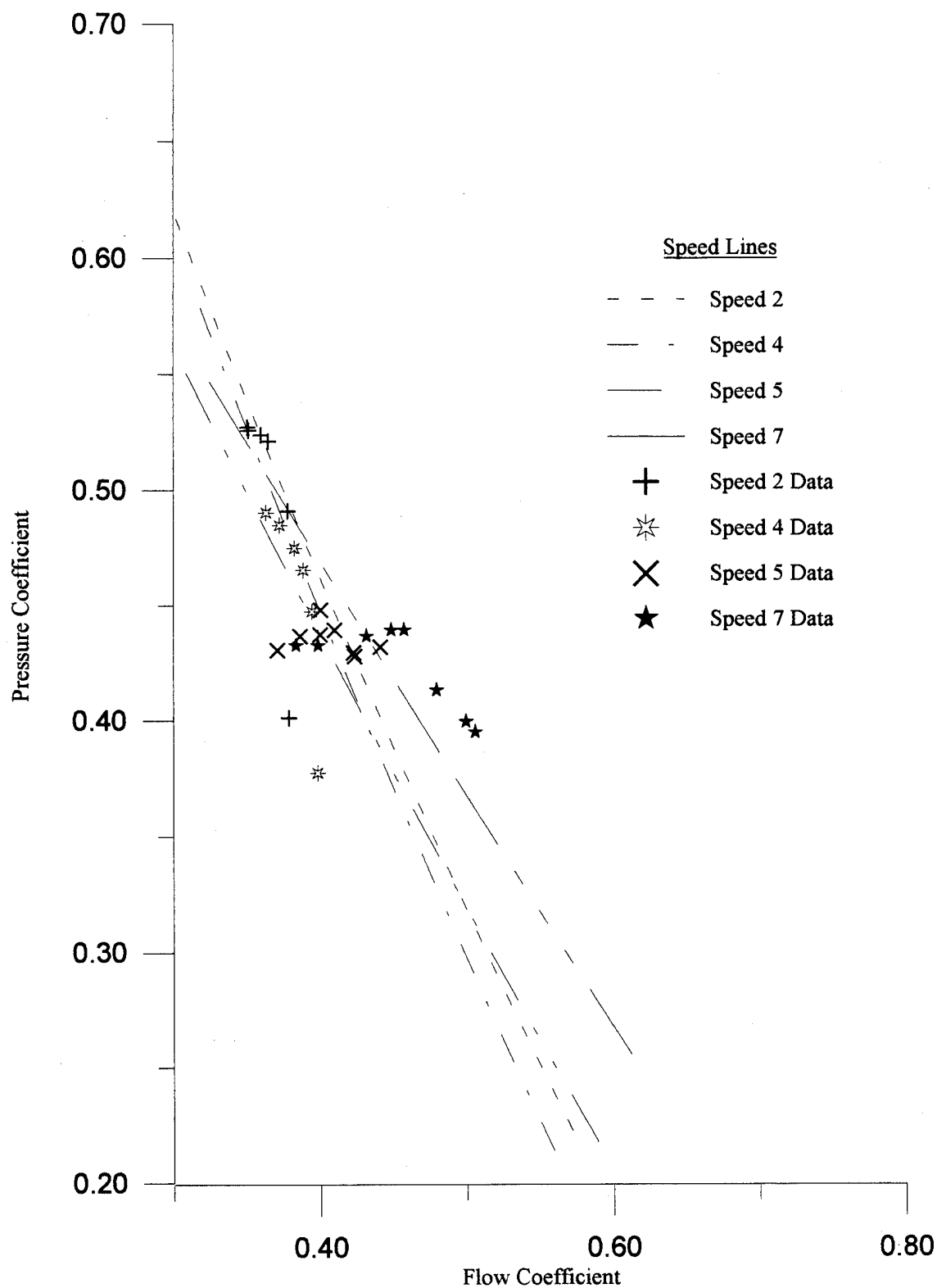
Figure 4.6 Stage 3 Pressure Characteristic
Prediction using Curve 3
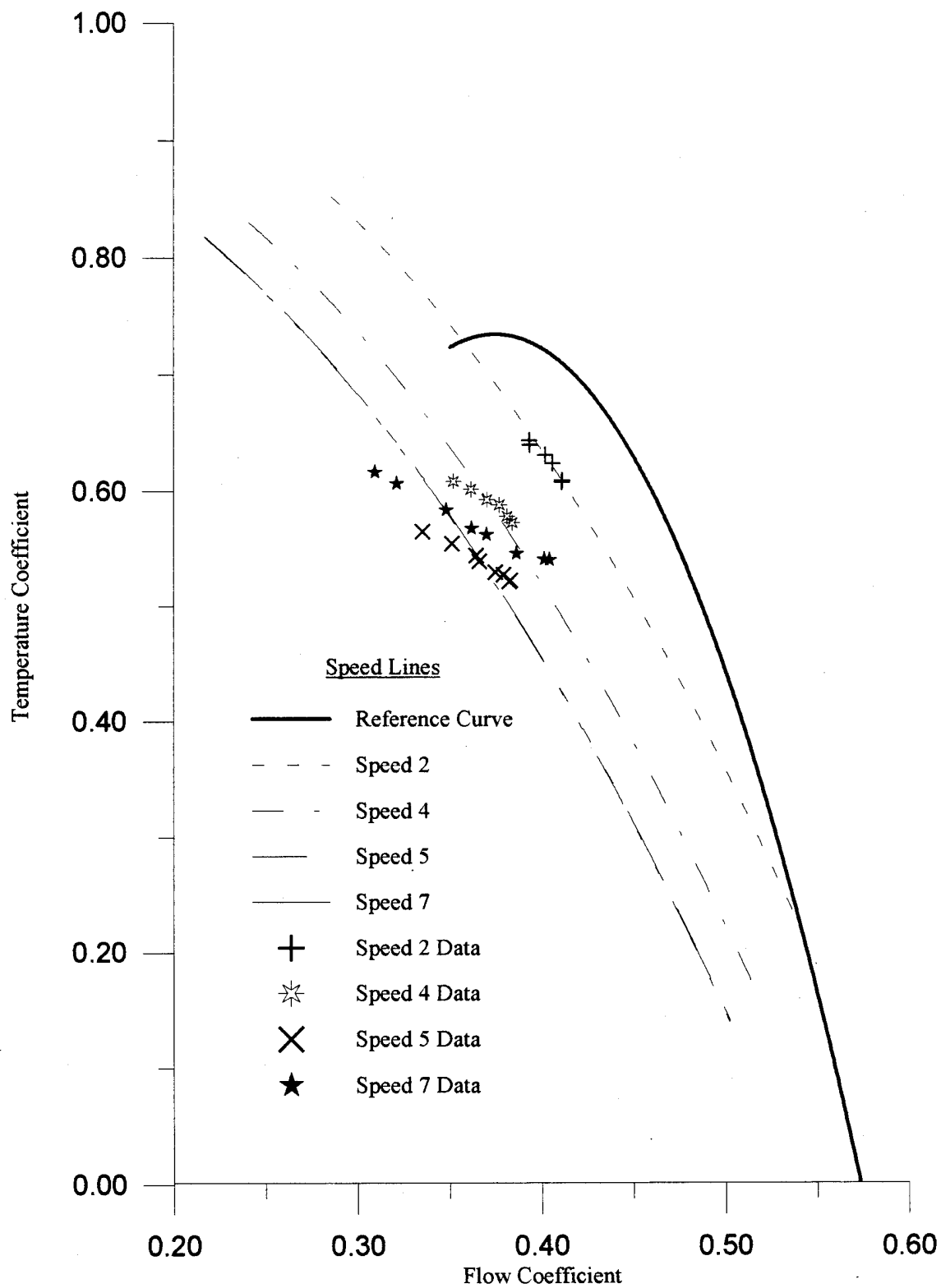
Figure 4.7 Stage 2 Temperature
Characteristic Prediction using Curve 1

Figure 4.8 Stage 2 Pressure Characteristic
Prediction using Curve 1

Figure 4.9 Stage 3 Temperature Characteristic
Prediction using Curve 1

Figure 4.10 Stage 3 Pressure Characteristic
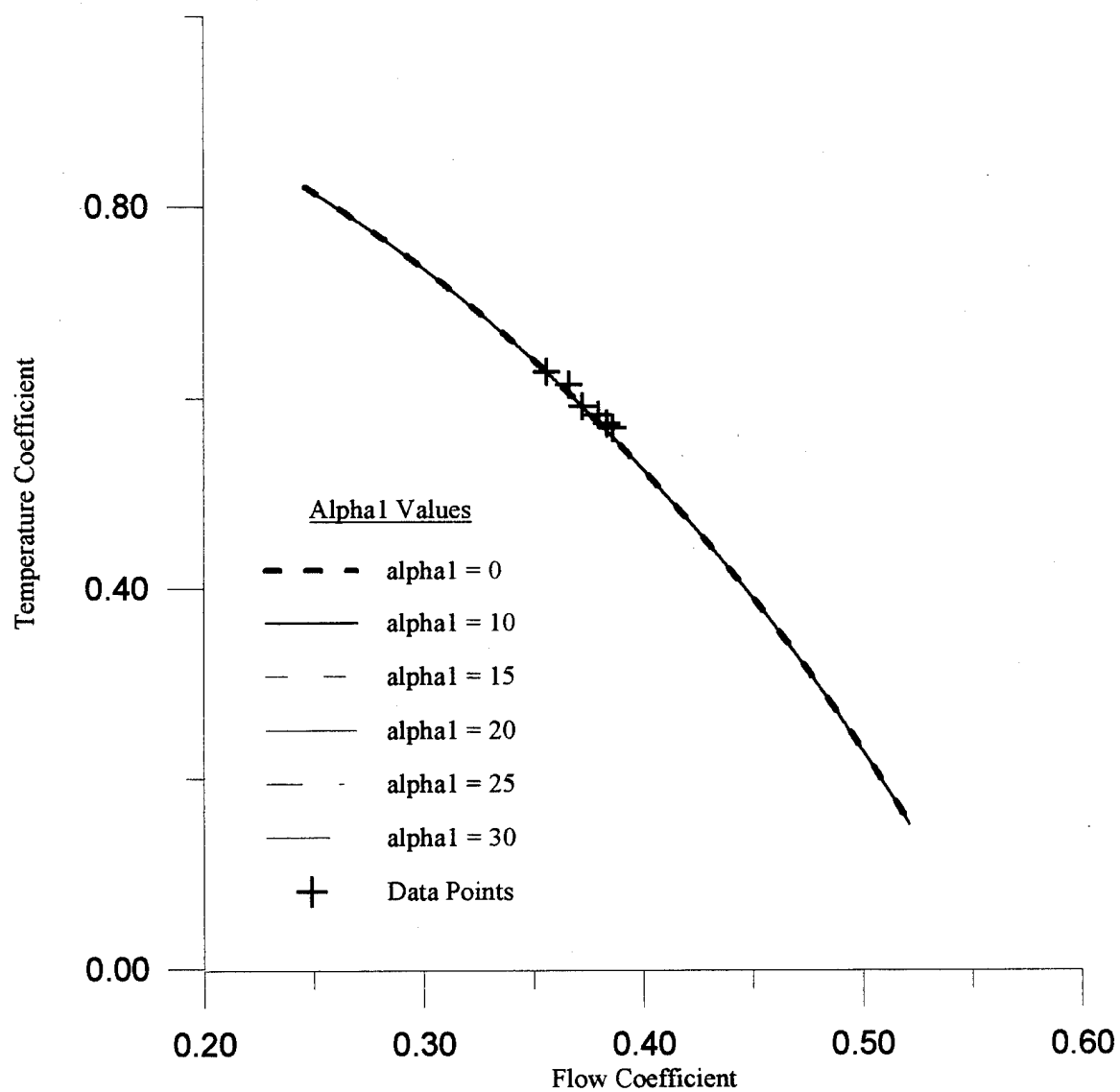Prediction using Curve 1

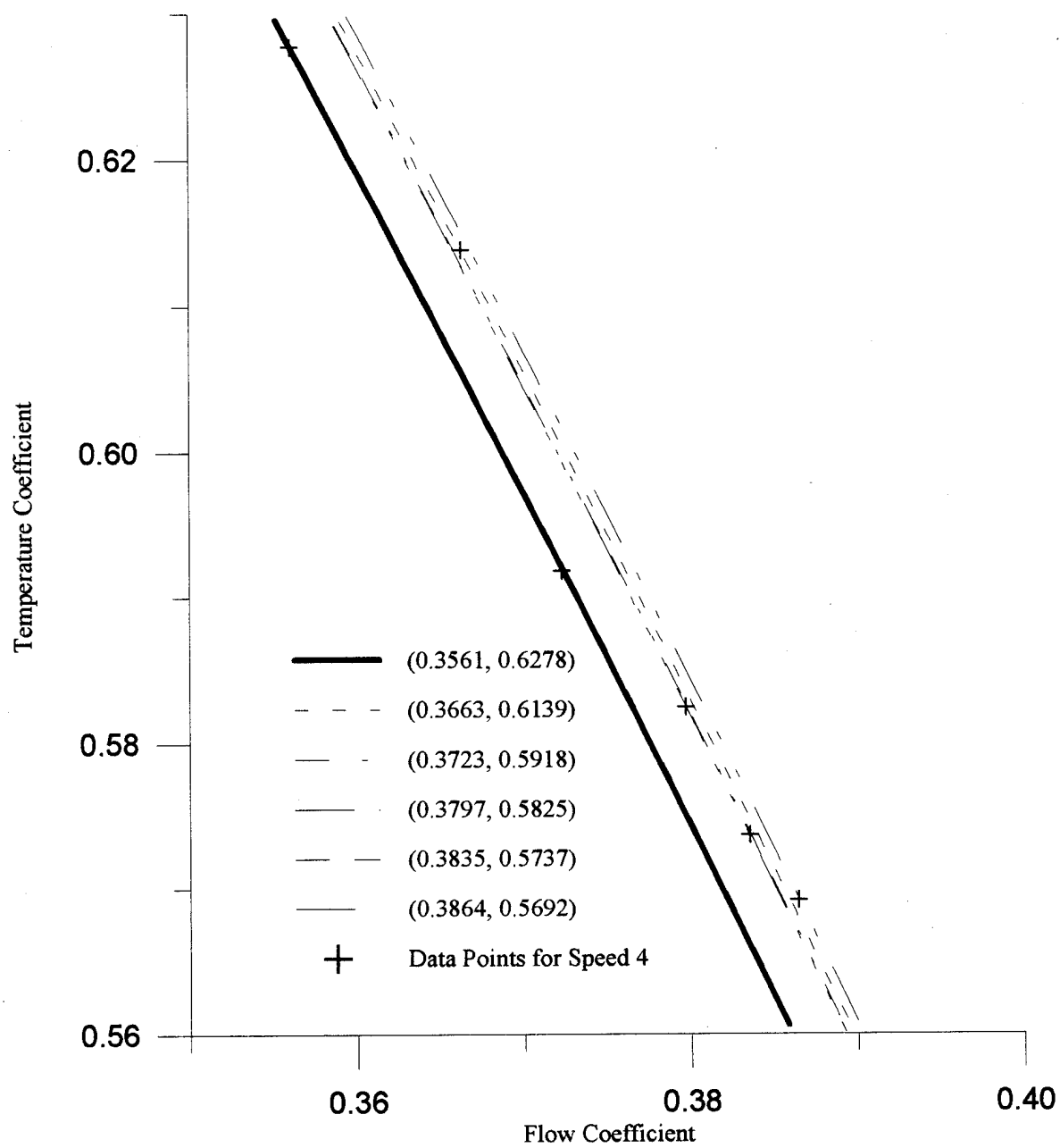Figure 4.11 Influence of Alpha1 on Characteristic Prediction

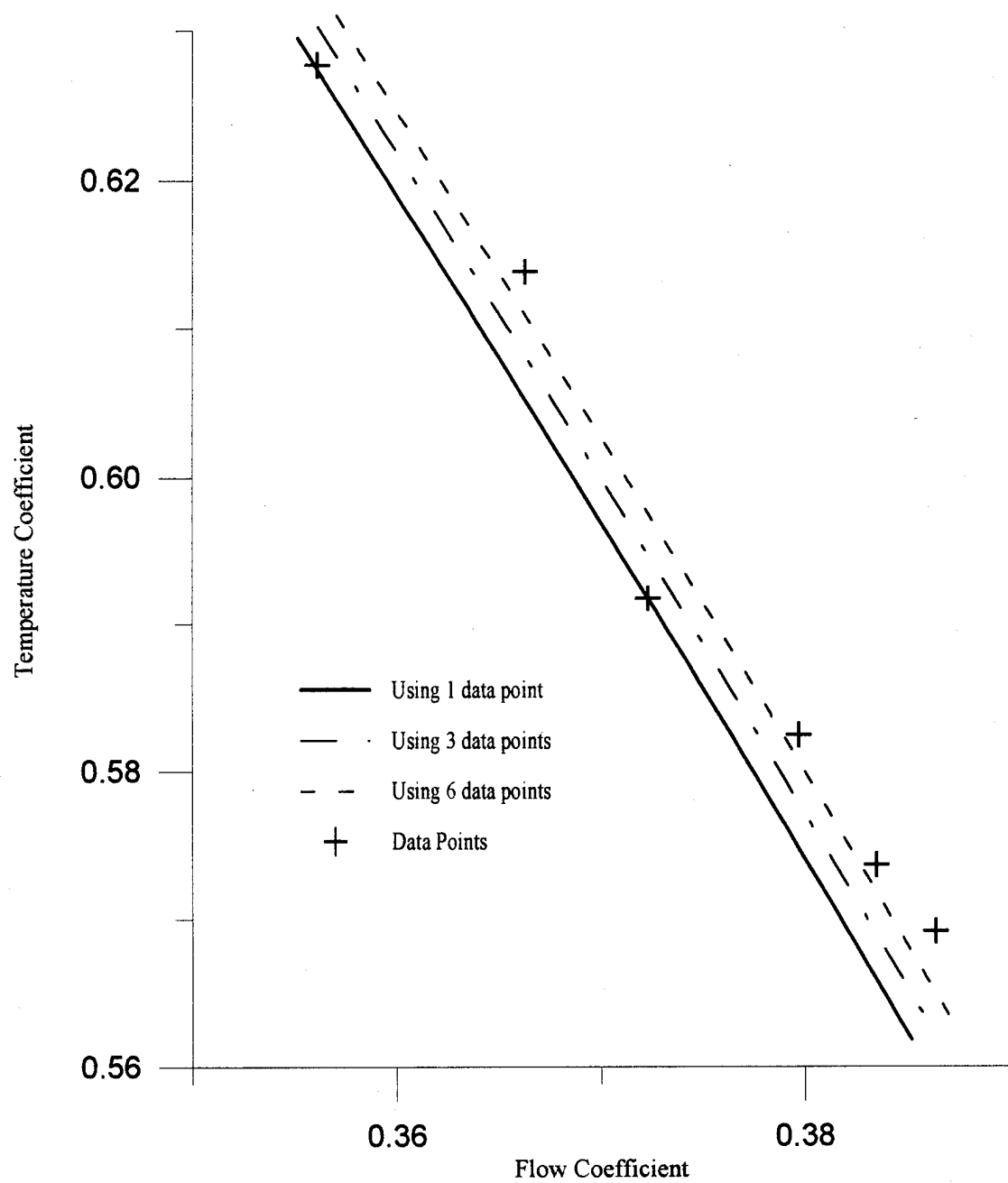Figure 4.12 Effect of Given Data Point on Curve Prediction

Figure 4.13 Improvement in Temperature Characteristic
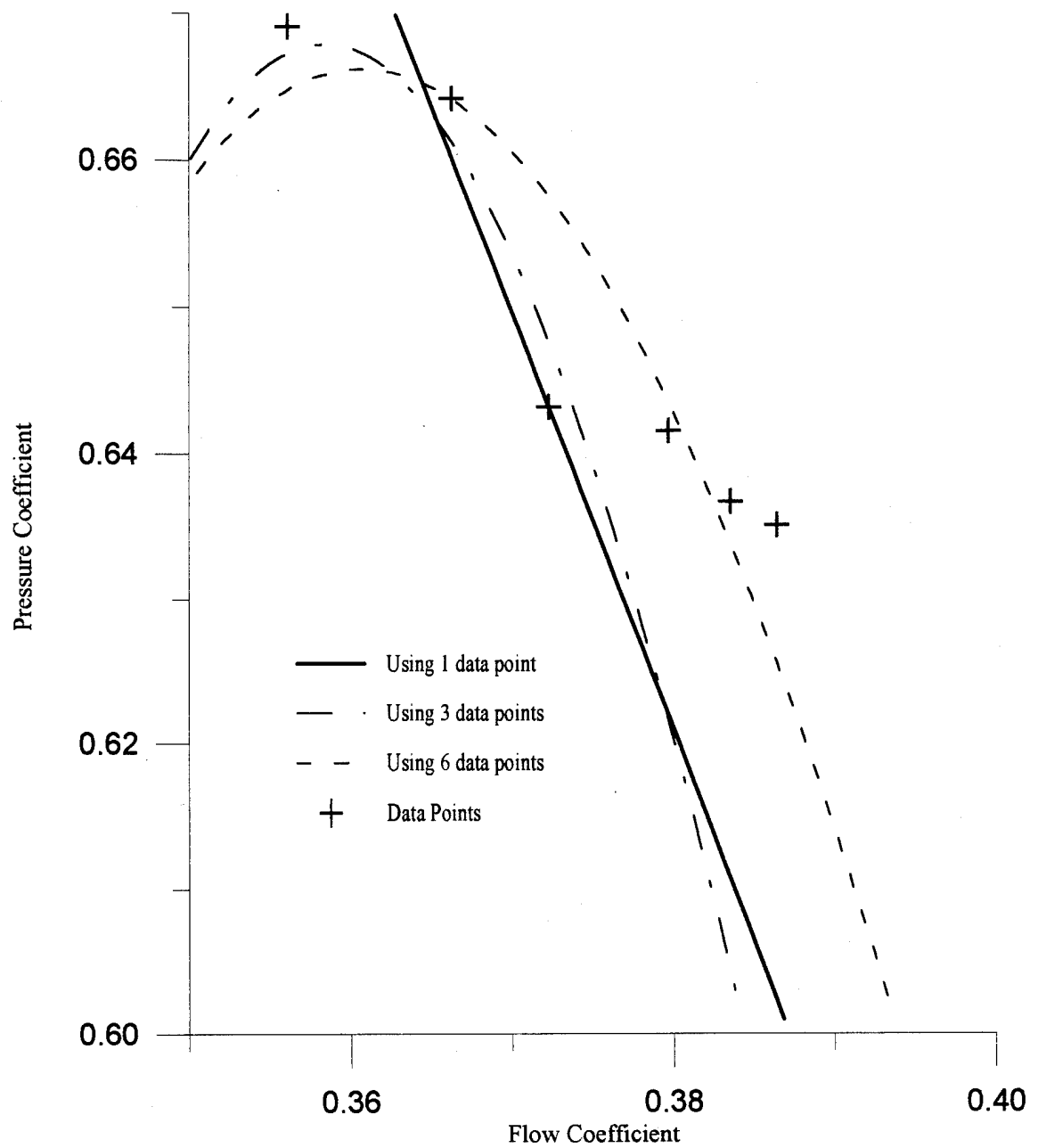Prediction due to Additional Data Points

Figure 4.14 Improvement in Pressure Characteristic
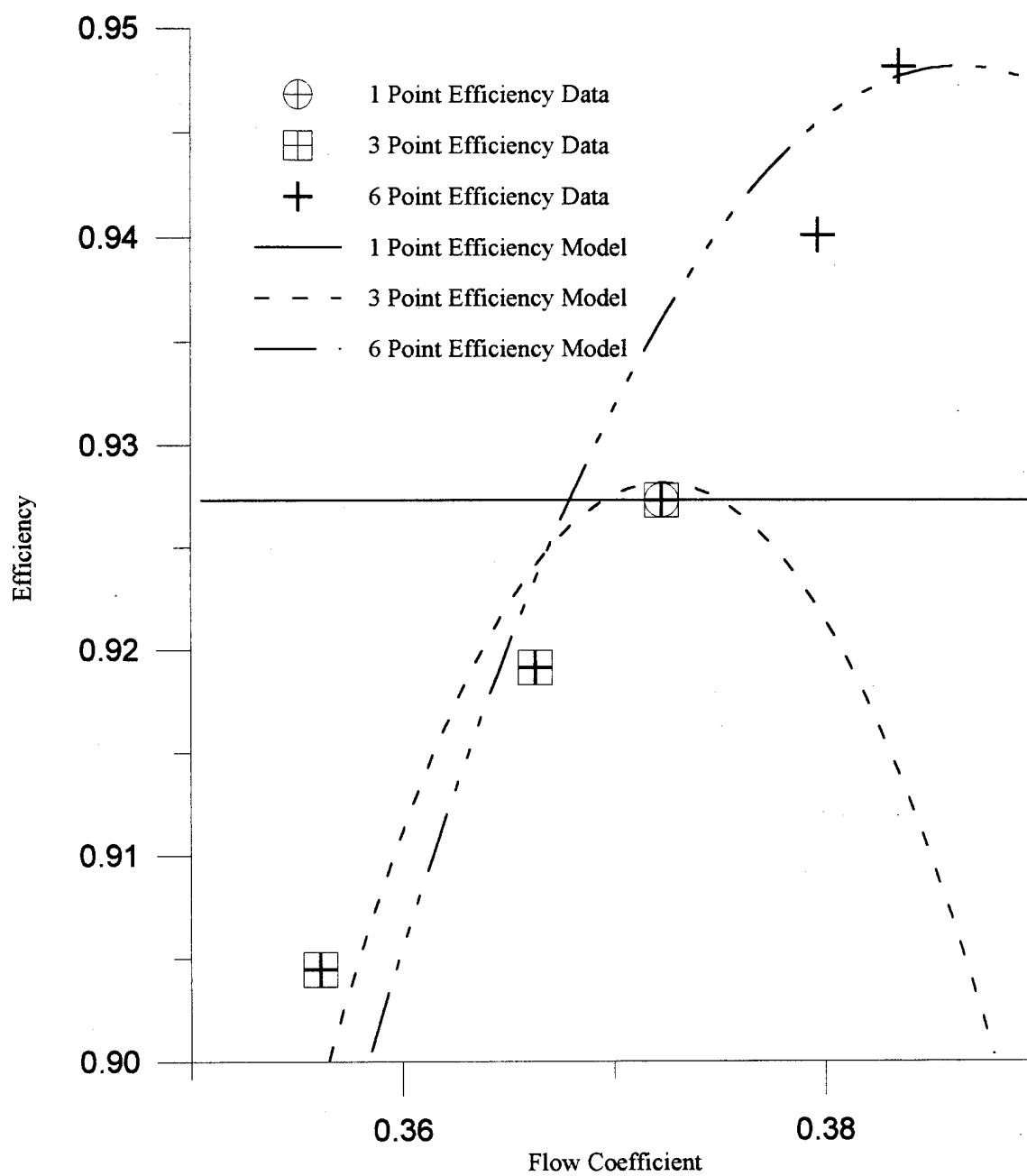Prediction due to Additional Data Points

Figure 4.15 Efficiency vs. Flow Coefficient Models for
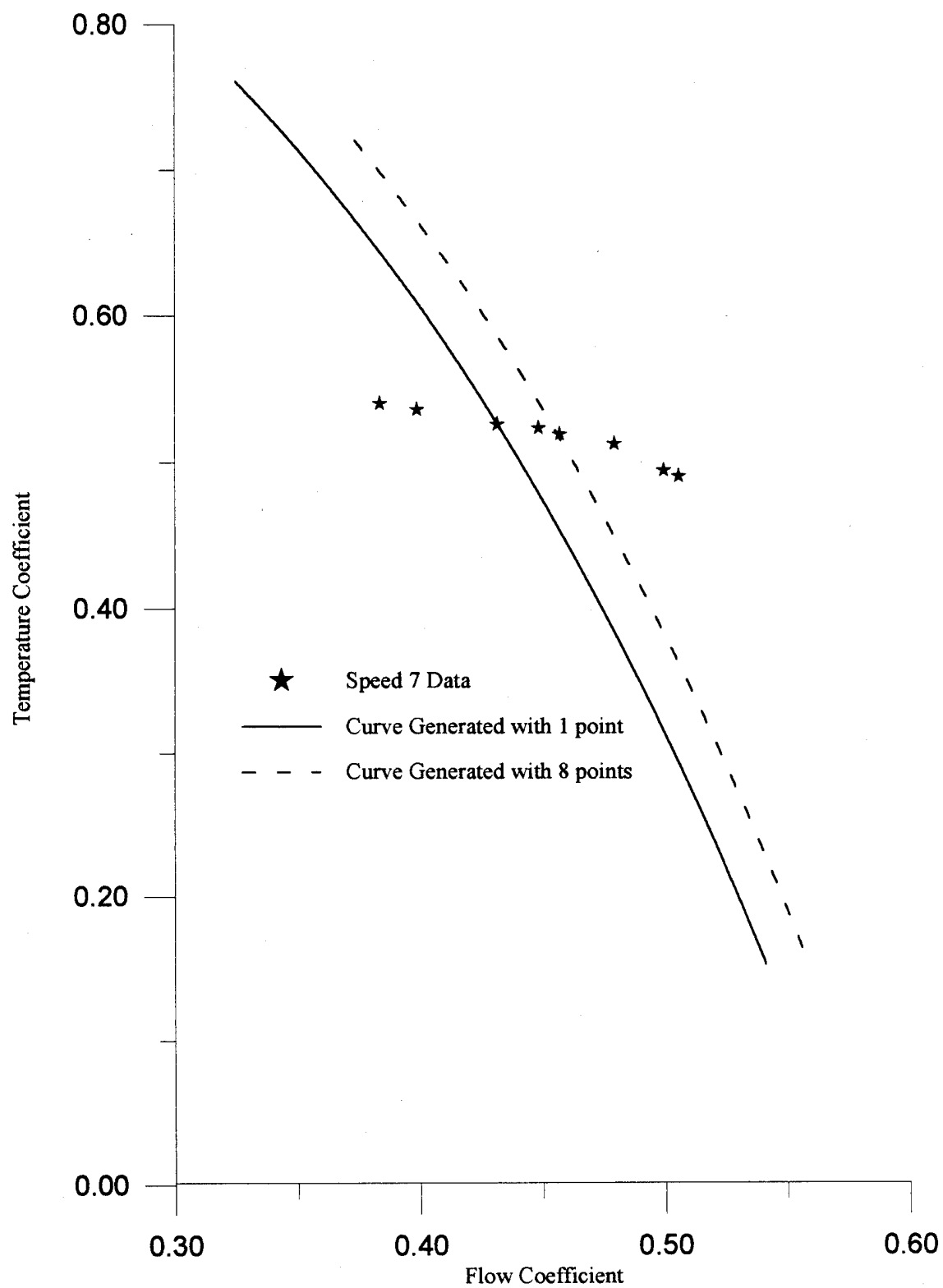Stage 1, Speed 4

Figure 4.16 Improvement in Stage 3, Speed 7 Temperature
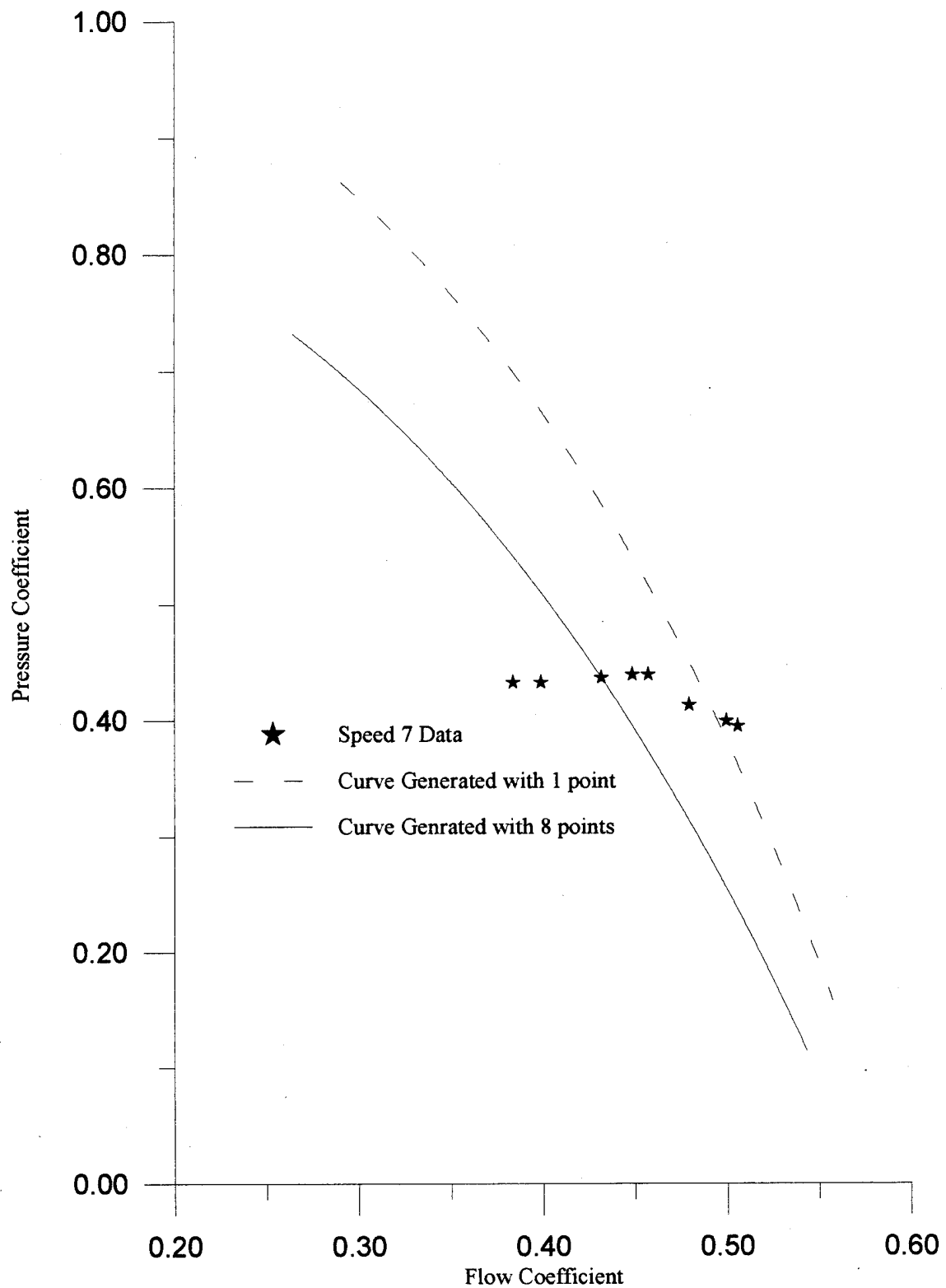Characteristic Prediction using Curve 1 and Additional Data

Figure 4.17 Improvement in Stage 3, Speed 7 Pressure
Characteristic Prediction using Curve 1 and Additional Data
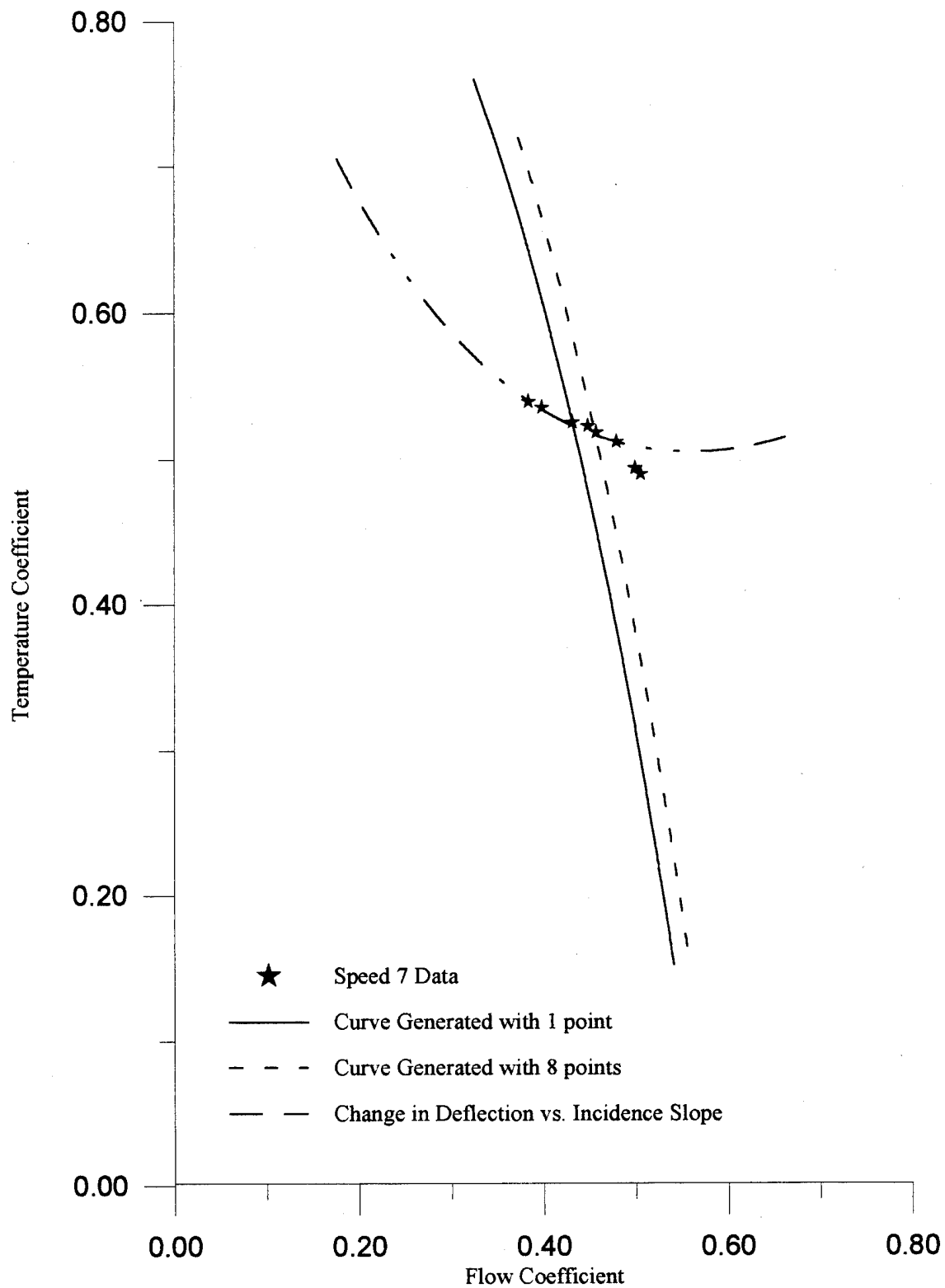
Figure 4.18 Improvement in Stage 3, Speed 7 Temperature
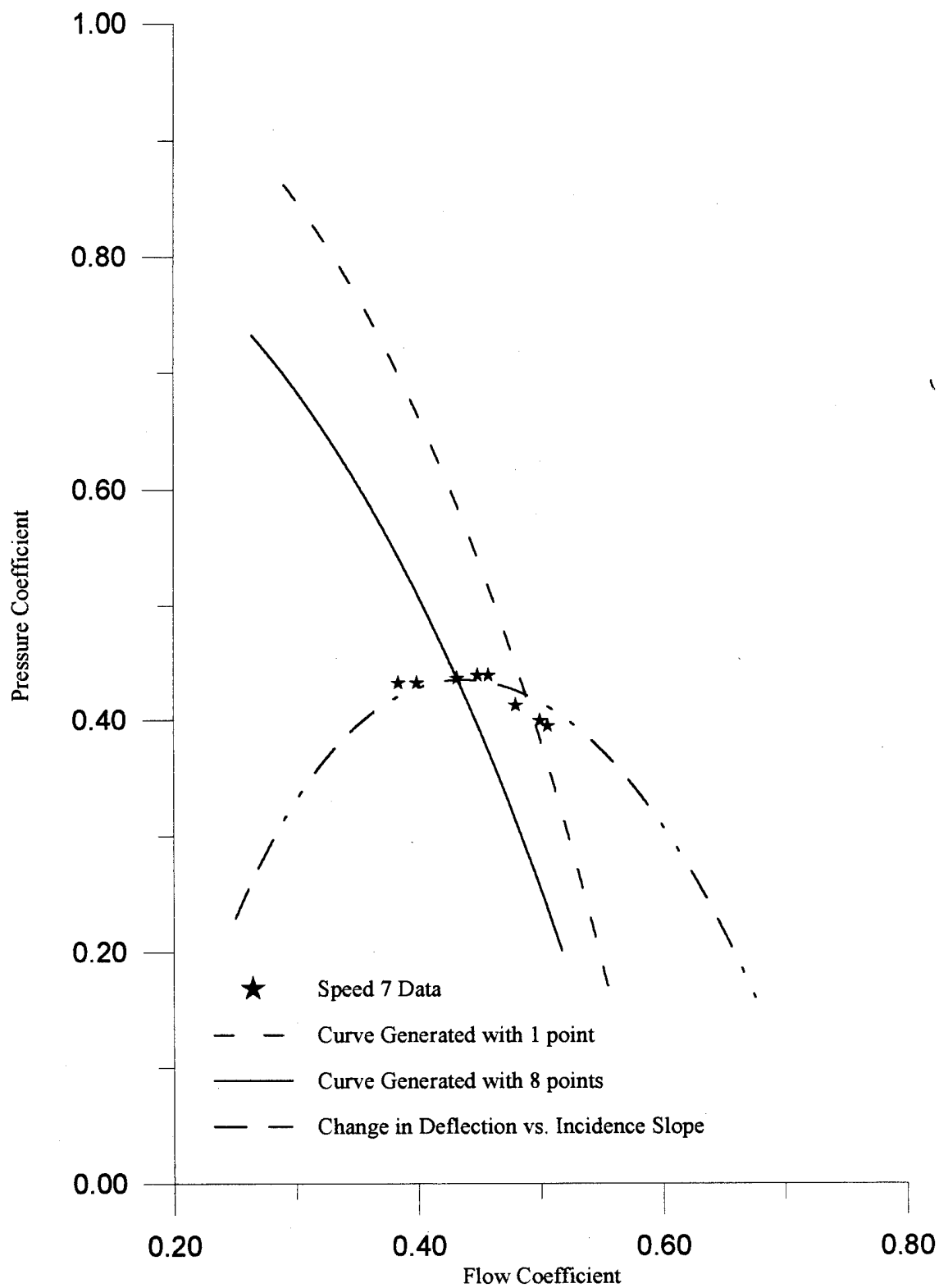Characteristic Prediction using Curve 1 and Changing ε'

Figure 4.19 Improvement in Stage 3, Speed 7 Pressure
Characteristic Prediction using Curve 1 and Changing ε'

REPORT DOCUMENTATION PAGE

Public reporting burden for this collection of information is estimated to average 1 hour per response, including the time for reviewing instructions, searching existing data sources, gathering and maintaining the data needed, and completing and reviewing the collection of information. Send comments regarding this burden estimate or any other aspect of this collection of information, including suggestions for reducing this burden, to Washington Headquarters Services, Directorate for Information Operations and Reports, 1215 Jefferson Davis Highway, Suite 1204, Arlington, VA 22202-4302, and to the Office of Management and Budget, Paperwork Reduction Project (0704-0188), Washington, DC 20503.

1. AGENCY USE ONLY (Leave blank)	2. REPORT DATE December 1995	3. REPORT TYPE AND DATES COVERED Master's Thesis

4. TITLE AND SUBTITLE
Prediction of an Axial Compressor Stage Characteristic from a One-Point Measurement

5. FUNDING NUMBERS

6. AUTHOR(S)
Shahnaz M. Punjani, Capt, USAF

7. PERFORMING ORGANIZATION NAME(S) AND ADDRESS(ES)
Air Force Institute of Technology
Wright-Patterson AFB, OH 45433-7765

8. PERFORMING ORGANIZATION REPORT NUMBER
AFIT/GAE/ENY/95D-21

9. SPONSORING/MONITORING AGENCY NAME(S) AND ADDRESS(ES)
Dr. Milt Davis
AEDC
1099 Avenue C
Arnold AFT, TN 37389-9013

10. SPONSORING/MONITORING AGENCY REPORT NUMBER

11. SUPPLEMENTARY NOTES

12a. DISTRIBUTION/AVAILABILITY STATEMENT
Approved for public release; distribution unlimited

12b. DISTRIBUTION CODE

13. ABSTRACT (Maximum 200 words)
This study focuses on predicting axial compressor stage characteristics using a single performance point comprised of mass flow, temperature and pressure rise coefficients obtained in experimental testing and a generic stage temperature characteristic. A new temperature characteristic is generated using a mapping technique where changes in stage blade angles are iterated from assumptions of free vortex flow and constant increment of flow turning angle with increased flow incidence. If additional data corresponding to the new curve are available, the characteristic is adjusted using non-linear least squares estimation. Essentially, the modified mapped curve results from a re-estimated change in the stator outlet angle which is iterated to minimize the total error between the new curve and the new aggregate of the given data. A pressure characteristic for the single data point may be predicted from the new temperature characteristic and an assumption of constant efficiency. Upon collection of additional data points, an improved pressure characteristic is obtained using an improved model for efficiency. The predicted characteristics agreed well with calibration data in pre-stall regions. For those data near stall, the assumed linear relationship between incidence and flow turning is invalid, and a new model for flow turning is required.

14. SUBJECT TERMS
Axial Compressors, Stage Characteristics, Pre-Stall Peformance

15. NUMBER OF PAGES
134

16. PRICE CODE

17. SECURITY CLASSIFICATION OF REPORT	18. SECURITY CLASSIFICATION OF THIS PAGE	19. SECURITY CLASSIFICATION OF ABSTRACT	20. LIMITATION OF ABSTRACT
Unclassified	Unclassified	Unclassified	UL

NSN 7540-01-280-5500

Standard Form 298 (Rev. 2-89)
Prescribed by ANSI Std. Z39-18
298-102

GENERAL INSTRUCTIONS FOR COMPLETING SF 298

The Report Documentation Page (RDP) is used in announcing and cataloging reports. It is important that this information be consistent with the rest of the report, particularly the cover and title page. Instructions for filling in each block of the form follow. It is important to *stay within the lines* to meet *optical scanning requirements*.

Block 1. Agency Use Only *(Leave blank)*.

Block 2. Report Date. Full publication date including day, month, and year, if available (e.g. 1 Jan 88). Must cite at least the year.

Block 3. Type of Report and Dates Covered. State whether report is interim, final, etc. If applicable, enter inclusive report dates (e.g. 10 Jun 87 - 30 Jun 88).

Block 4. Title and Subtitle. A title is taken from the part of the report that provides the most meaningful and complete information. When a report is prepared in more than one volume, repeat the primary title, add volume number, and include subtitle for the specific volume. On classified documents enter the title classification in parentheses.

Block 5. Funding Numbers. To include contract and grant numbers; may include program element number(s), project number(s), task number(s), and work unit number(s). Use the following labels:

C	-	Contract	**PR**	- Project
G	-	Grant	**TA**	- Task
PE	-	Program Element	**WU**	- Work Unit Accession No.

Block 6. Author(s). Name(s) of person(s) responsible for writing the report, performing the research, or credited with the content of the report. If editor or compiler, this should follow the name(s).

Block 7. Performing Organization Name(s) and Address(es). Self-explanatory.

Block 8. Performing Organization Report Number. Enter the unique alphanumeric report number(s) assigned by the organization performing the report.

Block 9. Sponsoring/Monitoring Agency Name(s) and Address(es). Self-explanatory.

Block 10. Sponsoring/Monitoring Agency Report Number. *(If known)*

Block 11. Supplementary Notes. Enter information not included elsewhere such as: Prepared in cooperation with...; Trans. of...; To be published in.... When a report is revised, include a statement whether the new report supersedes or supplements the older report.

Block 12a. Distribution/Availability Statement. Denotes public availability or limitations. Cite any availability to the public. Enter additional limitations or special markings in all capitals (e.g. NOFORN, REL, ITAR).

DOD	- See DoDD 5230.24, "Distribution Statements on Technical Documents."
DOE	- See authorities.
NASA	- See Handbook NHB 2200.2.
NTIS	- Leave blank.

Block 12b. Distribution Code.

DOD	- Leave blank.
DOE	- Enter DOE distribution categories from the Standard Distribution for Unclassified Scientific and Technical Reports.
NASA	- Leave blank.
NTIS	- Leave blank.

Block 13. Abstract. Include a brief *(Maximum 200 words)* factual summary of the most significant information contained in the report.

Block 14. Subject Terms. Keywords or phrases identifying major subjects in the report.

Block 15. Number of Pages. Enter the total number of pages.

Block 16. Price Code. Enter appropriate price code *(NTIS only)*.

Blocks 17. - 19. Security Classifications. Self-explanatory. Enter U.S. Security Classification in accordance with U.S. Security Regulations (i.e., UNCLASSIFIED). If form contains classified information, stamp classification on the top and bottom of the page.

Block 20. Limitation of Abstract. This block must be completed to assign a limitation to the abstract. Enter either UL (unlimited) or SAR (same as report). An entry in this block is necessary if the abstract is to be limited. If blank, the abstract is assumed to be unlimited.